Construction and Building Materials

Feasibility of 3DP cob walls under compression loads in low-rise construction

--Manuscript Draft--

Manuscript Number:	CONBUILDMAT-D-20-08200R2
Article Type:	Research Paper
Keywords:	Additive Manufacturing; 3D printing; Cob; compression test; Limit-state design; Structural performance optimisation
Corresponding Author:	Jaroslav Vaculik University of Adelaide Adelaide, AUSTRALIA
First Author:	Mohamed Gomaa, MSc
Order of Authors:	Mohamed Gomaa, MSc
	Jaroslav Vaculik, PhD
	Veronica Soebarto, PhD
	Michael Griffith, PhD
	Wassim Jabi, PhD
Abstract:	The rapid adoption of 3D-printing (3DP) technologies in construction, combined with an increased willingness to reduce the environmental impact of building industry, has facilitated reapproaching earth materials for modern building industry. The feasibility of 3DP earth-based materials has been under investigation in recent years, with a particular focus on cob due to its favourable characteristics toward the 3DP process. Yet, there is a lack of definitive information on the construction of 3DP cob. Hence this paper investigates the structural feasibility of 3D-printed cob walls in low-rise buildings. The investigation involved experimental compression tests on 3DP cob samples to obtain key mechanical properties including the compressive strength and elastic modulus. These properties were then used as inputs for structural analyses with respect to three alternate types of 3DP cob wall patterns to evaluate their load-carrying capacity based on a limit-state design framework. Results from the analyses were implemented in modelling an idealised low-rise cob building covering a range of floor spans and wall heights. The analytical study found that 3D-printed walls have the potential to sustain gravity loads typical of residential construction. Further, since the 3DP material was shown to have similar mechanical performance to conventional (non-3DP) cob on the material scale, the 3D-printing process provides the opportunity to produce wall sections that are structurally more efficient than the solid section used in conventional cob construction. This results in lower material consumption, making 3DP cob attractive from the point of view of resource efficiency. An important outcome of the study is the demonstration of a model design technique for low-rise 3DP cob buildings that could be implemented as part of a broader optimisation procedure to satisfy structural and architectural design objectives.

Feasibility of 3DP Cob Walls Under Compression Loads in Low-Rise Construction

Mohamed Gomaa[ae], Jaroslav Vaculik[b,c*], Veronica Soebarto[a], Michael Griffith[b,c], Wassim Jabi[d]

[a] School of Architecture and Built Environment, Horace Lamb Building, University of Adelaide, Adelaide SA5005, Australia.
[b] The School of Civil, Environmental and Mining Engineering, Engineering North Building, University of Adelaide, Adelaide SA5005, Australia.
[c] Bushfire and Natural Hazards Cooperative Research Centre, Melbourne, Australia
[d] The Welsh School of Architecture, Bute Building, Cardiff University, Cardiff CF10 3NB, UK.
[e] School of Engineering, B251- RMIT Bundoora East Campus, RMIT University, Melbourne VIC 3083, Australia.

*Corresponding Author
Postal address: The School of Civil, Environmental and Mining Engineering, Engineering North Building, University of Adelaide, Adelaide SA5005, Australia.
Phone: (+61 8 8313 5451)

Abstract

The rapid adoption of 3D-printing (3DP) technologies in construction, combined with an increased willingness to reduce the environmental impact of building industry, has facilitated reapproaching earth materials for modern building industry. The feasibility of 3DP earth-based materials has been under investigation in recent years, with a particular focus on cob due to its favourable characteristics toward the 3DP process. Yet, there is a lack of definitive information on the construction of 3DP cob. Hence this paper investigates the structural feasibility of 3D-printed cob walls in low-rise buildings. The investigation involved experimental compression tests on 3DP cob samples to obtain key mechanical properties including the compressive strength and elastic modulus. These properties were then used as inputs for structural analyses with respect to three alternate types of 3DP cob wall patterns to evaluate their load-carrying capacity based on a limit-state design framework. Results from the analyses were implemented in modelling an idealised low-rise cob building covering a range of floor spans and wall heights. The analytical study found that 3D-printed walls have the potential to sustain gravity loads typical of residential construction. Further, since the 3DP material was shown to have similar mechanical performance to conventional (non-3DP) cob on the material scale, the 3D-printing process provides the opportunity to produce wall sections that are structurally more efficient than the solid section used in conventional cob construction. This results in lower material consumption, making 3DP cob attractive from the point of view of resource efficiency. An important outcome of the study is the demonstration of a model design technique for low-rise 3DP cob buildings that could be implemented as part of a broader optimisation procedure to satisfy structural and architectural design objectives.

Keywords:

Additive manufacturing; 3D printing; Cob; Compression test; Limit-state design; Structural performance optimisation.

1 Introduction

Digital fabrication technologies, especially 3D printing (3DP), have been witnessing an increasing uptake in many areas of industry [1]. The construction industry has been adopting a scaled-up version of 3DP over the past two decades. The increased demand for 3DP technologies in construction industry has also encouraged researchers to develop novel ideas toward the full automation of the construction process. Several studies have proven that a well-developed digital-based process of construction offers various benefits such as larger design freedom, accelerated productivity, higher degree of customisation, and improved safety of construction personnel [2], [3].

Among the developed techniques of digital fabrication in construction, 3DP has been the most studied, and has seen a particular focus on cement-based materials [4]–[7]. This has led in recent years to a rapid spread of 3DP building prototypes around the world, as 3DP technology has been increasingly embraced by the construction industry [8]. Among the most notable examples are two concrete buildings constructed in 2019: One is the world's largest 3DP building, constructed by Apis Cor in Dubai, United Arab Emirates having two storeys, a plan area of 640 m^2 and height of 9.5 m (Figure 1a). The second is a 80 m^2 prototype house built by CyBe as part of their contract with the Saudi Arabia Ministry of Housing with an ambitious goal to build 1.5 million houses using 3D concrete printing [9] (Figure 1b).

Figure 1: Notable examples of 3DP concrete buildings: (a) Two-storey office building in Dubai constructed by Apis Cor (image credit: Apis Cor), and (b) House in Saudi Arabia constructed by CyBe (image credit: CyBe).

The accelerating rate of present-day global construction is well known to produce adverse environmental impacts. Fortunately, the implementation of digital technology in construction offers great potential for sustainability [10]. For instance, according to Ford and Despeisse [11], additive manufacturing (e.g. 3D printing) in construction has several sustainability benefits such as improving efficiency of resources, extending product life, and upgrading the value and supply chains.

The increased motivation to harness the sustainability benefits of 3DP technology in construction has also recently renewed the interest in earthen construction materials after decades of dormancy [11],[14]. Significantly, a recent study by Hamard et al. [12] has revealed that considerable sustainability benefits can be realised through the integration of digital fabrication techniques with earth-based materials, which have low embodied energy, are highly recyclable, and generate limited waste. Furthermore, these materials typically have high material density and thus high thermal mass, which can lead to favourable thermal comfort performance, particularly in areas where there is a large difference in daytime and night-time temperatures [12], [14], [15]. As a further benefit, earth-based materials are significantly cheaper per unit volume compared to conventional building materials such as concrete or steel [13], and can under many circumstances result in more economical small-scale structures.

Earthen construction has three famous forms: cob, adobe, and rammed earth. Cob, which is the focus of this study, is a traditional building material comprising a mixture of subsoil, water and straw (or other fibres). It differs from adobe and rammed earth by using a wet-based construction technique that offers freedom of design while not requiring formwork. It also exhibits excellent maintenance characteristics through the ability to apply add-ons or create cuts-out, even after the cob is dry [16]–[18]. This makes cob particularly attractive for 3D printing.

In recent years, the performance of cob manufactured digitally using 3D printing has been the focus of emergent research at several institutions such as IAAC, Cardiff University and Plymouth University [19]. A proof of concept of the idea has also been successfully demonstrated by the 3D-printer manufacturer WASP by constructing two prototypes of cob houses [20] (Figure 2). And while the focus of the studies to date has been to examine feasibility with regard to aspects such as geometry and fabrication process [21], thermal performance [22], and life cycle assessment [8], the examination of structural performance not yet been carried out in any significant detail. As a consequence, the pursuit of fully implementing 3D cob in modern construction remains hindered by a lack of engineering guidance for structural design. Overcoming this hurdle requires establishing a reliable body of experimental test data on the mechanical (structural engineering) properties of 3DP cob, as well the development of appropriate structural design and modelling tools that can be used by design engineers.

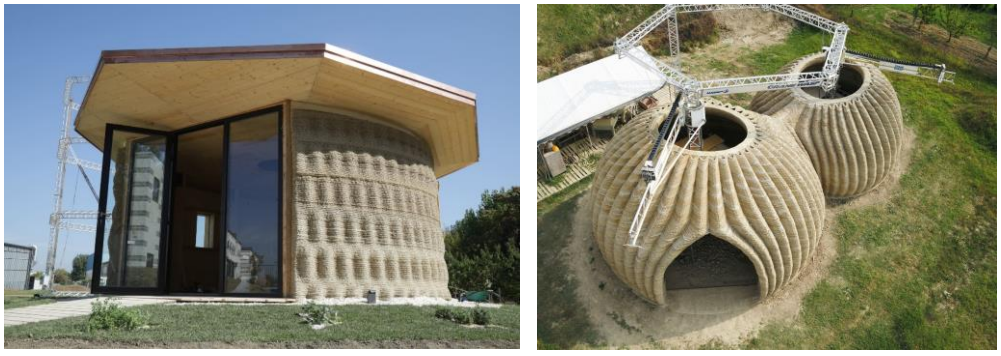

Figure 2: 3DP cob houses fabricated by WASP (image credit: WASP).

While numerous studies have focused on the mechanical properties of 3DP concrete [1][7], to the knowledge of the authors only a single study to date has investigated the mechanical properties of any 3DP cob-like material [23]. This study, by Perrot et al., tested material made from a mix of earth material and alginate seaweed biopolymer (as a substitute for straw which is traditionally used), and demonstrated compressive strength simliar to that of conventional (non-3DP) cob. Besides this study, however, there is no existing research into the mechanical properties of traditional (straw-fibre) cob passed through the 3DP process. Moreover, there are, to the authors' knowledge, no existing studies involving the translation of these fundamental properties toward engineering design of 3DP cob on neither the wall nor building scale.

To address these gaps, this study aims to provide insight into the expected loadbearing capability 3DP cob walls. This is approached in two stages: The first conducts an experimental compression test on 3DP cob samples to obtain the basic mechanical properties including compressive strength, elastic modulus, and Poisson's ratio. The second stage evaluates the wall section geometries (dimensions) necessary to perform a loadbearing function in typical residential construction for alternate 3DP patterns through a first-principles analysis approach. This is combined with an optimisation process to examine the relationship between structural efficiency and several design variables such as variable room size, floor heights, number of storeys, and wall section properties. The outcomes are expected to empower architects and engineers with a model approach for the structural design and construction process of 3DP cob. The paper also acts as an essential part of larger overarching research by the authors on the feasibility of 3DP cob in modern construction.

The paper is structured as follows: Section 2 undertakes a review of previous material testing of traditional (non-3DP) cob to establish typical range of material properties. Section 3 reports original compression tests on 3DP cob cylinders. Section 4 demonstrates a simplified design approach for estimating the loadbearing capability of 3DP walls, and examines their feasibility in residential construction, including an investigation of the sensitivity on material properties. Section 5 demonstrates the essential design process on a fictional small house, and Section 6 concludes with a summary and recommendations for future work.

2 Structural performance of cob as a building material

Cob buildings are well-known for their durability and resistance to weathering [24]. However, the lack of a binding agent (e.g. cement) makes the compressive strength of cob (typically < 2 MPa) much weaker compared to concrete (typically > 20 MPa) and even other traditional materials such as rammed earth (typically 5–20 MPa). This combined with the fact that cob buildings were historically built without reinforcement means that building heights are typically restricted to low-rise (i.e. between one to three storeys), with most being 2-storey [13]. Some very rare but notable examples of high-rise are found however, such as the world heritage-listed towers in Yemen which have up to 9 storeys [25][26]. The low compressive strength of cob compared to other traditional materials is generally compensated for by large wall thickness [27], [28].

Multi-storey cob houses typically incorporate light-weight floor and roof systems in the form of timber framing. Floors usually comprise joists with wooden decking, while roofs include timber rafters plus purlins and have a typically sloped profile with extended eaves to protect walls from rain. Walls in multi-storey houses are typically around 600 mm thick, and for efficiency they are typically made thinner at upper storeys relative to the ground floor [13], [28].

Mechanical properties of cob are dependent on a number of factors: subsoil composition including clay content, straw and water content, degree of compaction, and the general quality of the workmanship [29], [27], [30]. Studies into the influence of the mix composition have demonstrated compressive strength to be generally enhanced by increased straw content (due to acting as local tensile reinforcement) and reduced by higher moisture content [16], [31]. Table 1 provides a generalised overview of test studies to date, summarising the range of reported compressive strength (f_c) and elastic modulus (E). It is important to note that the cob mixtures in these studies vary in terms of their composition, with the intention of the table being to demonstrate the broad range of property values rather than parametric trends.

Compressive strength can be considered to be the fundamental engineering property of interest for earthen-material structures, as it controls the loadbearing capacity of walls under gravity loads [13], [32]. As demonstrated by Table 1, compressive strength usually falls between 0.4–1.35 MPa, although values less than 0.1 MPa and as high as 5 MPa have been reported. Notably, low values of strength (< 0.4 MPa) are usually for mixtures with high moisture content (> 15%) [13], [31]. Among the studies in Table 1, the range of scatter in compressive strength (where reported) varies between 2–21%. Stochastic variability has implications toward the lower-bound characteristic value that can be adopted in limit-state design as discussed later.

The reported elastic modulus varies drastically among the published studies. Most values fall within the range 4–200 MPa, but outlying values as low as 0.33 MPa and as high as 850 MPa have also been reported. As will be shown later (Section 4) the elastic modulus has particular importance toward the loadbearing capacity of 3DP cob walls due to the potential for local buckling of the printed sections.

Data on Poisson's ratio is limited to two studies [29] and [33], who reported mean values of 0.15 and 0.12 respectively.

Additionally, cob exhibits considerably higher material ductility than rammed earth and adobe [29], [33], as characterised by the ability to maintain stress resistance into the post-peak phase of stress-strain response. Miccoli et al. [29] demonstrated this to be the case under both compressive and shear loading. The observed ductility of cob can be attributed to the influence of fibres, with fibres used in cob being typically longer than in adobe. This favourable behaviour implies that cob may be able to outperform the alternate earthen materials under deformation-controlled loading such as earthquake. While this warrants further investigation, it is outside the scope of the current paper.

Table 1: Compressive strength (f_c), elastic modulus (E), and Poisson's ratio (ν) for non-3DP cob. Values presented as a range (a–b) cover different cob mixtures, if applicable. Percentages in brackets denote the intra-batch CoV if specified. Unless noted otherwise, the mixtures have moisture content (mc) < 15%.

Source	f_c (MPa)	E (MPa)	ν
Houben and Guillaud (1994) [34]	0.10	–	–
Saxton (1995) [31]	0.35–1.75 (mc<15%) 0–0.2 (mc>15%)	–	–
Ziegert (2003) [35]	0.45–1.40	170–335	–
Coventry (2004) [36]	0.48–1.24 (3%–10%)	0.33–1.25	–
Keefe (2005) [24]	0.6–1.4	–	–
Akinkurolere et al. (2006) [16]	0.6–2.2	–	–
Weismann and Bryce (2006) [28]	0.77	–	–
Quagliarini et al. (2010) [13]	0.24–0.40 (mc>15%)	4.0–40 *	–
Pullen and Scholz (2011) [32]	0.45–0.89 (22%)	11–69	–
Minke (2012) [37]	0.5–5.0	60–850	–
Miccoli et al. (2014) [29]	1.59 (2%)	651 (68%)	0.15 (4%)
Rizza and Bottger (2015) [38]	0.60 (13%)	71.5	–
Brunello et al. (2018) [39]	0.71–0.87 (8%–15%)	–	–
Quagliarini and Maracchini (2018) [33]	1.12 (5%)	16.9 (4%)	0.12 (66%)
Vinceslas et al. (2018) [40]	0.50–0.76	110–350	–
Wright (2019) [30]	1.22–1.53 ** (18%–21%) 0.77–2.45 ***	–	–
Jimenez Rios and O'Dwyer (2020) [41]	0.70 (12%)	143 (23%)	–

Notes:
* E determined from reported stress-strain curves
** Specimens with varied straw content
*** Specimens with varied soil clay content

The only study, to the authors' knowledge, that has undertaken material testing on any 3D-printed earthen material is a recent study by Perrot et al. [23], which used a cob-like material incorporating alginate seaweed biopolymer as a substitute for straw. The produced material achieved a compressive strength between 1.2–1.8 MPa, demonstrating that 3DP earth material has the potential to achieve compressive strength toward the higher end of that for conventional non-3DP cob (Table 1).

3 Compression tests on 3D-printed cob cylinders

This section reports laboratory tests performed on 3DP-cob cylinders to quantify fundamental mechanical properties necessary for design. Among the side objectives of these tests was also to ensure that the 3D-printing process did not produce any unexpected strength reduction compared to conventional non-3DP cob (Table 1). Such a reduction could be conceivable due

to the altered form of the material as a result of being stacked in layers rather than being a homogeneous mass. Due to the lack of a structural testing standard specific to earthen materials, the study adopted general principles for the testing of quasi-brittle materials, as recommended by [42].

3.1 Test specimens

3.1.1 Material mix preparation

In the 3D-printing process, for both concrete and earth-based materials, the material must flow efficiently through the system, be deposited as layers and harden properly to reach a structural integrity threshold within an acceptable time frame that meets the construction requirements [5] [23]. The properties of the input material must therefore be formulated carefully considering both their wet (pre-hardening) and hardened states. According to Weismann and Bryce [28] and Hamard et al. [12], traditional cob mixture typically comprises 78% subsoil, 20% water and 2% fibre (straw) by weight. This however produces a nearly dry mixture with low flowability, making it unsuitable for 3D printing. To overcome this, the adopted mixture followed an alternate, 3DP-suitable, mix developed by the authors in a precursor study [22]. In the adopted mix, the water content was increased to an average of 25%, subsoil was reduced to 73%, and straw was maintained at 2% (by weight). The mixture used locally-sourced wheat straw chopped into lengths of 30–50 mm, as longer straw lengths were found to be unsuitable by causing blockage inside the extrusion system. The composition of the subsoil (sourced from Cardiff, UK) was examined using methods recommended by [28], [43] and found to contain 19–20% clay and 80–81% aggregate/sand. This is in good agreement with subsoil composition recommended in the literature (15–25% clay to 75–85 % aggregate/sand) [28], [12].

It is worth mentioning that, despite the intentionally high moisture content of the input mixture, the moisture content of the final printed cob becomes slightly reduced by the 3DP extrusion process. This is caused by the pressurisation of the mixture inside the extrusion system, which leads to moisture release in the form of leakage around the cartridge connections. The moisture loss in this study was estimated at around 3%, leaving the printed cob at 22% moisture content. This reduction is considered favourable as it improves the structural stability of the printed layers and also reduces drying shrinkage. Note that while shrinkage is an important aspect of cob construction, it was not a specific focus of this study, especially as the observed shrinkage in the specimens was low (approx. 2%) and the specimens showed no signs of cracking during the drying period.

3.1.2 3D-printing of specimens

The test specimens in this study were printed using a 6-axis KUKA KR60 HA robotic arm (Figure 3). The software package for robotic control was Rhinoceros via Grasshopper and KUKA PRC®. An electromechanical dual ram extruder, developed by the authors in a previous study [21], was used for material delivery. The test specimens comprised 400 mm-tall cob cylinders with an average diameter of 200 mm (Figure 4). Each cylinder was contoured as 14 successive layers, with an average height of 29 mm per layer. The nozzle had a 45 mm

diameter. The robotic arm moved in a circular pattern at an average movement speed of 35 mm/sec.

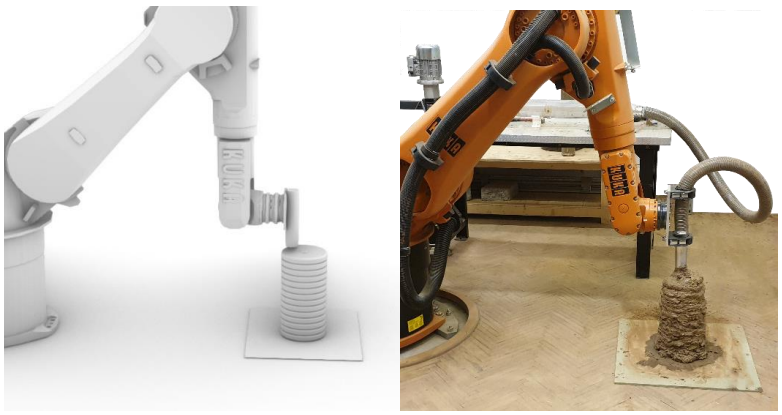

Figure 3: Robotic 3D printing of the cob specimens: virtual model on Rhino (left) and the real output (right).

3.2 Test arrangement and method

The test specimens were subjected to uniform axial load in a universal testing machine (Figure 4). Prior to the test, the machine loading platens were coated with grease to minimise frictional confinement. The rate of applied load was approximately 0.08 MPa/min, with each test taking about 10 minutes to perform. The test apparatus monitored the applied load and axial (longitudinal) displacement between the two platens using a built-in linear variable differential transformer (LVDT). Due to the impracticality of applying strain gauges to the irregular surface of the specimens, horizontal deformation (necessary to evaluate the Poisson's ratio) was quantified in post-processing by digital image correlation using high-resolution video footage captured during the test. A total of three samples were tested, with examples of the failed specimens shown in Figure 5.

Figure 4: Compression test setup (left) and the cylindrical specimen (right).

Figure 5: Typical examples of specimens after compressive failure.

3.3 Results

The observed stress-strain behaviour is shown in Figure 6. Each specimen exhibits quasi-brittle response with an approximately linear rising branch, followed by a reduction in slope up to the peak, and continued softening in the post-peak zone. The plotted stress was calculated as $\sigma = P/A$, where P is the applied force and A is the average cross-sectional area of the specimen (31,400 mm^2). Axial strain was computed as $\varepsilon_{axial} = \Delta/L$, where Δ is the displacement measured platen-to-platen, and L is the length of the specimen (400 mm).

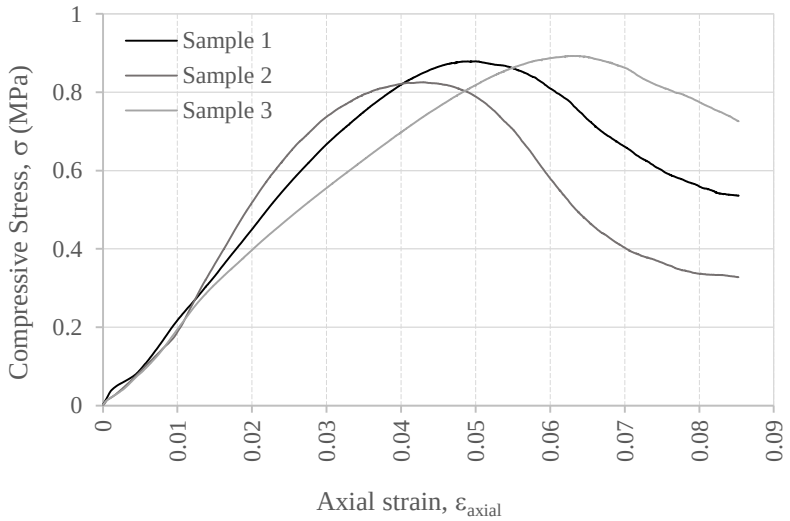

Figure 6: Stress-strain behaviour of compression test specimens.

The properties derived from the test, including the compressive strength, elastic modulus, and Poisson's ratio, are summarised in Table 2.

The average unconfined compressive strength (f_c) of the specimens is 0.87 MPa. This compares favourably to strength of non-3DP cob reported in the literature (Table 1) with most reported values falling within 0.4–1.35 MPa. On this basis there does not appear to be any obvious reduction in strength introduced by the 3DP process. Despite a limited number of samples, the variability is low (CoV = 4%). It should be noted that the reported compressive strength corresponds directly to the peak stress reached during the test. To account for the size-effect in quasi-brittle materials as well as confinement resulting from the compression apparatus platens, test standards typically apply a correction factor to the measured peak stress to obtain a size-invariant unconfined compressive strength. For instance if these results were to be interpreted according to the test standard for masonry units (EN 772-1, [44]) a correction factor of 1.25 would apply on the basis of the test specimen dimensions. However, for conservatism, the subsequent analysis in Section 4 takes this factor as 1.

Elastic modulus (E) was evaluated as the slope of the σ-ε curve along the initial rising branch before the onset of nonlinearity. Mean E of the tested specimens is 22.9 MPa (CoV = 10%). This falls into the lower end of values determined for non-3DP cob (Table 1) (median ≈ 60 MPa). As demonstrated later (Section 4), the elastic modulus is influential on wall loadbearing strength as it controls local buckling of the printed cross section, thus providing impetus for future investigations into 3DP-suitable cob mix design to focus on not just the material's strength but also stiffness.

Poisson's ratio (ν) was calculated as the ratio of lateral to longitudinal strain over the initial elastic portion of response, producing a mean value of 0.22. This is consistent with the range of scatter reported by [29] and [33] for non-3DP cob (Table 1).

Table 2: Results of compression test, including unconfined compressive strength (f_c), elastic modulus (E), and Poisson's ratio (ν).

Sample	f_c (MPa)	E (MPa)	ν
1	0.88	22.7	0.16
2	0.83	25.3	0.28
3	0.89	20.6	0.21
Mean value	0.87	22.9	0.22
CoV	4%	10%	28%

4 Evaluation of the feasibility of loadbearing 3DP cob walls

This section examines the feasibility of using 3DP cob walls as loadbearing in low-rise residential construction. The design actions considered are from gravity loads only, and do not include wind or earthquake loading which can be highly region-specific.

4.1 Method of structural analysis

Although the expected behaviour of 3DP cob walls under gravity loads is expected to resemble that of walls constructed using conventional materials such as unreinforced masonry or concrete, the design-code provisions for these established materials are not necessarily translatable to 3DP cob. Therefore, the wall's load-carrying capacity was evaluated using first principles while adhering to the concepts of limit-state design. This includes using characteristic values of material stress capacity (rather than mean values), and applying factors to upscale design loads and downgrade the design capacity.

4.1.1 Limit-state design

Capacity-adequacy checks were performed according to a limit-state design framework. With reference to the compressive strength, the design check can be expressed using the generalised form

$$N_c^* < \phi N_c. \quad (1)$$

In Eq. (1), N_c^* is the design compressive force acting on the wall, determined as γS, with S being the unfactored working load and γ being the load factor (greater than 1). In turn, ϕN_c is the design compressive capacity of the wall, determined as the basic capacity N_c multiplied by the capacity-reduction factor ϕ (less than 1). To account for the fact that the material stress capacities exhibit stochastic variability, capacity N_c was calculated using the characteristic compressive strength, f_c', defined as the lower-5th-percentile value.

4.1.2 Wall cross-section patterns

Three different types of printed patterns were considered as part of this feasibility study; these are referred to as A, B and C as shown in Figure 7. These three patterns align carefully with the wall sections in two previous studies that investigated thermal performance and life cycle assessment of 3D-printed cob by Gomaa et al. [22] and Alhumayani et al. [8] respectively. The criteria for choosing these wall sections are based on meeting multiple design requirements including adequate thermal insulation, efficient use of material, and structural integrity. A generic vertical cross section of a wall is shown in Figure 8. Because the 3D-printing process in the current study dispensed the cob material in circular cross sections while being flattened down into wider layers, the resulting vertical shells did not have a constant thickness (Figure 8). Rather, the shell thickness ranged between an inner value, t_{in}, and outer value, t_{out}, as shown. Both t_{in} and t_{out} could be estimated according to a number of parameters in the 3D-printing process setup, such as the layer height, nozzle size and the extrusion rate [21]. On the basis of typical printed patterns, $t_{out} - t_{in}$ was taken as 20 mm, with the average thickness (t) being in turn defined as $t = (t_{in} + t_{out})/2$. For each section type, the nominal wall depth (d) is defined as the distance between the centrelines of the two external 'face' shells; and a denotes the dimension between the internal 'web' shells (Figure 8). In all of the subsequent analyses, a is taken equal to d.

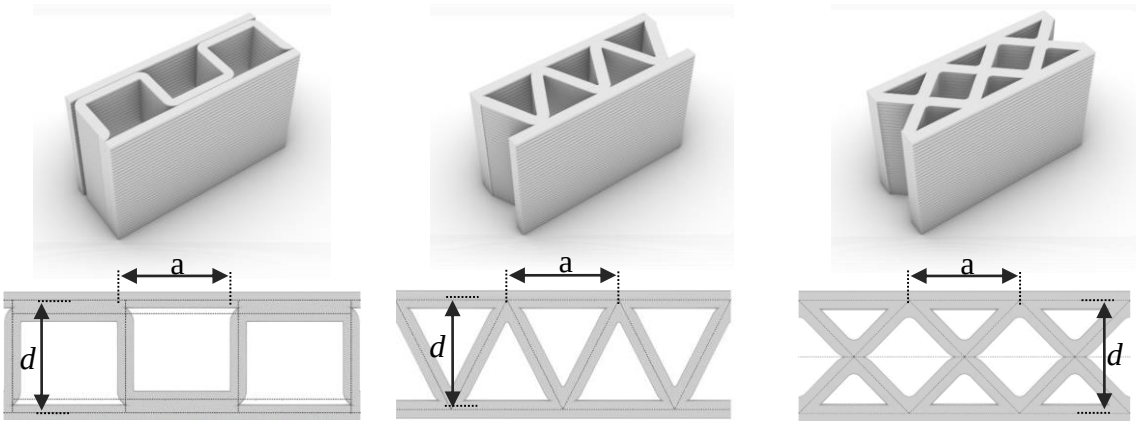

Figure 7: Alternate printed patterns considered in this study.

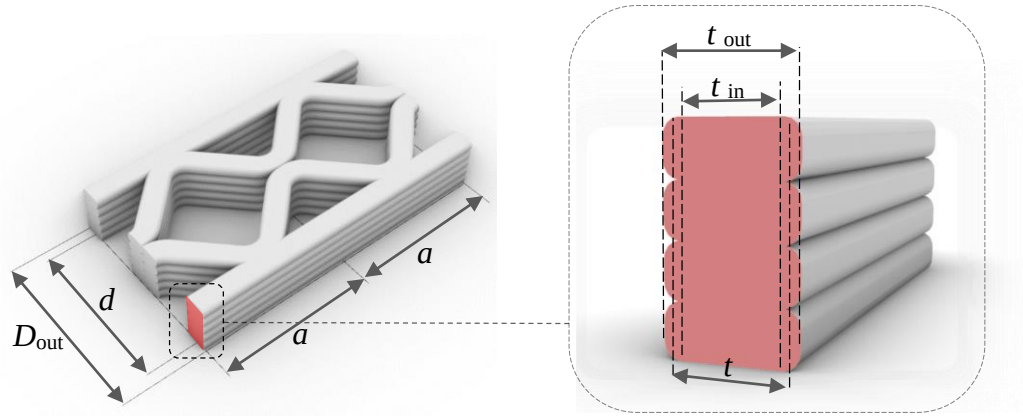

Figure 8: Definition of geometric properties along a generic cross section.

Evaluation of the wall's compressive capacity requires the wall's area (A) and out-of-plane moment of inertia (I). These were calculated for each type of section by conservatively taking the shell thickness as t_{in}. For comparative purposes, the sectional properties of the three pattern types are provided in Table 3.

Table 3: Section properties for the alternate printed patterns. Each considers a reference section with t_{in} = 50mm and d = 500mm. Properties accented by a bar ($\bar{X}$) denote the value per unit length run of the wall.

Wall Type	t_{in} (mm)	t (mm)	d (mm)	$\bar{A}$ (mm^2/m)	$\bar{I}$ (mm^4/m)	$\bar{P}_{buck,loc}$ (kN/m)
A	50	60	500	200,000	9.32×10^9	145
B	50	60	500	212,000	8.60×10^9	137
C	50	60	500	241,000	9.23×10^9	181

4.1.3 Wall compressive strength

The compressive strength of a generic (3DP or no-3DP) cob wall requires evaluation of its member capacity under combined axial load and eccentricity moment with the potential for global buckling combined with material failure. A 3DP wall however differs from a solid wall in that the section capacity can be governed by not just material crushing, but also by local buckling of the shell structure. Thus, the compressive stress capacity of the section was evaluated as

$$\sigma_{c,\max} = \min\left(\sigma_{\text{mat}}, \sigma_{\text{buck,loc}}\right), \tag{2}$$

i.e. the lesser of the stress to cause material crushing (σ_{mat}) and local buckling ($\sigma_{\text{buck,loc}}$).

The material crushing limit in Eq. (2) was taken as the characteristic (lower-5th-percentile) compressive strength ($\sigma_{\text{mat}} = f_c'$). The characteristic strength was estimated to be 0.62 MPa, based on the assumption that it follows a lognormal distribution with mean = 0.87 MPa (Table 1) and CoV = 20%.

The capacity of each of the three section types to withstand local buckling was determined using the finite-element analysis package ABAQUS. The model analysed for each type of printed section was built using shell elements and comprised a full-sized wall subjected to a uniform compressive force at its top and bottom boundaries. The length and height of each wall were taken as 2 m. These dimensions were chosen by trial-and-error so as to satisfy the conditions of: 1) being were sufficiently large not to influence the computed local-buckling stress, but 2) not excessive to cause global buckling. A visual examination of the resulting buckling mode shape was undertaken to confirm that it indeed corresponded to local buckling of the shell structure. A typical local-buckling shape is shown in Figure 9 and is characterised by the face- and web-shells deforming perpendicular to their local planes in an alternating pattern, while maintaining the original angle at shell junctions. The corresponding load capacities are summarised in the last column of Table 3 as the load per unit length of the wall ($\bar{P}_{\text{buck,loc}}$). These capacities were computed by assigning the material properties E = 22.9 MPa and ν = 0.22 as informed by the material tests. The local-buckling stress used in Eq (2), was evaluated as $\sigma_{\text{buck,loc}} = \bar{P}_{\text{buck,loc}}/\bar{A}$.

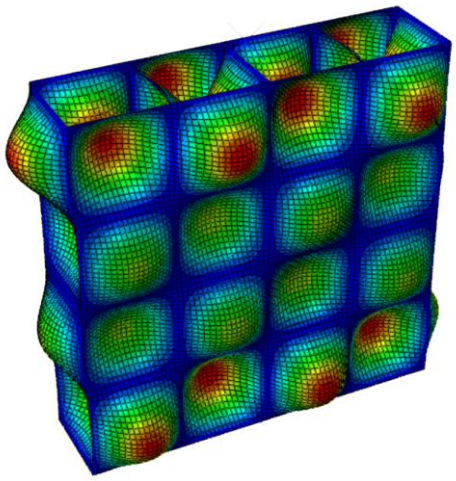

Figure 9: Visual representation of a typical local-buckling failure mode in a wall member as calculated by finite element analysis. Shown for section type A.

The member capacity of the wall was evaluated from first principles by treating it as a column under eccentric loading with potential for global buckling. In this treatment, the peak compressive stress $\sigma_{\max}$ along on the section can be expressed as:

$$\sigma_{\max} = P\left[\frac{1}{A} + \frac{ec}{I}\sec\left(\frac{\pi}{2}\sqrt{\frac{P}{P_{\text{buck,glob}}}}\right)\right] \quad (3)$$

where P is the applied axial load; e is the net eccentricity of the applied load (described later); A and I are the section's area and moment of inertia; c is the distance from the centreline to the extreme compressive fibre, equal to $(d+t_{in})/2$. The critical global buckling load of the wall, $P_{\text{buck,glob}}$, was obtained by Euler's formula:

$$P_{\text{buck,glob}} = \frac{\pi^2 EI}{L_e^2} \quad (4)$$

where L_e is the effective height of the wall being considered, taken as either the floor-to-floor or floor-to-roof height (indicated by H_w in Figure 9); and other properties as defined previously.

The wall's unfactored load capacity was evaluated by assigning $\sigma_{c,\max}$ [from Eq (2)] to $\sigma_{\max}$ in Eq (3) and solving for P. The limit-state design capacity was obtained by applying the capacity-reduction factor $\phi = 0.5$ as per AS3700 [45], such that:

$$\phi N_c = \phi P \ . \quad (5)$$

4.1.4 Modelling an idealised low-rise building

To examine the feasibility of using 3DP cob walls as loadbearing structural elements, the study considered an idealised 1- and 2-storey house. Schematic representations of the building's geometry are shown in Figure 10. In the case of a 1-storey house, the walls carry only the roof load, while in the 2-storey house they carry loads from the roof and suspended floor. In each

scenario, the total compressive force acting on the wall also incorporates self-weight calculated at the ground level.

The forces imparted to the wall by the roof and the floor depend on their respective dead load (self-weight plus superimposed permanent load), live load, and span. The roof and floor are treated as one-way-spanning, so the load that they apply to the wall can be calculated as the total pressure load multiplied by a tributary width (L_{trib}). The tributary width depends on the configuration of the wall within building. In the case of an external wall, it is equivalent to half the span of the floor/roof beam [LW(1) or (3) in Figure 10]. For an internal wall, it includes the sum of the contributions from each side [LW(2) in Figure 10]. Further, if the wall contains an opening, a simplistic treatment can be to scale the tributary width pro-rata depending on the proportion of solid wall to openings. For instance, if half of the wall is perforated by openings, then the tributary width becomes twice what it would be if the wall were solid.

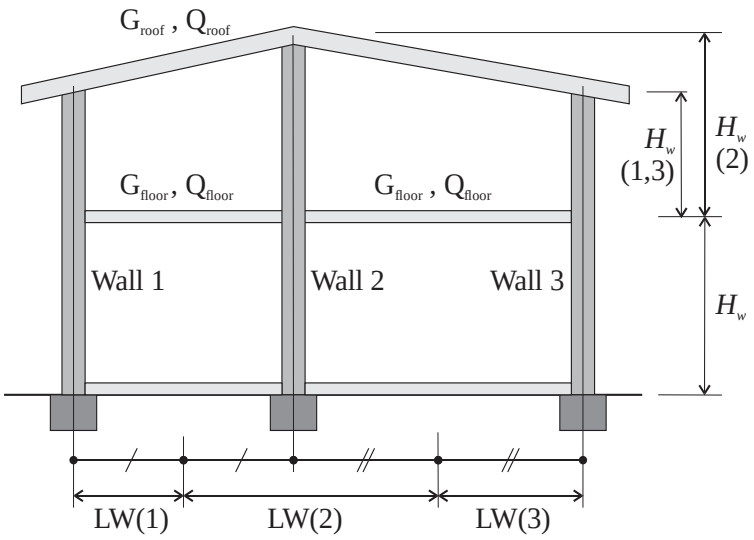

Figure 10: Overall building geometry, Two-storey (n_s = 2) double-bay building with internal and external walls, indicating the definition of wall height (H_w) and tributary width (denoted here as LW).

The gravity loads used in the analysis are representative of residential construction as prescribed by loading standards (e.g. [45]). The adopted unfactored loads are summarised in Table 4. The total dead load of the suspended floor is taken as 1.0 kPa, which allows for a timber joist plus timber deck floor (typically 0.5 kPa) in addition to a superimposed permanent load (0.5 kPa). The floor live load is taken as 1.5 kPa allowing for general residential occupancy. The dead load of the roof is taken as 0.9 kPa, making allowance for timber framing (rafters + purlins) with clay roof tiles. The live load on the roof is taken as 0.25 kPa.

The self-weight of the wall was calculated based on its section area, taking the weight density of the material as 18 kN/m^3. Thus, the total design compressive load was evaluated as:

$$N_c^* = \begin{cases} P_{\text{roof}}^* + P_{\text{wall}}^* & \dots 1 \text{ storey} \\ P_{\text{roof}}^* + P_{\text{floor}}^* + 2P_{\text{wall}}^* & \dots 2 \text{ storey} \end{cases} \quad (6)$$

where P^*_{roof} is the load applied by the roof, P^*_{floor} by the suspended floor, and P^*_{wall} is the self-weight of the wall over a single storey height H_w. Each P^* is taken at the ultimate limit state using the load combination $1.2G+1.5Q$ [45], with G being the dead load and Q the live load component.

Table 4: Summary of constant inputs used in the feasibility study. Explanations are provided in the text.

Property	**Value**
Cob material properties:	
Elastic modulus, E	22.9 MPa
Characteristic compressive strength, f_c' (See note 1)	0.62 MPa
Weight density, γ	18 kN/m^3
Poisson's ratio, ν	0.22
Unfactored loads:	
Roof dead load, G_{roof}	0.9 kPa
Roof live load, Q_{roof}	0.25 kPa
Floor dead load, G_{floor}	1.0 kPa
Floor live load, Q_{floor}	1.5 kPa
Limit-state design factors:	
Compressive strength capacity-reduction factor, ϕ	0.5
Ultimate limit-state design load combination	$1.2G + 1.5Q$
Eccentricities (e) of applied load (w.r.t. wall centreline): (See note 2)	
Load from roof	$0.1 \times D_{out}$
Load from floor	$0.25 \times D_{out}$
Self-weight of wall	$0.05 \times D_{out}$

Notes:

1. Determined from mean strength f_{cm} = 0.87 MPa by assuming lognormal distribution and CoV = 20%.
2. Where D_{out} is the full depth of the wall section measured between its outer edges (Figure 8).

4.1.5 Connection details and load eccentricity

It is important to consider that the floor and roof generally apply the load eccentrically with respect to the wall's centreline, and this generates an out-of-plane bending moment that can have a major influence on the wall's load-carrying capacity. The eccentricity of the applied load is controlled by the connection detail. While the development of the connection details

falls into the domain of detailed structural design and is outside the focus of this work, conceptual illustrations of the assumed connections are shown in Figure 11.

The connection between the roof and wall can be achieved by supporting the timber rafters using a timber bearing block, in turn resting on a spreader block that distributes the load onto the wall (Figure 11a). This detail is assumed to generate an eccentricity $e = 0.1\ D_{out}$, with D_{out} as defined in Figure 8. The assumed wall-to-floor connection involves partial penetration of the joists into the wall and are supported by a bearing block and spreader block (Figure 11b), which is assumed to produce an eccentricity of $0.25\ D_{out}$. It should be noted that a connection in which the floor is supported outside the extent of the wall is not advised, as it would generate an eccentricity > $0.5\ D_{out}$ and significantly diminish the loadbearing capacity. The aforementioned values of the assumed eccentricities are consistent with similar details for conventional clay brick masonry provided in AS3700 [46].

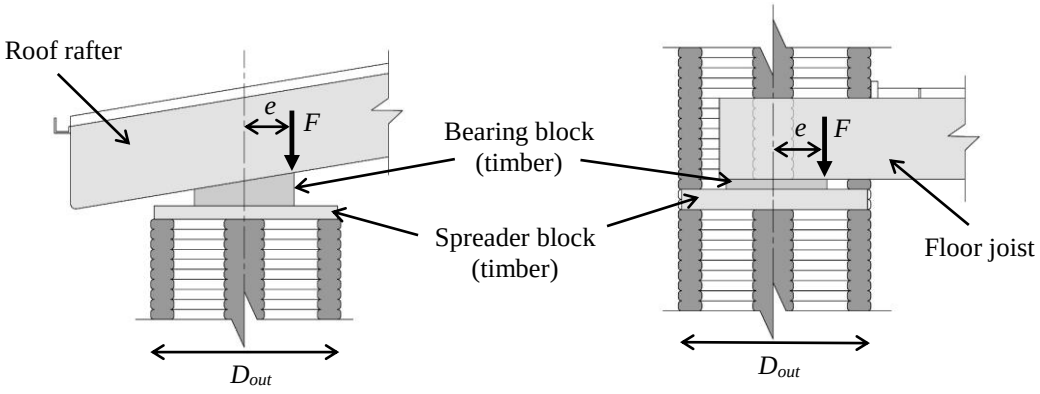

(a) Wall-to-roof connection (section view). *(b) Wall-to-floor connection (section view).*

Figure 11: Potential connection details and definition of eccentricities (e) of the applied load (F).

Additionally, for sake of conservatism the self-weight of the wall is assumed to act at an eccentricity of $0.05\ D_{out}$ to allow for any incidental geometric imperfection of the wall. The internal bending moment was calculated as the sum of each applied load P^* (i.e. P^*_{roof}, P^*_{floor}, P^*_{wall}) and its respective eccentricity, which dividing by the total compressive force N^*_c [from Eq. (6)] produces the net eccentricity:

$$e_{\text{net}} = \frac{\sum P_i^* e_i}{N_c^*} \tag{5}$$

The net eccentricity was used as the input value of e in Eq (3).

4.1.6 Optimisation of wall cross section geometry

The geometry of the 3D-printed sections in Figure 7 can be defined by two variables: the nominal wall depth (d) and average shell thickness (t). To characterise the most efficient section to fulfil a loadbearing function, an optimisation process was undertaken that minimises the material volume while ensuring that the load capacity remains sufficient to accommodate the

applied design load. As a metric of the structural adequacy, the limit-state design formula [Eq (1)] can be rearranged and expressed as the capacity utilisation (u), i.e. the ratio of the design load to the design capacity:

$$u = \frac{N_c^*(t,d)}{\phi N_c(t,d)} \tag{5}$$

where both the capacity and design load are functions of the optimisation variables d and t.

As a proxy for the material volume, we can adopt the area per unit length of the wall ($\bar{A}$), since the two are directly proportional. Therefore, the optimisation process to determine the optimal t and d can be expressed as:

Minimise $\bar{A}$, by varying t and d, subject to the constraints:

a. $u \leq 1$ (to ensure structural adequacy),
b. $t > 0, d > 0$ (positive values only),
c. $d \geq t$ (in valid sections the shell thickness must not exceed the effective depth).

To cater for varying architectural requirements on the building geometry, this optimisation was performed at different combinations of the wall height (H_w), tributary width (L_{trib}), and number of storeys (n_s). Constant inputs and their values are summarised in Table 4.

The optimisation problem was solved using two different methods in order to provide a means of cross-verifying the results and to examine alternate approaches to the representation of results. The first approach used a continuous optimiser in MATLAB, in which t and d can adopt any values along a continuous domain. The second approach used the evolutionary optimiser Galapagos in the Rhino-Grasshopper package [47] (Figure 12). The continuous-optimisation algorithm in MATLAB is the computationally faster of the two approaches; yet, implementing the optimisation in Grasshopper provides certain advantages, such as:

1) Direct link to the 3DP system (i.e. 3D printers and robotic arms), providing the ability to interface the design software with the printing tools.

2) Inclusive control over the design-to-fabrication framework, incorporating design of the geometry and other performance objectives such as thermal, lighting and environmental impacts.

3) The ability to provide visual representation of the modelling results in real time, including the building geometry and its aesthetics (Figure 13).

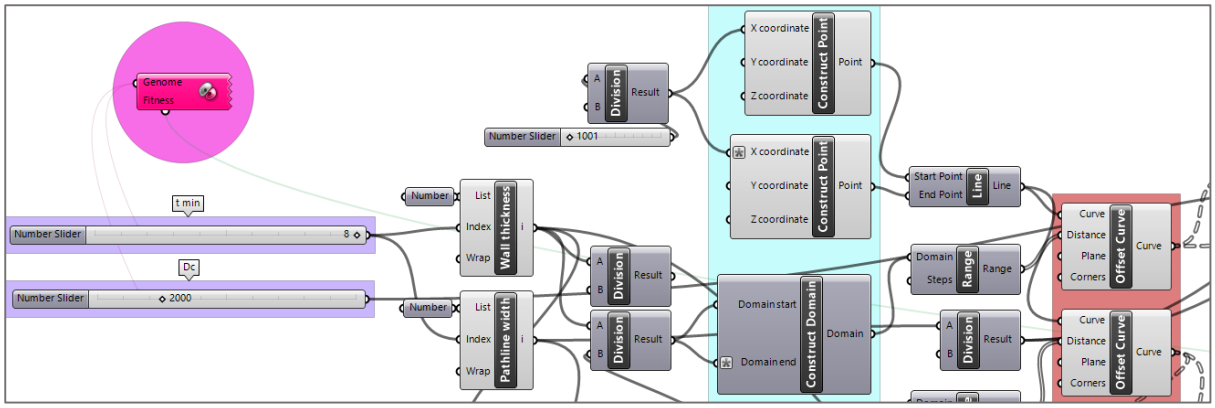

Figure 12: Part of the Grasshopper defintion for the optimisation of the wall models.

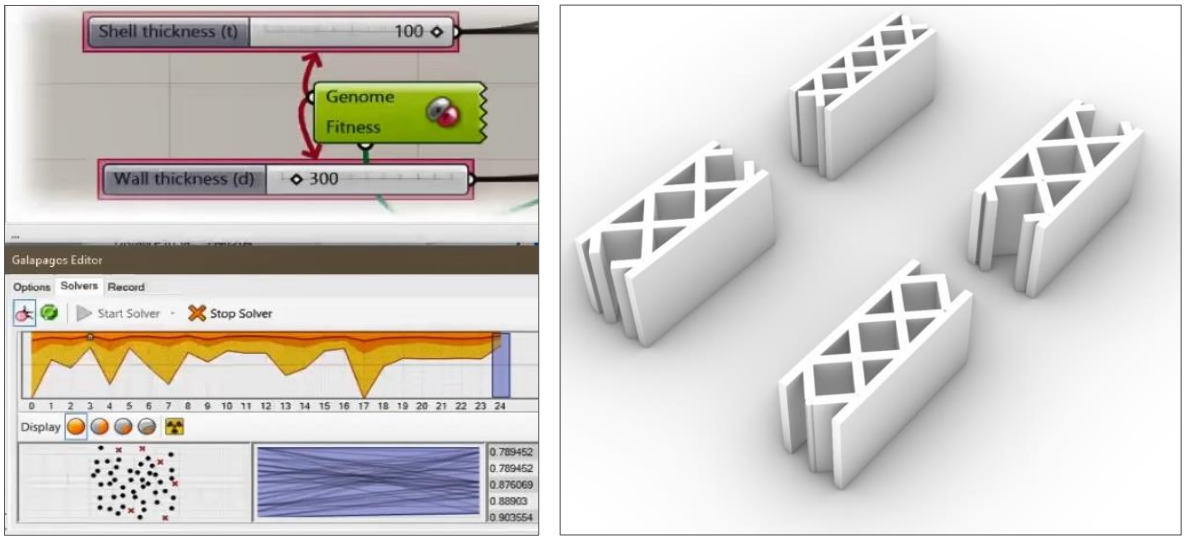

Figure 13: Visual representation of the optimisation process of Galapagos (left) and a sample of the visual generation of results for wall type C in Grasshopper (right).

4.2 Results and discussion

4.2.1 Single-scenario analysis

The typical relationship between structural adequacy versus the wall section geometry is illustrated in Figure 14, which plots contour lines of constant utilisation (u) as a function of shell thickness (t) and nominal wall depth (d). The graph corresponds to a single scenario where H_w = 2.5 m, L_{trib} = 3.5 m, and n_s = 2; however, the general trends are representative regardless of the selected values of these inputs. The thick black contour line corresponding to u=1 represents sections whose capacity exactly matches the design load. Thus, the grey-shaded area above u=1 encompasses sections that are structurally adequate. The red dashed line delineates the zones where the section is compact (governed by the material crushing) as opposed to slender (governed by local buckling), as per Eq (2). The black dashed lines bound the range of t values that correspond to available nozzle sizes in the 3DP system used in the present experimental study.

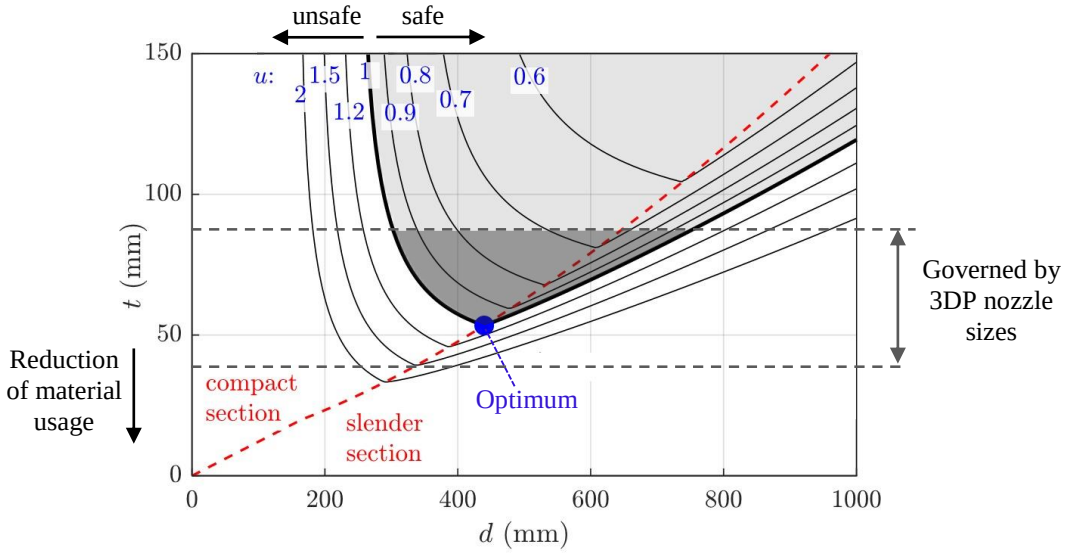

Figure 14: Typical utilisation-contour plot for varied shell thickness (t) and nominal wall depth (d). Shaded grey area indicates the zone where the wall's capacity is adequate for the design load. The dashed red line delineates compact sections (material stress failure) from slender sections (local-buckling failure). In this example: H_w = 2.5m, L_{trib} = 3.5m, n_s = 2.

For any of the printed patterns (A, B, C) the area-per-unit-length is approximately proportional to shell thickness (i.e. $t \propto \bar{A}$), thus allowing the shell thickness to be used as a proxy for material consumption. Therefore, in the graphical representation in Figure 14, the optimal section occurs at the trough of the u=1 contour line where t is minimised. Notably, the u contours follow different trajectories in the compact- and slender-section zones, and the optimal solution always occurs at the boundary that delineates them. In the compact-section zone, there is a roughly inverse relationship between t and d; this is because a section with a reduced depth requires a thicker shell to maintain the necessary section area and moment of inertia. In the slender-section zone the capacity is governed by local buckling of the shell, and hence increasing the section depth requires an increase to the shell thickness to maintain a constant capacity. The existence of an optimal section also demonstrates that hollow 3DP sections offer improved material efficiency compared to equivalent solid sections. These observations also highlight that in the practical range of interest, the design capacity of the wall is governed both by the material's compressive strength and elastic modulus, underscoring the importance of both these properties.

4.2.2 Design charts based on experimentally quantified material properties

The loadbearing capability of 3DP cob walls is examined in Figure 15 and Figure 16 by presenting model design charts for varied tributary width and wall height respectively. The figures plot the smallest required shell thickness (t) and accompanying wall thickness (d) of the optimised wall section that minimises material consumption. The constant inputs used to generate these figures are summarised in Table 4 and include the material properties established in Section 3. Figure 15 maintains a constant wall height of 3.0 m while varying the tributary width up to a maximum of 6 m. Conversely, Figure 16 maintains a constant tributary width at

4.0 m while varying the wall height between 2.5 to 3.5 m. These ranges of dimensions were selected to reflect the practical bounds of interest in a typical residential building. Each figure considers separately the alternate printed patterns (A, B, C) in either a 1- or 2-storey building. The relative efficiency of the alternate sections is presented in Figure 17 and Figure 18 by plotting the section area per unit length (a proxy for the material consumption).

Overall, the plots demonstrate that, on the assumption of the mechanical properties matching those established in the accompanying tests, loadbearing structural function in typical residential construction can be accomplished using wall section sizes that are reasonable and within the capability of the 3D printer system. The indicative range of shell thickness and wall thickness is summarised in Table 5. It is seen that in a single-storey house the section size can be kept small (t = 25–40 mm, d = 250–400 mm) relative to a 2-storey house (t = 35–120 mm, d = 320–800 mm).

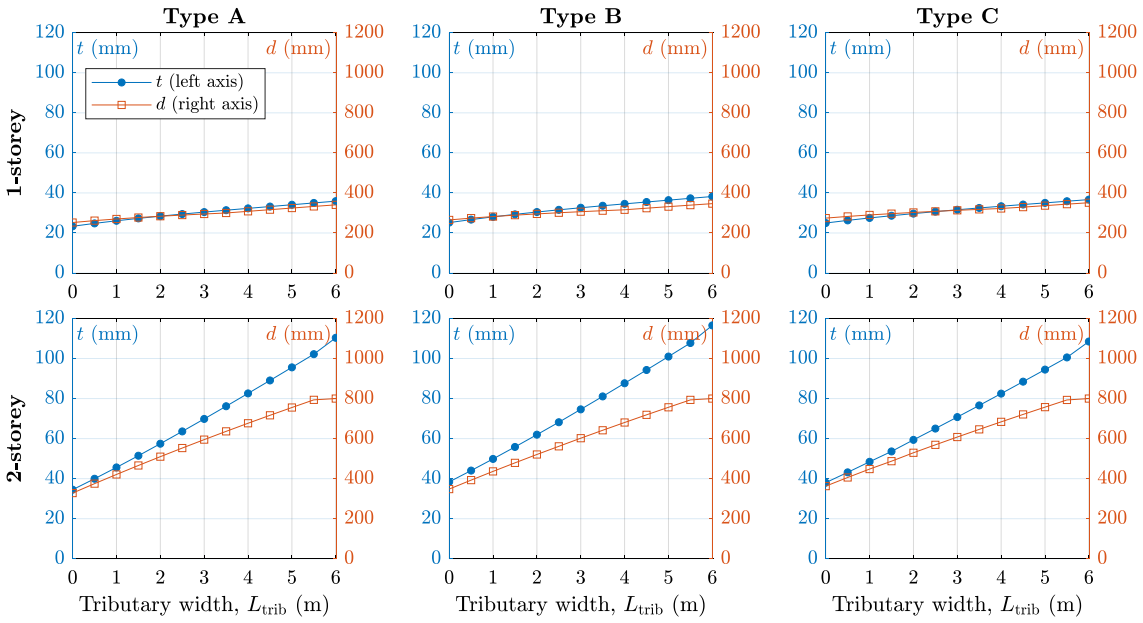

Figure 15: Dimensions t and d of optimised sections for varied tributary width (constant wall height of 3 m). All inputs including material properties are as per Table 4. Considers section types A, B, C, and either a 1- or 2-storey building. Each plot shows t on the left y-axis and d on the right y-axis.

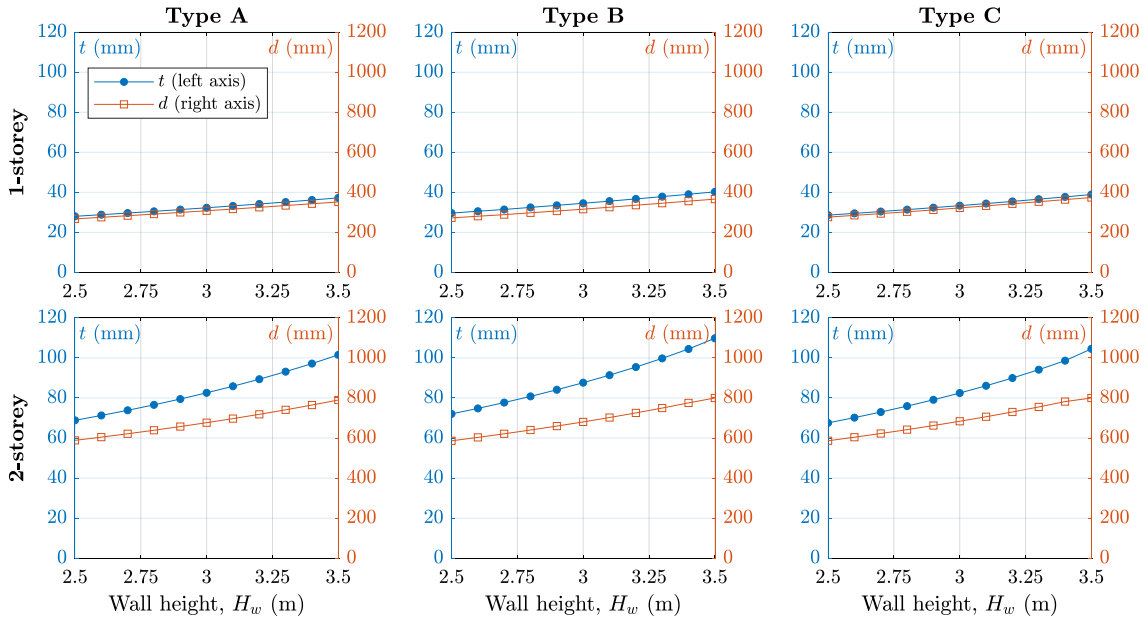

Figure 16: Dimensions t and d of optimised sections for varied wall height (constant tributary width of 4 m). All inputs including material properties are as per Table 4. Considers section types A, B, C, and either a 1- or 2-storey building. Each plot shows t on the left y-axis and d on the right y-axis.

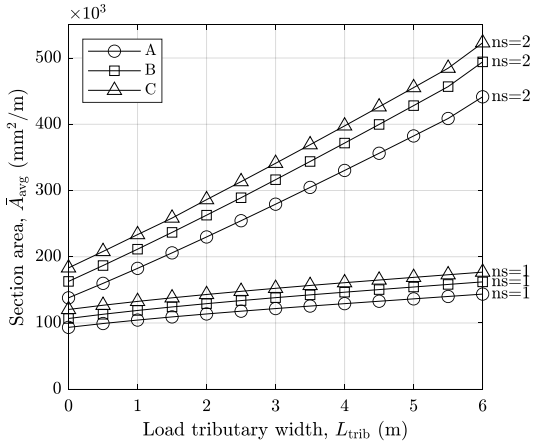

Figure 17: Section area per unit length for the optimised sections in Figure 15.

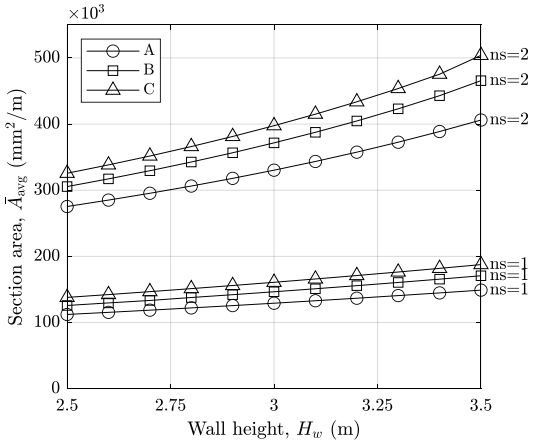

Figure 18: Section area per unit length for the optimised sections in Figure 16.

Table 5: The range of the section-defining parameters *t* and *d* corresponding to the design charts in Figure 15 and Figure 16.

	1 storey		2 stories	
	Min (mm)	Max (mm)	Min (mm)	Max (mm)
Shell thickness (*t*)	25	40	35	115
Wall thickness (*d*)	250	400	320	800

Note that in scenarios where a small section geometry may be permitted by structural considerations alone, the actual section could in practicality be dictated by other factors such as architectural requirements, aesthetics, thermal performance, standardisation of the construction process, and the capability of the 3D-printing system. For instance, a previous study by Gomaa et al. [21] found that 3D printing of large-scale cob walls requires a nozzle size of at least 40 mm, which can be used to generate an 'average' shell thickness (t) between 50–80 mm. Smaller nozzle diameters can slow down the printing process and also cause clogging of the extrusion system. On the other hand, using larger nozzles leads to reduced control over material consumption and accuracy.

The plots in Figure 17 and Figure 18 indicate that based solely on their structural performance, of the three section types, A is the most efficient, followed by B and then C. However, on any project it may also be necessary to consider other factors that may be impacted by the type of wall section. For example, from an architectural perspective, the notion of efficiency also includes considerations such as the design function, thermal performance, and environmental impacts. For instance, the thermal performance efficiency of 3DP cob was explored thoroughly in a recent study by Gomaa et al. [22], which demonstrated that the voids present in 3DP wall patterns dramatically improve thermal efficiency compared to solid cob walls. This means that the relative thermal performance of the alternate wall sections A, B or C may not necessarily match their relative structural performance. Hence, it is recommended that selecting the wall section type should be undertaken using a holistic approach that considers their structural, thermal, and environmental efficiency.

4.2.3 Parametric study into the influence of the material properties

As demonstrated by the review of experimental studies (Table 1), the mechanical properties of cob can exhibit drastic variation depending on the mix composition. To account for the limited number of material tests in the current study, a parametric study was undertaken to examine the sensitivity of the feasibility study findings on the quality of the material. To this end, the mean compressive strength (f_{cm}) and elastic modulus (E) were varied so as to cover a realistic range of the respective properties as identified through the review of past testing (Table 1).

Three scenarios were considered (Note: Symbol '*' refers to the value being representative of the accompanying tests in Section 3):

1. Varied f_{cm} = 0.6/0.9*/1.35 MPa, at constant E = 23* MPa,
2. Varied E = 20*/40/80 MPa, at constant f_{cm} = 0.87* MPa,
3. E and f_{cm} both varied in equal proportion: [f_{cm}, E] = [0.4,20*], [0.8*,40], and [1.6,80] MPa.

The purpose of the first two scenarios was to gain insight into the parametric influence of the respective properties by varying them in isolation, while the third was meant to represent variation of the overall quality of the material by changing both properties simultaneously.

The study considers wall pattern type C and varies the tributary width while keeping H_w = 3 m. Aside from f_c and E, the remaining inputs listed in Table 4 remain unchanged. The results are presented in Figures 19–24 respectively.

- Scenario 1

The first scenario (Figures 19 and 20) looks at variation of compressive strength between 0.6/0.9/1.35 MPa while maintaining E as per the current tests (23 MPa). Note that the intermediate strength level (0.9 MPa) is similar to the result of the current tests. It is observed that in the 1-storey case, the required cross section is relatively insensitive over the three levels of strength. In the 2-storey case however, the reduced strength (0.6 MPa) requires a cross section that becomes excessively large for any tributary width exceeding 1m, thus making the walls effectively incapable of performing a loadbearing function. Conversely, the improved strength (1.35 MPa) allows for a smaller section to be used, saving up to 30% in material volume.

- Scenario 2

The second scenario (Figures 21 and 22) looks at variation of the elastic modulus at levels of 20/40/80 MPa while maintaining f_{cm} as per the current tests (0.87 MPa). The lowest E value (i.e. 20 MPa) is comparable to the material of the current tests. For both the 1- and 2-storey cases, a higher elastic modulus leads to a reduction in the necessary cross section size. The improvement in increasing E from 20 to 80 MPa results in a material saving between 10–50%. It is also interesting to note that a higher elastic modulus results in an optimal cross section that has an increased wall thickness (d) while having a lower shell thickness (t); this can be explained by improved resistance to local buckling.

- Scenario 3

The last scenario (Figures 23 and 24) examines the effect of proportionally increasing both f_{cm} and E, which can be considered analogous to an overall variation in the quality of the material, i.e. low (0.4/40MPa), intermediate (0.8/40MPa) and high (1.6/80MPa) quality. The graphs indicate a strong dependence between the loadbearing capacity (i.e. required section size) and the input material properties in both the 1- and 2-storey cases. While not being directly comparable to the previous two scenarios because of different input values, a general comparison indicates that the most efficient improvement in overall loadbearing performance is achieved by simultaneously enhancing both f_{cm} and E, rather than by increasing either of these properties alone.

Overall, the sensitivity study indicates that the feasibility of cob walls to act as loadbearing is conditional on a minimum required level of material performance. The 3DP cob tested in this study meets this threshold, but it is evident that a reduced compressive strength (< 0.75 MPa) may not be sufficient for loadbearing walls in a 2-storey house. On the other hand, even weak cob (≈ 0.4 MPa) may still be sufficient to construct loadbearing walls in a single-storey house.

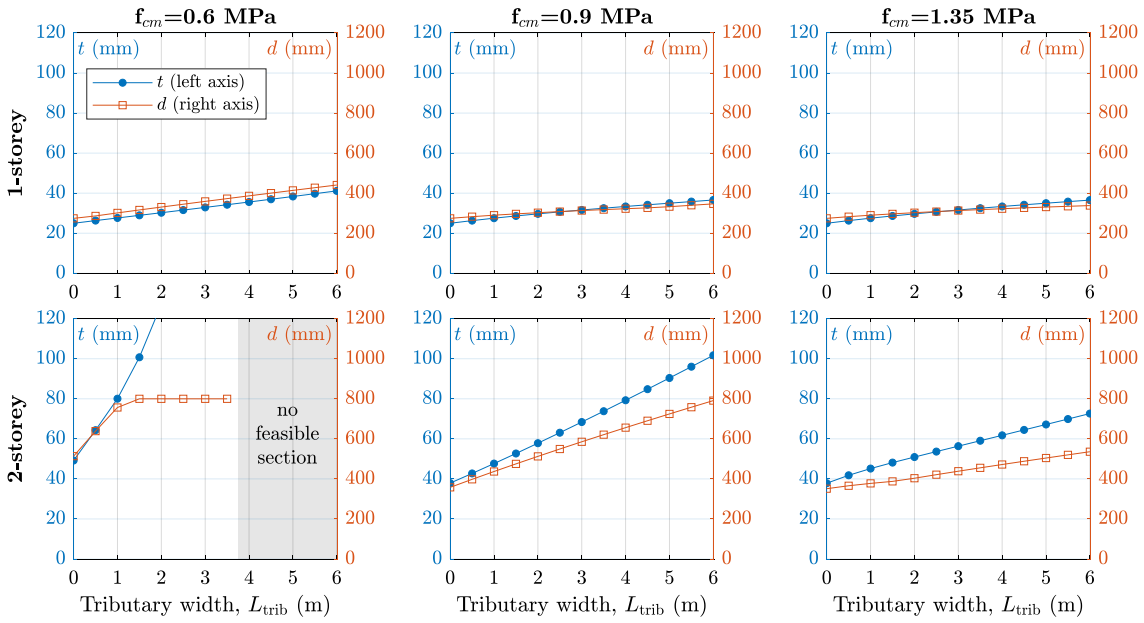

Figure 19: Dimensions t and d of optimised sections for varied compressive strength (constant E).

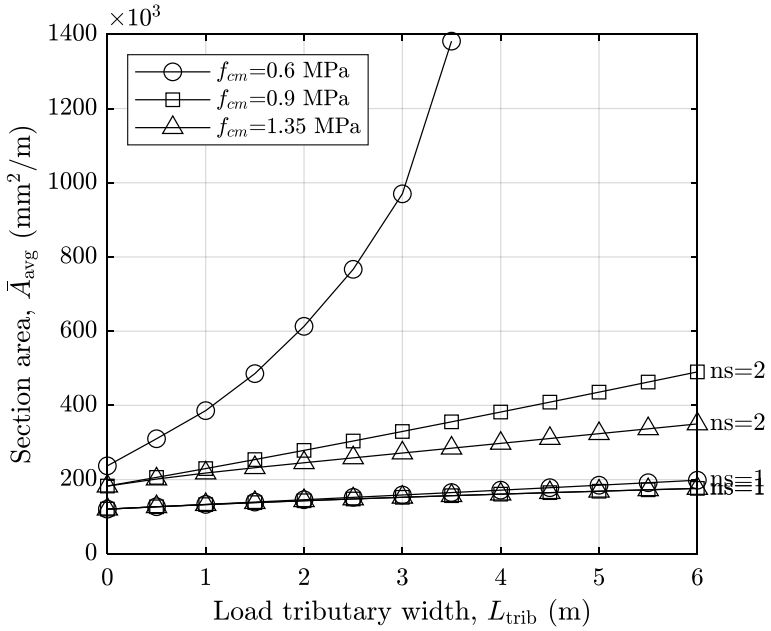

Figure 20: Material consumption of the optimised sections plotted in Figure 19.

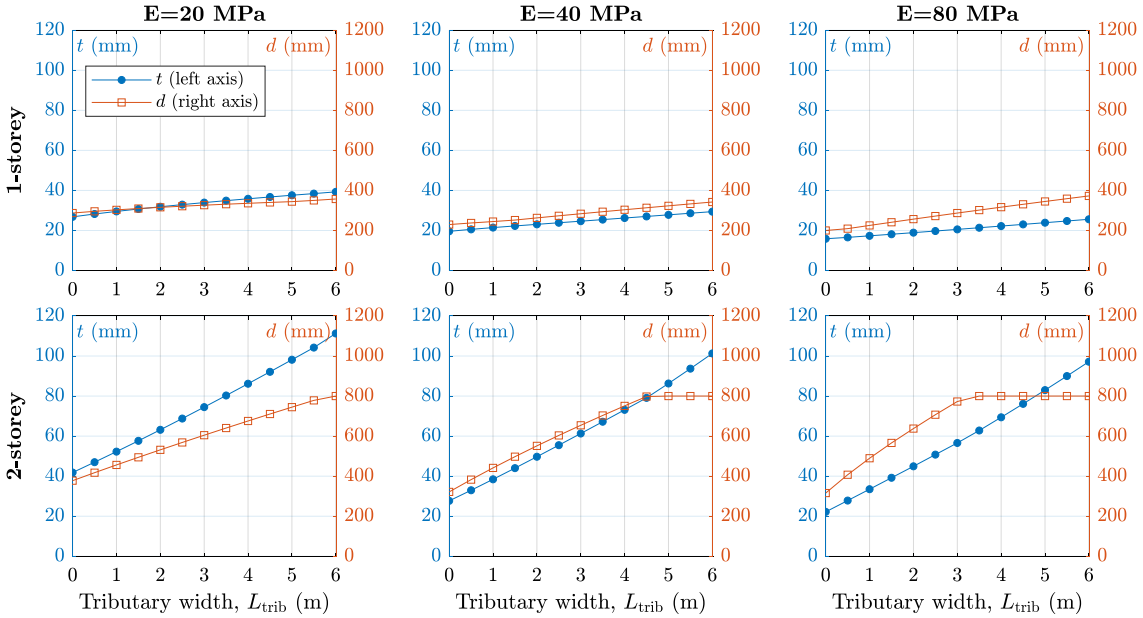

Figure 21: Dimensions t and d of optimised sections for varied elastic modulus (constant f_{cm}).

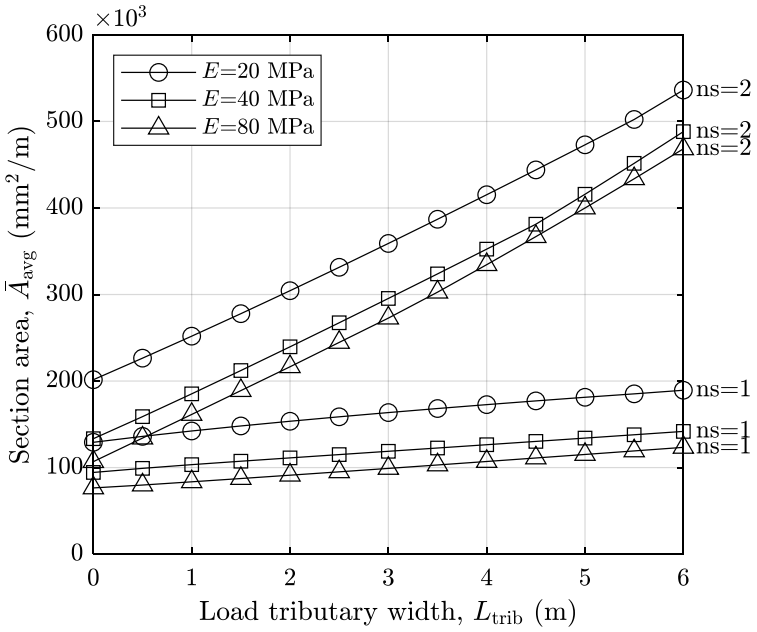

Figure 22: Material consumption of the optimised sections plotted in Figure 21.

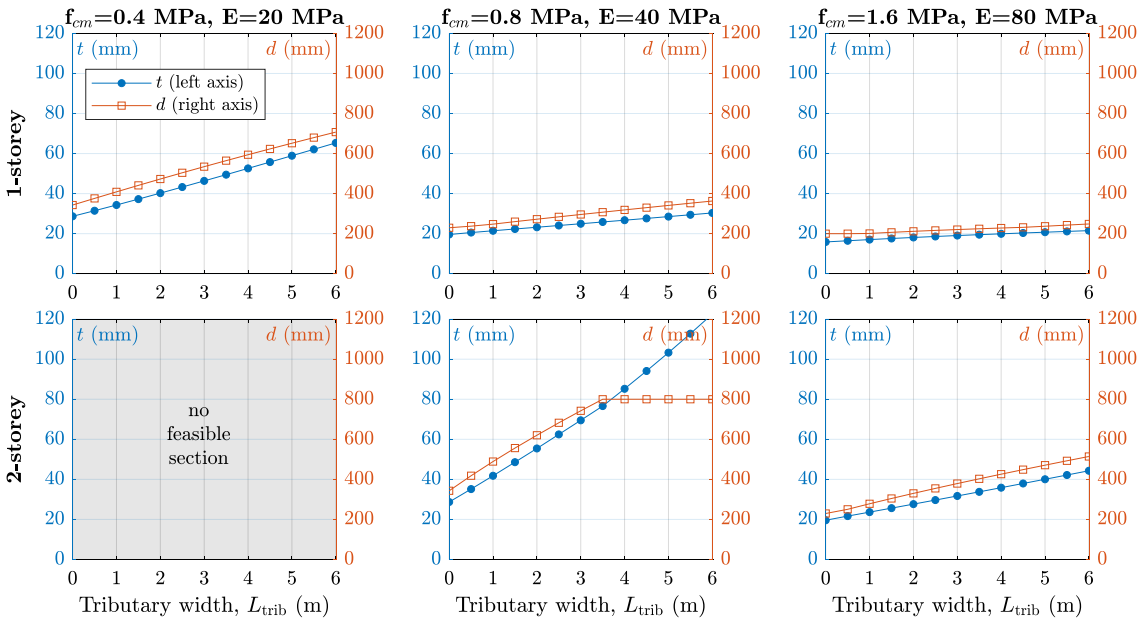

Figure 23: Dimensions t and d of optimised sections for varied f_{cm} and E, with ratio f_{cm}/E held fixed.

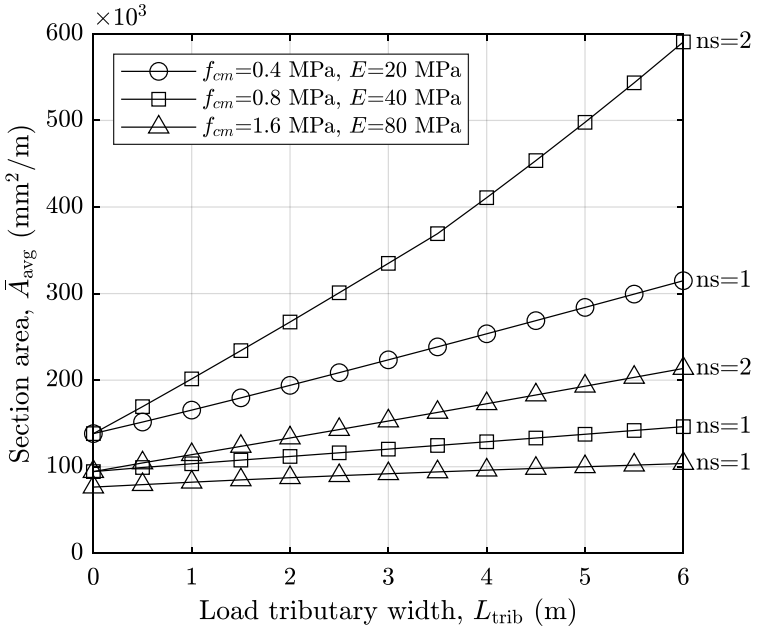

Figure 24: Material consumption of the optimised sections plotted in Figure 23.

5 Case study of a small 3DP cob house

As explained previously, the approach to leveraging the wall sizing charts (e.g. Figure 15) depends both on structural and architectural design considerations. To demonstrate the essential design process, a case study involving a small house will now be presented. The process starts with a floor plan defining the zoning and dimensions of the spaces (Figure 25). For illustrative purposes, the hypothetical house incorporates four spaces with different sizes and opening configurations, representing typical design requirements. The dimensions of the spaces range from 2m to 4 m, wall heights are set at 3m, and the number of storeys is taken as either 1 or 2. The roof (in the 1 and 2-storey cases) and the suspended floor (in the 2-storey case) are treated as one-way spanning in the directions indicated on Figure 25.

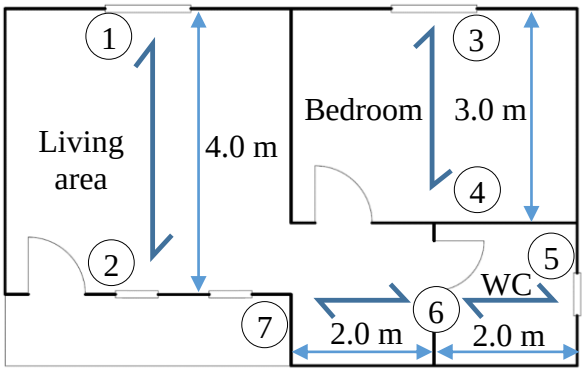

Figure 25: Basic floor plan of the idealised 3DP cob house. Half-headed arrows indicate the span direction of the suspended floor and roof. Loadbearing walls are numbered from 1 to 7.

The design parameters and final sizing of each wall are summarised in Tables 6 and 7 for the single and double storey alternatives respectively. The procedure to determine the minimum section sizes is as follows:

1. Establish which walls are loadbearing by considering the span direction of the floor/roof. In this example, walls 1–7 are loadbearing (Figure 25).
2. The 'basic' tributary width of each loadbearing wall is determined by considering whether the wall is internal or external and the effective span of the floor/roof being supported, using gross dimensions (refer to Figure 10).
3. If the wall has an opening, the basic tributary width is upscaled in relation to the ratio of the openings (as described in Section 4.1.4). For instance, a wall containing 50% openings (in plan view) carries an effective tributary width equal to double the basic tributary width. Note that for simplicity, the effective tributary widths in Tables 6 and 7 are rounded-up to the nearest 1m.
4. Non-loadbearing walls are analogous to having a zero effective tributary width.
5. The effective tributary width is then used to select *t* and *d* from the relevant design chart (Figure 15).

Note that the nominated section sizes in Tables 6 and 7 assume the material properties quantified in the accompanying material tests (i.e. using Figure 15). Also note that consideration is given here only to gravity loads and not to out-of-plane loads due to wind or earthquake, which are region-specific and outside the scope of the current paper.

Figure 26 illustrates the floor plan by assigning the minimum section sizes to each wall. Since the minimum required section size can be different for each wall, the designer has the choice of standardising the sizes as needed to suit the other project requirements (e.g. thermal and architectural) which may also serve to reduce the complexity of the design and improve the efficiency of the construction process.

Table 6: Design of loadbearing (1–7) and non-loadbearing (NLB) walls in the 1-storey example house.

Wall	Basic L_{trib} (m)	Opening ratio (%)	Tributary scale factor	Effective L_{trib} (m)	Corresponding t and d (mm)					
					Type A		Type B		Type C	
					t	d	t	d	t	d
1	2	25	1.5	3	30	300	35	310	35	320
2	2	50	2.0	4	**35**	**310**	**35**	**320**	**35**	**330**
3	1.5	30	1.6	3	30	300	35	310	35	320
4	1.5	15	1.3	2	30	290	35	300	35	310
5	1	5	1.1	1	**30**	**280**	**30**	**290**	**30**	**300**
6	2	30	1.6	3	30	300	35	310	35	320
7	1	40	1.8	2	30	290	35	300	35	310
NLB	0	0	n/a	0	25	320	25	350	25	380

Table 7: Design of loadbearing (1–7) and non-loadbearing (NLB) walls in the 2-storey example house.

Wall	Basic L_{trib} (m)	Opening ratio (%)	Tributary scale factor	Effective L_{trib} (m)	Corresponding t and d (mm)					
					Type A		Type B		Type C	
					t	d	t	d	t	d
1	2	25	1.5	3	70	600	75	600	70	600
2	2	50	2.0	4	**80**	**700**	**85**	**640**	**80**	**700**
3	1.5	30	1.6	3	70	600	75	600	70	600
4	1.5	15	1.3	2	60	500	60	520	60	520
5	1	5	1.1	1	**45**	**420**	**50**	**420**	**50**	**420**
6	2	30	1.6	3	70	600	75	600	70	600
7	1	40	1.8	2	60	500	60	520	60	520
NLB	0	0	n/a	0	35	350	40	370	40	390

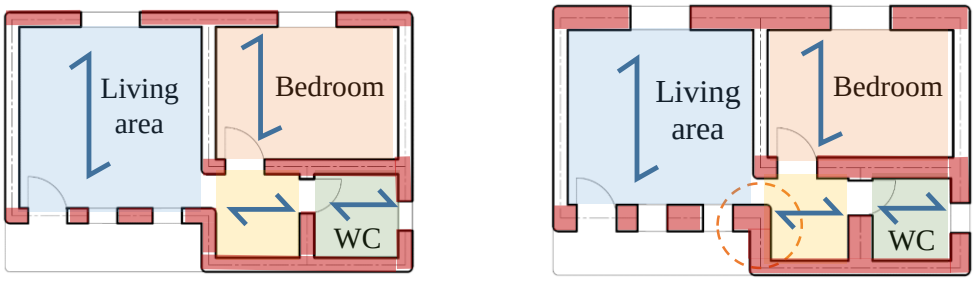

(a) Single-storey house *(b) Double-storey house*

Figure 26: Floor plan showing the minimum required wall sizes walls to scale. (Shown for pattern type A for illustrative purposes)

From Table 6 and Figure 26a, it can be seen that in the case of 1-storey house, the required sections are relatively consistent across all of the walls present (in terms of *t* and *d*), regardless of the chosen pattern (A, B, C). For example, if we consider pattern A, the required *t* varies between 30–35 mm, and *d* between 280–310 mm. The consistency in wall sizes in the case of a 1-storey building results from the required cross section being relatively insensitive to the tributary width, as reflected by Figure 15. For construction simplicity, the designer may therefore choose to standardise the wall sizes by assigning the largest required section to every wall.

In contrast to the 1-storey house, in the case of the 2-storey house the required section sizes (Table 7) vary substantially between the walls present (e.g. for type A: t = 45–80 mm, d = 420–700 mm). The resulting floor plan (Figure 26b) visually illustrates the difference in the wall thickness demands, especially between loadbearing and non-loadbearing walls. Therefore, in the case of the 2-storey building, the designer may opt for a suitable compromise between standardising the wall section sizes and economical material usage, for instance by adopting two or three different sizes across the building. Large wall thickness can also negatively impact the architectural functionality of the spaces, where, as highlighted in this example by the dotted circle in Figure 26b, the aisle linking the living area with the bedroom becomes severely narrowed due to the large thickness of the walls on both sides. Such considerations may require an iterative re-adjustment of the floor plan until both the structural and architectural requirements are satisfied.

An alternate way that the designer can balance the structural and architectural requirements in relation to wall section sizes is by dictating the gravity load path by controlling: 1) the span directivity of the floor/roof system being carried by the walls, 2) which cob walls act as loadbearing, and 3) which internal walls can be formed using lightweight partitions. To demonstrate this, Figure 27 illustrates three alternatives that maintain the same space layout as the original arrangement (Figure 25) but are reconfigured by altering the floor (or roof) spans and by implementing internal partitions to affect which walls are loadbearing.

Arrangement (a) is similar to the original configuration but rotates the floor span in south-east zone, thus allowing cob wall no. 6 (see Figure 25) to be replaced by a lightweight partition and also to reduce the size of wall no. 7. By removing some of the internal cob walls, configuration (a) arguably reduces the overall 3DP construction complexity compared to the original layout.

It does however increase the load demand on internal wall no. 4, therefore enlarging its section, and potentially hindering the functionality of the smaller rooms (i.e. toilets and lobby).

The presence of the internal cob wall (no. 4) in the original arrangement and configuration (a) also limits the freedom for future architectural changes to the internal space layout. Configurations (b) and (c) address this by replacing the internal walls in the east side of the house with lightweight partitions, thus improving the versatility for future layout alternations, but at the cost of requiring larger external walls because of a longer floor span in the east half out the house [compared to (a)].

Comparing configurations (b) and (c), a possible downside of (b) is that the central wall requires a large section since it acts as an internal loadbearing wall. By altering the direction of the floor span in the east half of the house, configuration (c) approximately halves the load on the central wall, but it does so at the cost of making the north and south outer walls loadbearing. Overall this would act to make the required wall sizes in option (c) more uniform across the house than in option (b), thus making (c) the potentially preferable option from a constructability point-of-view.

Overall, this example demonstrates that the process of selecting of the structural configuration is and exercise that involves compromise between a number of factors, including

- the dimensions and functionality of the spaces and location of openings,
- constructability and economical use of material,
- allowance for future alterations to the internal layout, and
- other factors not considered here, such as thermal insulation performance.

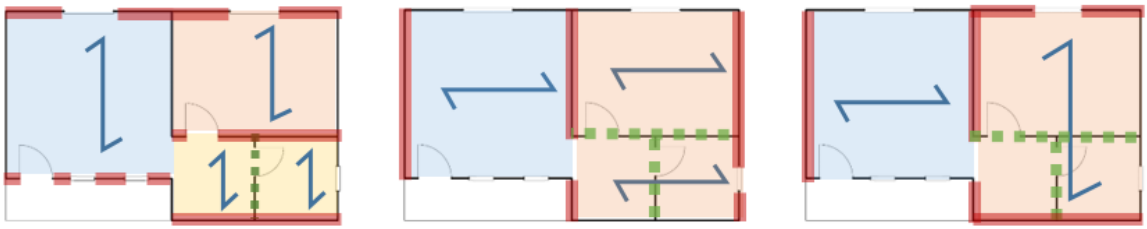

(a) *(b)* *(c)*

Figure 27. Examples of alternative arrangements of the floor/roof span directivity in the example small 3DP cob house. The loadbearing walls in each instance are highlighted in red. The lightweight partitions are highlighted in green dotted lines.

6 Conclusion

The increased uptake of 3DP technologies in construction, accompanied by a movement toward environmentally efficient materials has led to leveraging earthen materials in a contemporary 3DP process. 3DP cob has been a subject of investigation for several years now; however, while those investigations have focused mostly on the architectural aspects and environmental performance, investigation into the material's feasibility to be used for load-carrying building elements has not yet been undertaken sufficiently.

This study has conducted a comprehensive feasibility investigation into the structural capacity of 3DP cob walls under gravity loads. This was accomplished by first quantifying the basic mechanical properties of 3DP cob using a standardised compression test. The tests demonstrated that 3DP cob appears to exhibit similar mechanical performance to conventional cob in terms of compressive strength and elastic modulus. The expected load-carrying capacity of 3DP walls was then predicted using established structural mechanics concepts and limit-state design principles. These predictions demonstrate that 3DP cob walls are expected to have sufficient capacity to act as loadbearing in residential buildings up to two storeys.

The feasibility study also demonstrated the following:

- Due to the favourable geometric properties of printable hollow sections, 3DP cob walls can perform a loadbearing function with more efficient material usage compared to traditional (non-3DP) solid cob walls.
- The model design approach demonstrated in this paper provides a means for integrating the structural design process of 3DP cob into the design-to-construction framework. The generated design guidelines can be directly implemented to a Rhino-Grasshopper definition that enables visual modelling and direct interfacing with the 3D-printing system.
- The range of wall section sizes (as informed by the analysis) required for loadbearing functionality in buildings up to 2-storeys can be efficiently fabricated using available 3DP technologies and extrusion systems.

The findings of this study complete a broader feasibility investigation of 3DP cob for modern construction which combines structural performance with three other aspects: 1) constructability and fabrication process, 2) thermal performance, and 3) life cycle assessment. The results lead to the conclusion that 3DP cob construction emerges as a strong competitor to conventional and 3DP concrete construction. 3DP cob can substitute concrete-based construction in small to medium size low-rise residential projects, especially as it provides higher environmental efficiency and rationalised energy use. It can also provide novel design opportunities in addition to higher precision compared to manually constructed cob, especially for producing complex geometries. Moreover, 3DP cob construction can provide quick sheltering solutions with low cost and efficient use of local materials in expeditionary and hostile environments.

It is however important to highlight that while the current study provides promising and necessary first insight into the structural feasibility of 3DP cob walls, the findings are based on structural analysis with input from small-scale material tests. Therefore, proof-of-concept structural testing on full printed wall sections is envisaged as a crucial next step of this research.

Furthermore, while the outcomes of this study are positive overall, the accompanying sensitivity study undertaken demonstrates that the quality of the material in terms of its mechanical properties (compression strength and elastic modulus) is highly influential on the resulting loadbearing capability of the walls. Therefore, further research into the development of 3DP-suitable cob mixtures with a focus on ensuring consistently high-quality mechanical performance could yield significant additional benefit to this form of construction. Accompanying focus into other material performance aspects, in particular shrinkage and creep, is also required.

Acknowledgements

We would like to acknowledge Dr Alejandro Veliz Reyes for his valuable collaboration and support (University of Plymouth). We also extend our gratitude to Aikaterini Chatzivasileiadi and Anas Lila (Cardiff University) for their invaluable help.

Funding Resources

This work was supported financially by the Engineering and Physical Sciences Research Council (EPSRC) and The University of Nottingham under the Network Plus: Industrial Systems in the Digital Age, Grant number: EP/P001246/1. This work is also partially supported by the University of Adelaide through the Research Abroad Scholarship scheme.

References

[1] P. Feng, X. Meng, J.-F. Chen, and L. Ye, "Mechanical properties of structures 3D printed with cementitious powders," *Constr. Build. Mater.*, vol. 93, pp. 486–497, 2015, doi: 10.1016/j.conbuildmat.2015.05.132.

[2] A. Kazemian, X. Yuan, E. Cochran, and B. Khoshnevis, "Cementitious materials for construction-scale 3D printing: Laboratory testing of fresh printing mixture," *Constr. Build. Mater.*, vol. 145, pp. 639–647, 2017, doi: 10.1016/j.conbuildmat.2017.04.015.

[3] B. Zareiyan and B. Khoshnevis, "Interlayer adhesion and strength of structures in Contour Crafting - Effects of aggregate size, extrusion rate, and layer thickness," *Autom. Constr.*, vol. 81, pp. 112–121, 2017, doi: 10.1016/j.autcon.2017.06.013.

[4] B. Khoshnevis, "Automated construction by contour crafting — related robotics and information technologies," vol. 13, pp. 5–19, 2004, doi: 10.1016/j.autcon.2003.08.012.

[5] T. T. Le, S. A. Austin, S. Lim, R. A. Buswell, A. G. F. Gibb, and T. Thorpe, "Mix design and fresh properties for high-performance printing concrete," *Mater. Struct. Constr.*, vol. 45, pp. 1221–1232, 2012, doi: 10.1617/s11527-012-9828-z.

[6] A. Perrot, D. Rangeard, and A. Pierre, "Structural built-up of cement-based materials used for 3D- printing extrusion techniques," *Mater. Struct.*, vol. 49, pp. 1213–1220, 2016, doi: 10.1617/s11527-015-0571-0.

[7] L. Wang, H. Jiang, Z. Li, and G. Ma, "Mechanical behaviors of 3D printed lightweight concrete structure with hollow section," *Arch. Civ. Mech. Eng.*, vol. 20, pp. 1–17, Mar. 2020, doi: 10.1007/s43452-020-00017-1.

[8] H. Alhumayani, M. Gomaa, V. Soebarto, and W. Jabi, "Environmental Assessment of large-Scale 3D Printing in Construction: A Comparative Study between Cob and Concrete," *J. Clean. Prod.*, vol. 270, pp. 122463, Jun. 2020, doi: 10.1016/j.jclepro.2020.122463.

[9] CyBe, "3D Studio 2030 — CyBe Construction," 2019. https://cybe.eu/case/3d-studio-2030/ (accessed Nov. 20, 2019).

[10] C. Shrubsole *et al.*, "Bridging the gap: The need for a systems thinking approach in understanding and addressing energy and environmental performance in buildings," *Indoor Built Environ.*, vol. 28, pp. 100–117, 2019, doi: 10.1177/1420326X17753513.

[11] S. Ford and M. Despeisse, "Additive manufacturing and sustainability: an exploratory study of the advantages and challenges," *J. Clean. Prod.*, vol. 137, pp. 1573–1587, 2016, doi: 10.1016/j.jclepro.2016.04.150.

[12] E. Hamard, B. Cazacliu, A. Razakamanantsoa, and J. C. Morel, "Cob, a vernacular earth construction process in the context of modern sustainable building," *Build. Environ.*, vol. 106, pp. 103–119, 2016, doi: 10.1016/j.buildenv.2016.06.009.

[13] E. Quagliarini, A. Stazi, E. Pasqualini, and E. Fratalocchi, “Cob construction in Italy: Some lessons from the past,” *Sustainability*, vol. 2, pp. 3291–3308, 2010, doi: 10.3390/su2103291.
[14] T. Morton, F. Stevenson, B. Taylor, and N. C. Smith, “Low Cost Earth Brick Construction: Monitoring & Evaluation,” Fife, UK, 2005. [Online]. Available: http://www.arc-architects.com/downloads/Low-Cost-Earth-Masonry-Monitoring-Evaluation-Report-2005.pdf.
[15] L. Ben-Alon, V. Loftness, K. A. Harries, and E. Cochran Hameen, “Integrating Earthen Building Materials and Methods into Mainstream Construction Using Environmental Performance Assessment and Building Policy,” *IOP Conf. Ser. Earth Environ. Sci.*, vol. 323, pp. 012139, 2019, doi: 10.1088/1755-1315/323/1/012139.
[16] O. O. Akinkurolere, C. Jiang, A. T. Oyediran, O. I. Dele-Salawu, and A. K. Elensinnla, “Engineering properties of Cob as a building material,” *Journal of Applied Sciences*, vol. 6, pp. 1882–1885, 2006, doi: 10.3923/jas.2006.1882.1885.
[17] J. Fordice and L. Ben-Alon, “A research project dedicated to making cob legally accessible to the public,” 2017.
[18] E. Kianfar and V. Toufigh, “Reliability analysis of rammed earth structures,” *Constr. Build. Mater.*, vol. 127, pp. 884–895, 2016, doi: 10.1016/j.conbuildmat.2016.10.052.
[19] A. Veliz Reyes, W. Jabi, M. Gomaa, A. Chatzivasileiadi, L. Ahmad, and N. M. Wardhana, “Negotiated matter: a robotic exploration of craft-driven innovation,” *Archit. Sci. Rev.*, vol. 62, pp. 1–11, 2019, doi: 10.1080/00038628.2019.1651688.
[20] 3D-WASP, “3D Printers | WASP | Leading Company in the 3d printing industry,” 2020. https://www.3dwaspp.com/en/ (accessed Jan. 10, 2020).
[21] M. Gomaa, W. Jabi, A. Veliz Reyes, and V. Soebarto, “3D Printing System for Earth-based construction: Case Study of Cob Walls,” *Autom. Constr.*, vol. 124, pp. 103577, 2021, doi: https://doi.org/10.1016/j.autcon.2021.103577.
[22] M. Gomaa, J. Carfrae, S. Goodhew, W. Jabi, and A. Veliz Reyez, “Thermal performance exploration of 3D printed cob,” *Archit. Sci. Rev.*, vol. 62, pp. 1–8, Apr. 2019, doi: 10.1080/00038628.2019.1606776.
[23] A. Perrot, D. Rangeard, and E. Courteille, “3D printing of earth-based materials: Processing aspects,” *Constr. Build. Mater.*, vol. 172, pp. 670–676, 2018, doi: 10.1016/j.conbuildmat.2018.04.017.
[24] L. Keefe, *Earth building : methods and materials, repair and conservation*, 1st ed. New York: Taylor and Francis Ltd., 2005.
[25] S. S. Damluji, *The Architecture of Yemen: From Yafi to Hadramut*. London: Laurence King Publishing, 2008.
[26] Green Home Buildings, “Mixing and Applying Cob,” 2020. http://www.greenhomebuilding.com/QandA/cob/mixing.htm (accessed Jul. 03, 2020).
[27] Earth Devon, “Cob Dwellings: Compliance with The Building Regulations,” *Cob Unbaked Earth Dwellings*, vol. 2000, pp. 1–21, 2008.
[28] A. Weismann and K. Bryce, *Building with cob: a step-by-step guide*. Devon: Green Books ltd, 2006.
[29] L. Miccoli, U. Müller, and P. Fontana, “Mechanical behaviour of earthen materials: A comparison between earth block masonry, rammed earth and cob,” *Constr. Build. Mater.*, vol. 61, pp. 327–339, 2014, doi: 10.1016/j.conbuildmat.2014.03.009.
[30] D. J. Wright, “Building From The Ground Up : Understanding and Predicting The Strength of Cob , An Earthen Construction Material,” The University of Tulsa. PhD thesis, 2019.
[31] R. H. Saxton, “Performance of cob as a building material,” *Struct. Eng. London*, vol. 73, pp. 111–115, 1995.

[32] Q. M. Pullen and T. V. Scholz, “Index and engineering properties of Oregon Cob,” *J. Green Build.*, vol. 6, pp. 88–106, 2011, doi: 10.3992/jgb.6.2.88.
[33] E. Quagliarini and G. Maracchini, “Experimental and FEM Investigation of Cob Walls under Compression,” *Adv. Civ. Eng.*, vol. 2018, pp. 21–29, 2018, doi: 10.1155/2018/7027432.
[34] H. Houben and H. Guillaud, *Earth construction: a comprehensive guide*, 1st ed. London: Intermediate Technology Publications, 1994.
[35] L. Ziegert, “Konstruktion, Schäden und Sanierung, Berichte aus dem Konstruktiven Ingenieurbau,” Technical University of Berlin. PhD Thesis., 2003.
[36] K. A. Coventry, “Specification Development for the Use of Devon Cob in Earthen Construction,” University of Plymouth. PhD thesis, 2004.
[37] G. Minke, *Building with Earth: design and technology of a sustainable architecture*. Basel: Walter de Gruyter, 2012.
[38] M. Rizza and H. Bottger, *Effect of Straw Length and Quantity on Mechanical Properties of Cob*. San Francisco, 2015.
[39] G. Brunello, J. Espinoza, and A. Golitz, “Cob Property Analysis,”. Dep of Civil & Environemntal Engineering. Santa Clara University. MSc Thesis., 2018.
[40] T. Vinceslas, E. Hamard, A. Razakamanantsoa, and F. Bendahmane, “Further development of a laboratory procedure to assess the mechanical performance of cob,” *Environ. Geotech.*, vol. 7, pp. 200–207, 2018, doi: 10.1680/jenge.17.00056.
[41] A. Jiménez Rios and D. O’Dwyer, “Experimental validation for the application of the flat jack test in cob walls,” *Constr. Build. Mater.*, vol. 254, 2020, doi: 10.1016/j.conbuildmat.2020.119148.
[42] A. Fabbri, J.-C. Morel, and D. Gallipoli, “Assessing the performance of earth building materials: a review of recent developments,” *RILEM Tech. Lett.*, vol. 3, pp. 46–58, 2018, doi: 10.21809/rilemtechlett.2018.71.
[43] S. Goodhew, PP. C. Grindley, and S. D. Probeif, “Composition, Effective Thermal Conductivity And Specific Heat Of Cob Earth-walling,” *Trans. Built Environ.*, vol. 15, pp. 205–213, Jan. 1995, doi: 10.2495/STR950231.
[44] CEN, “EN 772-1. Methods of test for masonry units - Part 1: Determination of compressive strength,” 2011. [Online]. Available: https://infostore.saiglobal.com/en-us/Standards/EN-772-1-2011-A1-2015-331320_SAIG_CEN_CEN_761952/.
[45] Standards Australia, *AS 1170.1–2002 (R2016) Structural design actions Part 1 : Permanent , imposed and other actions*. Sydney, NSW: Australian / New Zealand Standard ™, 2002.
[46] Standards Australia, *Australian Standard for Masonry structures (AS 3700:2018)*. Sydney, NSW: Australian / New Zealand Standard ™, 2018.
[47] R. McNeel, “Grasshopper - in Rhino 6,” 2020. https://www.rhino3d.com/6/new/grasshopper (accessed Jul. 30, 2020).

Feasibility of 3DP Cob Walls Under Compression Loads in Low-Rise Construction

Mohamed Gomaa[ae], Jaroslav Vaculik[b,c*], Veronica Soebarto[a], Michael Griffith[b,c], Wassim Jabi[d]

[a] School of Architecture and Built Environment, Horace Lamb Building, University of Adelaide, Adelaide SA5005, Australia.
[b] The School of Civil, Environmental and Mining Engineering, Engineering North Building, University of Adelaide, Adelaide SA5005, Australia.
[c] Bushfire and Natural Hazards Cooperative Research Centre, Melbourne, Australia
[d] The Welsh School of Architecture, Bute Building, Cardiff University, Cardiff CF10 3NB, UK.
[e] School of Engineering, B251- RMIT Bundoora East Campus, RMIT University, Melbourne VIC 3083, Australia.

*Corresponding Author
Postal address: The School of Civil, Environmental and Mining Engineering, Engineering North Building, University of Adelaide, Adelaide SA5005, Australia.
Phone: (+61 8 8313 5451)

Abstract

The rapid adoption of 3D-printing (3DP) technologies in construction, combined with an increased willingness to reduce the environmental impact of building industry, has facilitated reapproaching earth materials for modern building industry. The feasibility of 3DP earth-based materials has been under investigation in recent years, with a particular focus on cob due to its favourable characteristics toward the 3DP process. Yet, there is a lack of definitive information on the construction of 3DP cob. Hence this paper investigates the structural feasibility of 3D-printed cob walls in low-rise buildings. The investigation involved experimental compression tests on 3DP cob samples to obtain key mechanical properties including the compressive strength and elastic modulus. These properties were then used as inputs for structural analyses with respect to three alternate types of 3DP cob wall patterns to evaluate their load-carrying capacity based on a limit-state design framework. Results from the analyses were implemented in modelling an idealised low-rise cob building covering a range of floor spans and wall heights. The analytical study found that 3D-printed walls have the potential to sustain gravity loads typical of residential construction. Further, since the 3DP material was shown to have similar mechanical performance to conventional (non-3DP) cob on the material scale, the 3D-printing process provides the opportunity to produce wall sections that are structurally more efficient than the solid section used in conventional cob construction. This results in lower material consumption, making 3DP cob attractive from the point of view of resource efficiency. An important outcome of the study is the demonstration of a model design technique for low-rise 3DP cob buildings that could be implemented as part of a broader optimisation procedure to satisfy structural and architectural design objectives.

Keywords:

Additive manufacturing; 3D printing; Cob; Compression test; Limit-state design; Structural performance optimisation.

1 Introduction

Digital fabrication technologies, especially 3D printing (3DP), have been witnessing an increasing uptake in many areas of industry [1]. The construction industry has been adopting a scaled-up version of 3DP over the past two decades. The increased demand for 3DP technologies in construction industry has also encouraged researchers to develop novel ideas toward the full automation of the construction process. Several studies have proven that a well-developed digital-based process of construction offers various benefits such as larger design freedom, accelerated productivity, higher degree of customisation, and improved safety of construction personnel [2], [3].

Among the developed techniques of digital fabrication in construction, 3DP has been the most studied, and has seen a particular focus on cement-based materials [4]–[7]. This has led in recent years to a rapid spread of 3DP building prototypes around the world, as 3DP technology has been increasingly embraced by the construction industry [8]. Among the most notable examples are two concrete buildings constructed in 2019: One is the world's largest 3DP building, constructed by Apis Cor in Dubai, United Arab Emirates having two storeys, a plan area of 640 m^2 and height of 9.5 m (Figure 1a). The second is a 80 m^2 prototype house built by CyBe as part of their contract with the Saudi Arabia Ministry of Housing with an ambitious goal to build 1.5 million houses using 3D concrete printing [9] (Figure 1b).

Figure 1: Notable examples of 3DP concrete buildings: (a) Two-storey office building in Dubai constructed by Apis Cor (image credit: Apis Cor), and (b) House in Saudi Arabia constructed by CyBe (image credit: CyBe).

The accelerating rate of present-day global construction is well known to produce adverse environmental impacts. Fortunately, the implementation of digital technology in construction offers great potential for sustainability [10]. For instance, according to Ford and Despeisse [11], additive manufacturing (e.g. 3D printing) in construction has several sustainability benefits such as improving efficiency of resources, extending product life, and upgrading the value and supply chains.

The increased motivation to harness the sustainability benefits of 3DP technology in construction has also recently renewed the interest in earthen construction materials after decades of dormancy [11],[14]. Significantly, a recent study by Hamard et al. [12] has revealed that considerable sustainability benefits can be realised through the integration of digital fabrication techniques with earth-based materials, which have low embodied energy, are highly recyclable, and generate limited waste. Furthermore, these materials typically have high material density and thus high thermal mass, which can lead to favourable thermal comfort performance, particularly in areas where there is a large difference in daytime and night-time temperatures [12], [14], [15]. As a further benefit, earth-based materials are significantly cheaper per unit volume compared to conventional building materials such as concrete or steel [13], and can under many circumstances result in more economical small-scale structures.

Earthen construction has three famous forms: cob, adobe, and rammed earth. Cob, which is the focus of this study, is a traditional building material comprising a mixture of subsoil, water and straw (or other fibres). It differs from adobe and rammed earth by using a wet-based construction technique that offers freedom of design while not requiring formwork. It also exhibits excellent maintenance characteristics through the ability to apply add-ons or create cuts-out, even after the cob is dry [16]–[18]. This makes cob particularly attractive for 3D printing.

In recent years, the performance of cob manufactured digitally using 3D printing has been the focus of emergent research at several institutions such as IAAC, Cardiff University and Plymouth University [19]. A proof of concept of the idea has also been successfully demonstrated by the 3D-printer manufacturer WASP by constructing two prototypes of cob houses [20] (Figure 2). And while the focus of the studies to date has been to examine feasibility with regard to aspects such as geometry and fabrication process [21], thermal performance [22], and life cycle assessment [8], the examination of structural performance not yet been carried out in any significant detail. As a consequence, the pursuit of fully implementing 3D cob in modern construction remains hindered by a lack of engineering guidance for structural design. Overcoming this hurdle requires establishing a reliable body of experimental test data on the mechanical (structural engineering) properties of 3DP cob, as well the development of appropriate structural design and modelling tools that can be used by design engineers.

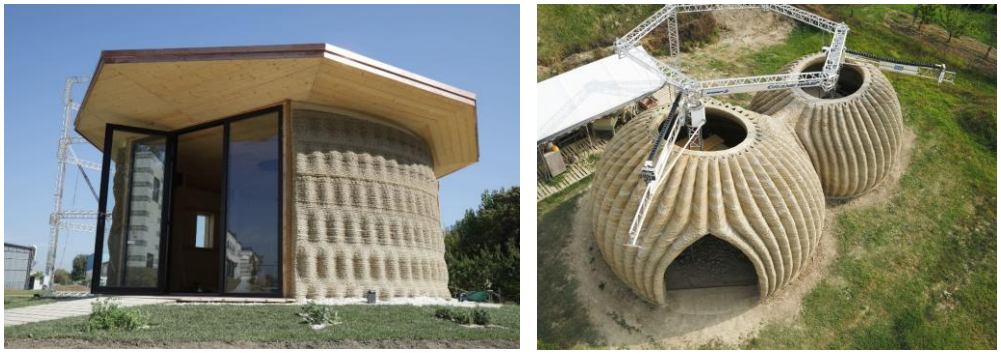

Figure 2: 3DP cob houses fabricated by WASP (image credit: WASP).

While numerous studies have focused on the mechanical properties of 3DP concrete [1][7], to the knowledge of the authors only a single study to date has investigated the mechanical properties of any 3DP cob-like material [23]. This study, by Perrot et al., tested material made from a mix of earth material and alginate seaweed biopolymer (as a substitute for straw which is traditionally used), and demonstrated compressive strength simliar to that of conventional (non-3DP) cob. Besides this study, however, there is no existing research into the mechanical properties of traditional (straw-fibre) cob passed through the 3DP process. Moreover, there are, to the authors' knowledge, no existing studies involving the translation of these fundamental properties toward engineering design of 3DP cob on neither the wall nor building scale.

To address these gaps, this study aims to provide insight into the expected loadbearing capability 3DP cob walls. This is approached in two stages: The first conducts an experimental compression test on 3DP cob samples to obtain the basic mechanical properties including compressive strength, elastic modulus, and Poisson's ratio. The second stage evaluates the wall section geometries (dimensions) necessary to perform a loadbearing function in typical residential construction for alternate 3DP patterns through a first-principles analysis approach. This is combined with an optimisation process to examine the relationship between structural efficiency and several design variables such as variable room size, floor heights, number of storeys, and wall section properties. The outcomes are expected to empower architects and engineers with a model approach for the structural design and construction process of 3DP cob. The paper also acts as an essential part of larger overarching research by the authors on the feasibility of 3DP cob in modern construction.

The paper is structured as follows: Section 2 undertakes a review of previous material testing of traditional (non-3DP) cob to establish typical range of material properties. Section 3 reports original compression tests on 3DP cob cylinders. Section 4 demonstrates a simplified design approach for estimating the loadbearing capability of 3DP walls, and examines their feasibility in residential construction, including an investigation of the sensitivity on material properties. Section 5 demonstrates the essential design process on a fictional small house, and Section 6 concludes with a summary and recommendations for future work.

2 Structural performance of cob as a building material

Cob buildings are well-known for their durability and resistance to weathering [24]. However, the lack of a binding agent (e.g. cement) makes the compressive strength of cob (typically < 2 MPa) much weaker compared to concrete (typically > 20 MPa) and even other traditional materials such as rammed earth (typically 5–20 MPa). This combined with the fact that cob buildings were historically built without reinforcement means that building heights are typically restricted to low-rise (i.e. between one to three storeys), with most being 2-storey [13]. Some very rare but notable examples of high-rise are found however, such as the world heritage-listed towers in Yemen which have up to 9 storeys [25][26]. The low compressive strength of cob compared to other traditional materials is generally compensated for by large wall thickness [27], [28].

Multi-storey cob houses typically incorporate light-weight floor and roof systems in the form of timber framing. Floors usually comprise joists with wooden decking, while roofs include timber rafters plus purlins and have a typically sloped profile with extended eaves to protect walls from rain. Walls in multi-storey houses are typically around 600 mm thick, and for efficiency they are typically made thinner at upper storeys relative to the ground floor [13], [28].

Mechanical properties of cob are dependent on a number of factors: subsoil composition including clay content, straw and water content, degree of compaction, and the general quality of the workmanship [29], [27], [30]. Studies into the influence of the mix composition have demonstrated compressive strength to be generally enhanced by increased straw content (due to acting as local tensile reinforcement) and reduced by higher moisture content [16], [31]. Table 1 provides a generalised overview of test studies to date, summarising the range of reported compressive strength (f_c) and elastic modulus (E). It is important to note that the cob mixtures in these studies vary in terms of their composition, with the intention of the table being to demonstrate the broad range of property values rather than parametric trends.

Compressive strength can be considered to be the fundamental engineering property of interest for earthen-material structures, as it controls the loadbearing capacity of walls under gravity loads [13], [32]. As demonstrated by Table 1, compressive strength usually falls between 0.4–1.35 MPa, although values less than 0.1 MPa and as high as 5 MPa have been reported. Notably, low values of strength (< 0.4 MPa) are usually for mixtures with high moisture content (> 15%) [13], [31]. Among the studies in Table 1, the range of scatter in compressive strength (where reported) varies between 2–21%. Stochastic variability has implications toward the lower-bound characteristic value that can be adopted in limit-state design as discussed later.

The reported elastic modulus varies drastically among the published studies. Most values fall within the range 4–200 MPa, but outlying values as low as 0.33 MPa and as high as 850 MPa have also been reported. As will be shown later (Section 4) the elastic modulus has particular importance toward the loadbearing capacity of 3DP cob walls due to the potential for local buckling of the printed sections.

Data on Poisson's ratio is limited to two studies [29] and [33], who reported mean values of 0.15 and 0.12 respectively.

Additionally, cob exhibits considerably higher material ductility than rammed earth and adobe [29], [33], as characterised by the ability to maintain stress resistance into the post-peak phase of stress-strain response. Miccoli et al. [29] demonstrated this to be the case under both compressive and shear loading. The observed ductility of cob can be attributed to the influence of fibres, with fibres used in cob being typically longer than in adobe. This favourable behaviour implies that cob may be able to outperform the alternate earthen materials under deformation-controlled loading such as earthquake. While this warrants further investigation, it is outside the scope of the current paper.

Table 1: Compressive strength (f_c), elastic modulus (E), and Poisson's ratio (ν) for non-3DP cob. Values presented as a range (a–b) cover different cob mixtures, if applicable. Percentages in brackets denote the intra-batch CoV if specified. Unless noted otherwise, the mixtures have moisture content (mc) < 15%.

Source	f_c (MPa)	E (MPa)	ν
Houben and Guillaud (1994) [34]	0.10	–	–
Saxton (1995) [31]	0.35–1.75 (mc<15%) 0–0.2 (mc>15%)	–	–
Ziegert (2003) [35]	0.45–1.40	170–335	–
Coventry (2004) [36]	0.48–1.24 (3%–10%)	0.33–1.25	–
Keefe (2005) [24]	0.6–1.4	–	–
Akinkurolere et al. (2006) [16]	0.6–2.2	–	–
Weismann and Bryce (2006) [28]	0.77	–	–
Quagliarini et al. (2010) [13]	0.24–0.40 (mc>15%)	4.0–40 *	–
Pullen and Scholz (2011) [32]	0.45–0.89 (22%)	11–69	–
Minke (2012) [37]	0.5–5.0	60–850	–
Miccoli et al. (2014) [29]	1.59 (2%)	651 (68%)	0.15 (4%)
Rizza and Bottger (2015) [38]	0.60 (13%)	71.5	–
Brunello et al. (2018) [39]	0.71–0.87 (8%–15%)	–	–
Quagliarini and Maracchini (2018) [33]	1.12 (5%)	16.9 (4%)	0.12 (66%)
Vinceslas et al. (2018) [40]	0.50–0.76	110–350	–
Wright (2019) [30]	1.22–1.53 ** (18%–21%) 0.77–2.45 ***	–	–
Jimenez Rios and O'Dwyer (2020) [41]	0.70 (12%)	143 (23%)	–

Notes:
* E determined from reported stress-strain curves
** Specimens with varied straw content
*** Specimens with varied soil clay content

The only study, to the authors' knowledge, that has undertaken material testing on any 3D-printed earthen material is a recent study by Perrot et al. [23], which used a cob-like material incorporating alginate seaweed biopolymer as a substitute for straw. The produced material achieved a compressive strength between 1.2–1.8 MPa, demonstrating that 3DP earth material has the potential to achieve compressive strength toward the higher end of that for conventional non-3DP cob (Table 1).

3 Compression tests on 3D-printed cob cylinders

This section reports laboratory tests performed on 3DP-cob cylinders to quantify fundamental mechanical properties necessary for design. Among the side objectives of these tests was also to ensure that the 3D-printing process did not produce any unexpected strength reduction compared to conventional non-3DP cob (Table 1). Such a reduction could be conceivable due

to the altered form of the material as a result of being stacked in layers rather than being a homogeneous mass. Due to the lack of a structural testing standard specific to earthen materials, the study adopted general principles for the testing of quasi-brittle materials, as recommended by [42].

3.1 Test specimens

3.1.1 Material mix preparation

In the 3D-printing process, for both concrete and earth-based materials, the material must flow efficiently through the system, be deposited as layers and harden properly to reach a structural integrity threshold within an acceptable time frame that meets the construction requirements [5] [23]. The properties of the input material must therefore be formulated carefully considering both their wet (pre-hardening) and hardened states. According to Weismann and Bryce [28] and Hamard et al. [12], traditional cob mixture typically comprises 78% subsoil, 20% water and 2% fibre (straw) by weight. This however produces a nearly dry mixture with low flowability, making it unsuitable for 3D printing. To overcome this, the adopted mixture followed an alternate, 3DP-suitable, mix developed by the authors in a precursor study [22]. In the adopted mix, the water content was increased to an average of 25%, subsoil was reduced to 73%, and straw was maintained at 2% (by weight). The mixture used locally-sourced wheat straw chopped into lengths of 30–50 mm, as longer straw lengths were found to be unsuitable by causing blockage inside the extrusion system. The composition of the subsoil (sourced from Cardiff, UK) was examined using methods recommended by [28], [43] and found to contain 19–20% clay and 80–81% aggregate/sand. This is in good agreement with subsoil composition recommended in the literature (15–25% clay to 75–85 % aggregate/sand) [28], [12].

It is worth mentioning that, despite the intentionally high moisture content of the input mixture, the moisture content of the final printed cob becomes slightly reduced by the 3DP extrusion process. This is caused by the pressurisation of the mixture inside the extrusion system, which leads to moisture release in the form of leakage around the cartridge connections. The moisture loss in this study was estimated at around 3%, leaving the printed cob at 22% moisture content. This reduction is considered favourable as it improves the structural stability of the printed layers and also reduces drying shrinkage. Note that while shrinkage is an important aspect of cob construction, it was not a specific focus of this study, especially as the observed shrinkage in the specimens was low (approx. 2%) and the specimens showed no signs of cracking during the drying period.

3.1.2 3D-printing of specimens

The test specimens in this study were printed using a 6-axis KUKA KR60 HA robotic arm (Figure 3). The software package for robotic control was Rhinoceros via Grasshopper and KUKA PRC®. An electromechanical dual ram extruder, developed by the authors in a previous study [21], was used for material delivery. The test specimens comprised 400 mm-tall cob cylinders with an average diameter of 200 mm (Figure 4). Each cylinder was contoured as 14 successive layers, with an average height of 29 mm per layer. The nozzle had a 45 mm

diameter. The robotic arm moved in a circular pattern at an average movement speed of 35 mm/sec.

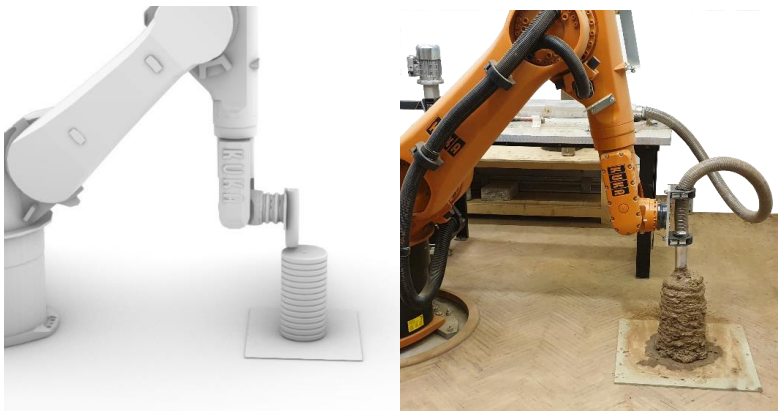

Figure 3: Robotic 3D printing of the cob specimens: virtual model on Rhino (left) and the real output (right).

3.2 Test arrangement and method

The test specimens were subjected to uniform axial load in a universal testing machine (Figure 4). Prior to the test, the machine loading platens were coated with grease to minimise frictional confinement. The rate of applied load was approximately 0.08 MPa/min, with each test taking about 10 minutes to perform. The test apparatus monitored the applied load and axial (longitudinal) displacement between the two platens using a built-in linear variable differential transformer (LVDT). Due to the impracticality of applying strain gauges to the irregular surface of the specimens, horizontal deformation (necessary to evaluate the Poisson's ratio) was quantified in post-processing by digital image correlation using high-resolution video footage captured during the test. A total of three samples were tested, with examples of the failed specimens shown in Figure 5.

Figure 4: Compression test setup (left) and the cylindrical specimen (right).

Figure 5: Typical examples of specimens after compressive failure.

3.3 Results

The observed stress-strain behaviour is shown in Figure 6. Each specimen exhibits quasi-brittle response with an approximately linear rising branch, followed by a reduction in slope up to the peak, and continued softening in the post-peak zone. The plotted stress was calculated as $\sigma = P/A$, where P is the applied force and A is the average cross-sectional area of the specimen (31,400 mm^2). Axial strain was computed as $\varepsilon_{axial} = \Delta/L$, where Δ is the displacement measured platen-to-platen, and L is the length of the specimen (400 mm).

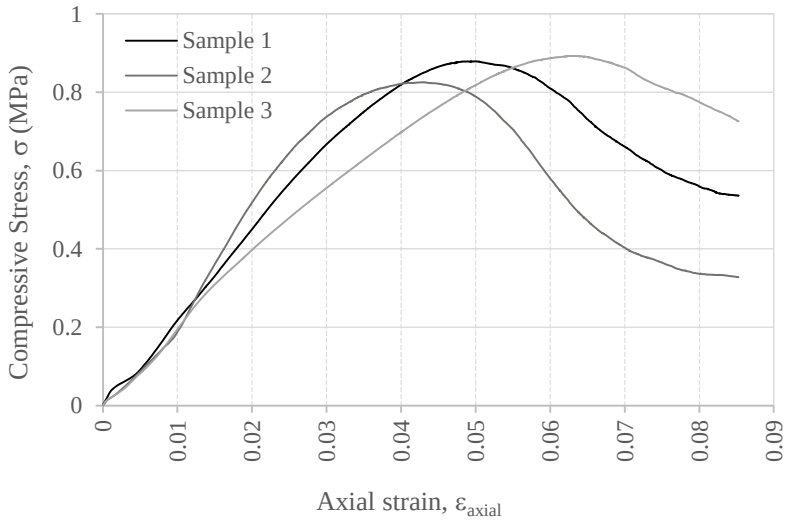

Figure 6: Stress-strain behaviour of compression test specimens.

The properties derived from the test, including the compressive strength, elastic modulus, and Poisson's ratio, are summarised in Table 2.

The average unconfined compressive strength (f_c) of the specimens is 0.87 MPa. This compares favourably to strength of non-3DP cob reported in the literature (Table 1) with most reported values falling within 0.4–1.35 MPa. On this basis there does not appear to be any obvious reduction in strength introduced by the 3DP process. Despite a limited number of samples, the variability is low (CoV = 4%). It should be noted that the reported compressive strength corresponds directly to the peak stress reached during the test. To account for the size-effect in quasi-brittle materials as well as confinement resulting from the compression apparatus platens, test standards typically apply a correction factor to the measured peak stress to obtain a size-invariant unconfined compressive strength. For instance if these results were to be interpreted according to the test standard for masonry units (EN 772-1, [44]) a correction factor of 1.25 would apply on the basis of the test specimen dimensions. However, for conservatism, the subsequent analysis in Section 4 takes this factor as 1.

Elastic modulus (E) was evaluated as the slope of the σ-ε curve along the initial rising branch before the onset of nonlinearity. Mean E of the tested specimens is 22.9 MPa (CoV = 10%). This falls into the lower end of values determined for non-3DP cob (Table 1) (median ≈ 60 MPa). As demonstrated later (Section 4), the elastic modulus is influential on wall loadbearing strength as it controls local buckling of the printed cross section, thus providing impetus for future investigations into 3DP-suitable cob mix design to focus on not just the material's strength but also stiffness.

Poisson's ratio (ν) was calculated as the ratio of lateral to longitudinal strain over the initial elastic portion of response, producing a mean value of 0.22. This is consistent with the range of scatter reported by [29] and [33] for non-3DP cob (Table 1).

Table 2: Results of compression test, including unconfined compressive strength (f_c), elastic modulus (E), and Poisson's ratio (ν).

Sample	f_c (MPa)	E (MPa)	ν
1	0.88	22.7	0.16
2	0.83	25.3	0.28
3	0.89	20.6	0.21
Mean value	0.87	22.9	0.22
CoV	4%	10%	28%

4 Evaluation of the feasibility of loadbearing 3DP cob walls

This section examines the feasibility of using 3DP cob walls as loadbearing in low-rise residential construction. The design actions considered are from gravity loads only, and do not include wind or earthquake loading which can be highly region-specific.

4.1 Method of structural analysis

Although the expected behaviour of 3DP cob walls under gravity loads is expected to resemble that of walls constructed using conventional materials such as unreinforced masonry or concrete, the design-code provisions for these established materials are not necessarily translatable to 3DP cob. Therefore, the wall's load-carrying capacity was evaluated using first principles while adhering to the concepts of limit-state design. This includes using characteristic values of material stress capacity (rather than mean values), and applying factors to upscale design loads and downgrade the design capacity.

4.1.1 Limit-state design

Capacity-adequacy checks were performed according to a limit-state design framework. With reference to the compressive strength, the design check can be expressed using the generalised form

$$N_c^* < \phi N_c. \quad (1)$$

In Eq. (1), N_c^* is the design compressive force acting on the wall, determined as γS, with S being the unfactored working load and γ being the load factor (greater than 1). In turn, ϕN_c is the design compressive capacity of the wall, determined as the basic capacity N_c multiplied by the capacity-reduction factor ϕ (less than 1). To account for the fact that the material stress capacities exhibit stochastic variability, capacity N_c was calculated using the characteristic compressive strength, f_c', defined as the lower-5th-percentile value.

4.1.2 Wall cross-section patterns

Three different types of printed patterns were considered as part of this feasibility study; these are referred to as A, B and C as shown in Figure 7. These three patterns align carefully with the wall sections in two previous studies that investigated thermal performance and life cycle assessment of 3D-printed cob by Gomaa et al. [22] and Alhumayani et al. [8] respectively. The criteria for choosing these wall sections are based on meeting multiple design requirements including adequate thermal insulation, efficient use of material, and structural integrity. A generic vertical cross section of a wall is shown in Figure 8. Because the 3D-printing process in the current study dispensed the cob material in circular cross sections while being flattened down into wider layers, the resulting vertical shells did not have a constant thickness (Figure 8). Rather, the shell thickness ranged between an inner value, t_{in}, and outer value, t_{out}, as shown. Both t_{in} and t_{out} could be estimated according to a number of parameters in the 3D-printing process setup, such as the layer height, nozzle size and the extrusion rate [21]. On the basis of typical printed patterns, $t_{out} - t_{in}$ was taken as 20 mm, with the average thickness (t) being in turn defined as $t = (t_{in} + t_{out})/2$. For each section type, the nominal wall depth (d) is defined as the distance between the centrelines of the two external 'face' shells; and a denotes the dimension between the internal 'web' shells (Figure 8). In all of the subsequent analyses, a is taken equal to d.

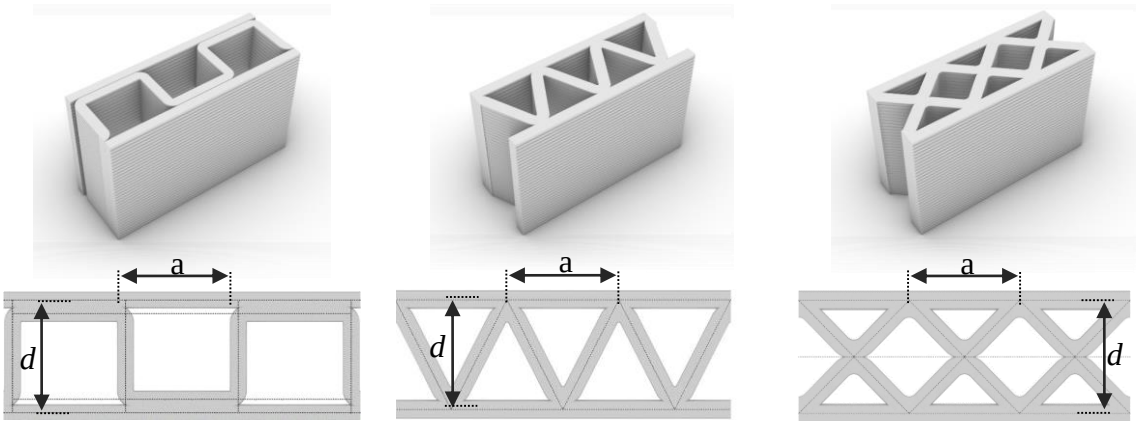

Figure 7: Alternate printed patterns considered in this study.

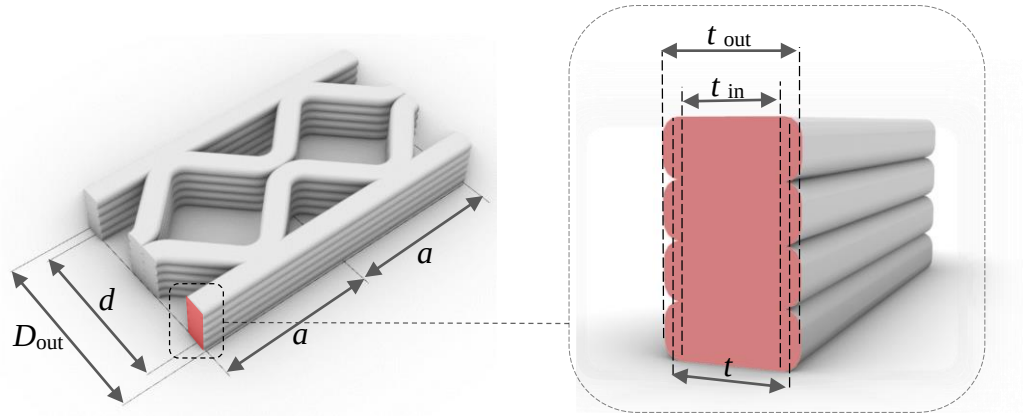

Figure 8: Definition of geometric properties along a generic cross section.

Evaluation of the wall's compressive capacity requires the wall's area (A) and out-of-plane moment of inertia (I). These were calculated for each type of section by conservatively taking the shell thickness as t_{in}. For comparative purposes, the sectional properties of the three pattern types are provided in Table 3.

Table 3: Section properties for the alternate printed patterns. Each considers a reference section with t_{in} = 50mm and d = 500mm. Properties accented by a bar ($\bar{X}$) denote the value per unit length run of the wall.

Wall Type	t_{in} (mm)	t (mm)	d (mm)	$\bar{A}$ (mm^2/m)	$\bar{I}$ (mm^4/m)	$\bar{P}_{buck,loc}$ (kN/m)
A	50	60	500	200,000	9.32×10^9	145
B	50	60	500	212,000	8.60×10^9	137
C	50	60	500	241,000	9.23×10^9	181

4.1.3 Wall compressive strength

The compressive strength of a generic (3DP or no-3DP) cob wall requires evaluation of its member capacity under combined axial load and eccentricity moment with the potential for global buckling combined with material failure. A 3DP wall however differs from a solid wall in that the section capacity can be governed by not just material crushing, but also by local buckling of the shell structure. Thus, the compressive stress capacity of the section was evaluated as

$$\sigma_{c,\max} = \min\left(\sigma_{\text{mat}}, \sigma_{\text{buck,loc}}\right), \tag{2}$$

i.e. the lesser of the stress to cause material crushing (σ_{mat}) and local buckling ($\sigma_{\text{buck,loc}}$).

The material crushing limit in Eq. (2) was taken as the characteristic (lower-5th-percentile) compressive strength ($\sigma_{\text{mat}} = f_c'$). The characteristic strength was estimated to be 0.62 MPa, based on the assumption that it follows a lognormal distribution with mean = 0.87 MPa (Table 1) and CoV = 20%.

The capacity of each of the three section types to withstand local buckling was determined using the finite-element analysis package ABAQUS. The model analysed for each type of printed section was built using shell elements and comprised a full-sized wall subjected to a uniform compressive force at its top and bottom boundaries. The length and height of each wall were taken as 2 m. These dimensions were chosen by trial-and-error so as to satisfy the conditions of: 1) being were sufficiently large not to influence the computed local-buckling stress, but 2) not excessive to cause global buckling. A visual examination of the resulting buckling mode shape was undertaken to confirm that it indeed corresponded to local buckling of the shell structure. A typical local-buckling shape is shown in Figure 9 and is characterised by the face- and web-shells deforming perpendicular to their local planes in an alternating pattern, while maintaining the original angle at shell junctions. The corresponding load capacities are summarised in the last column of Table 3 as the load per unit length of the wall ($\bar{P}_{\text{buck,loc}}$). These capacities were computed by assigning the material properties E = 22.9 MPa and ν = 0.22 as informed by the material tests. The local-buckling stress used in Eq (2), was evaluated as $\sigma_{\text{buck,loc}} = \bar{P}_{\text{buck,loc}}/\bar{A}$.

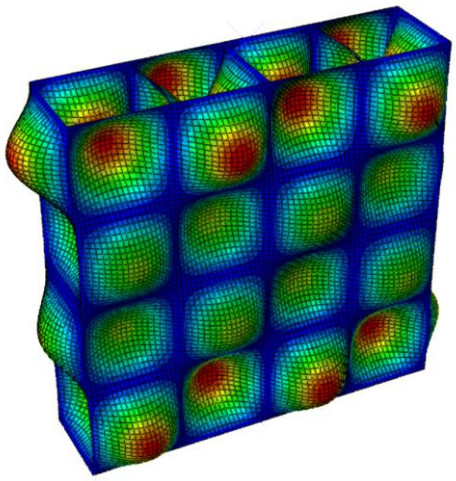

Figure 9: Visual representation of a typical local-buckling failure mode in a wall member as calculated by finite element analysis. Shown for section type A.

The member capacity of the wall was evaluated from first principles by treating it as a column under eccentric loading with potential for global buckling. In this treatment, the peak compressive stress $\sigma_{\max}$ along on the section can be expressed as:

$$\sigma_{\max} = P\left[\frac{1}{A} + \frac{ec}{I}\sec\left(\frac{\pi}{2}\sqrt{\frac{P}{P_{\text{buck,glob}}}}\right)\right] \quad (3)$$

where P is the applied axial load; e is the net eccentricity of the applied load (described later); A and I are the section's area and moment of inertia; c is the distance from the centreline to the extreme compressive fibre, equal to $(d+t_{in})/2$. The critical global buckling load of the wall, $P_{\text{buck,glob}}$, was obtained by Euler's formula:

$$P_{\text{buck,glob}} = \frac{\pi^2 EI}{L_e^2} \quad (4)$$

where L_e is the effective height of the wall being considered, taken as either the floor-to-floor or floor-to-roof height (indicated by H_w in Figure 9); and other properties as defined previously.

The wall's unfactored load capacity was evaluated by assigning $\sigma_{c,\max}$ [from Eq (2)] to $\sigma_{\max}$ in Eq (3) and solving for P. The limit-state design capacity was obtained by applying the capacity-reduction factor ϕ = 0.5 as per AS3700 [45], such that:

$$\phi N_c = \phi P \ . \quad (5)$$

4.1.4 Modelling an idealised low-rise building

To examine the feasibility of using 3DP cob walls as loadbearing structural elements, the study considered an idealised 1- and 2-storey house. Schematic representations of the building's geometry are shown in Figure 10. In the case of a 1-storey house, the walls carry only the roof load, while in the 2-storey house they carry loads from the roof and suspended floor. In each

scenario, the total compressive force acting on the wall also incorporates self-weight calculated at the ground level.

The forces imparted to the wall by the roof and the floor depend on their respective dead load (self-weight plus superimposed permanent load), live load, and span. The roof and floor are treated as one-way-spanning, so the load that they apply to the wall can be calculated as the total pressure load multiplied by a tributary width (L_{trib}). The tributary width depends on the configuration of the wall within building. In the case of an external wall, it is equivalent to half the span of the floor/roof beam [LW(1) or (3) in Figure 10]. For an internal wall, it includes the sum of the contributions from each side [LW(2) in Figure 10]. Further, if the wall contains an opening, a simplistic treatment can be to scale the tributary width pro-rata depending on the proportion of solid wall to openings. For instance, if half of the wall is perforated by openings, then the tributary width becomes twice what it would be if the wall were solid.

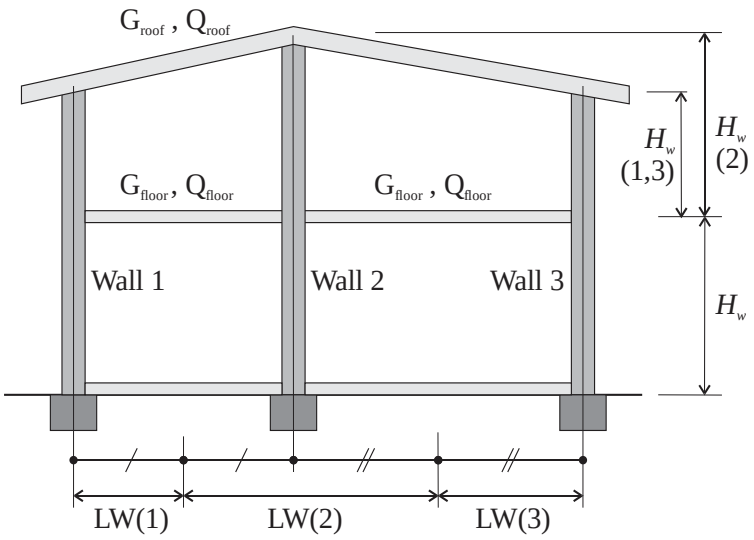

Figure 10: Overall building geometry, Two-storey (n_s = 2) double-bay building with internal and external walls, indicating the definition of wall height (H_w) and tributary width (denoted here as LW).

The gravity loads used in the analysis are representative of residential construction as prescribed by loading standards (e.g. [45]). The adopted unfactored loads are summarised in Table 4. The total dead load of the suspended floor is taken as 1.0 kPa, which allows for a timber joist plus timber deck floor (typically 0.5 kPa) in addition to a superimposed permanent load (0.5 kPa). The floor live load is taken as 1.5 kPa allowing for general residential occupancy. The dead load of the roof is taken as 0.9 kPa, making allowance for timber framing (rafters + purlins) with clay roof tiles. The live load on the roof is taken as 0.25 kPa.

The self-weight of the wall was calculated based on its section area, taking the weight density of the material as 18 kN/m^3. Thus, the total design compressive load was evaluated as:

$$N_c^* = \begin{cases} P_{\text{roof}}^* + P_{\text{wall}}^* & \dots 1 \text{ storey} \\ P_{\text{roof}}^* + P_{\text{floor}}^* + 2P_{\text{wall}}^* & \dots 2 \text{ storey} \end{cases} \quad (6)$$

where P^*_{roof} is the load applied by the roof, P^*_{floor} by the suspended floor, and P^*_{wall} is the self-weight of the wall over a single storey height H_w. Each P^* is taken at the ultimate limit state using the load combination $1.2G+1.5Q$ [45], with G being the dead load and Q the live load component.

Table 4: Summary of constant inputs used in the feasibility study. Explanations are provided in the text.

Property	**Value**
Cob material properties:	
Elastic modulus, E	22.9 MPa
Characteristic compressive strength, f_c' (See note 1)	0.62 MPa
Weight density, γ	18 kN/m^3
Poisson's ratio, ν	0.22
Unfactored loads:	
Roof dead load, G_{roof}	0.9 kPa
Roof live load, Q_{roof}	0.25 kPa
Floor dead load, G_{floor}	1.0 kPa
Floor live load, Q_{floor}	1.5 kPa
Limit-state design factors:	
Compressive strength capacity-reduction factor, ϕ	0.5
Ultimate limit-state design load combination	$1.2G + 1.5Q$
Eccentricities (e) of applied load (w.r.t. wall centreline): (See note 2)	
Load from roof	$0.1 \times D_{out}$
Load from floor	$0.25 \times D_{out}$
Self-weight of wall	$0.05 \times D_{out}$

Notes:

1. Determined from mean strength f_{cm} = 0.87 MPa by assuming lognormal distribution and CoV = 20%.
2. Where D_{out} is the full depth of the wall section measured between its outer edges (Figure 8).

4.1.5 Connection details and load eccentricity

It is important to consider that the floor and roof generally apply the load eccentrically with respect to the wall's centreline, and this generates an out-of-plane bending moment that can have a major influence on the wall's load-carrying capacity. The eccentricity of the applied load is controlled by the connection detail. While the development of the connection details

falls into the domain of detailed structural design and is outside the focus of this work, conceptual illustrations of the assumed connections are shown in Figure 11.

The connection between the roof and wall can be achieved by supporting the timber rafters using a timber bearing block, in turn resting on a spreader block that distributes the load onto the wall (Figure 11a). This detail is assumed to generate an eccentricity $e = 0.1\ D_{out}$, with D_{out} as defined in Figure 8. The assumed wall-to-floor connection involves partial penetration of the joists into the wall and are supported by a bearing block and spreader block (Figure 11b), which is assumed to produce an eccentricity of $0.25\ D_{out}$. It should be noted that a connection in which the floor is supported outside the extent of the wall is not advised, as it would generate an eccentricity > $0.5\ D_{out}$ and significantly diminish the loadbearing capacity. The aforementioned values of the assumed eccentricities are consistent with similar details for conventional clay brick masonry provided in AS3700 [46].

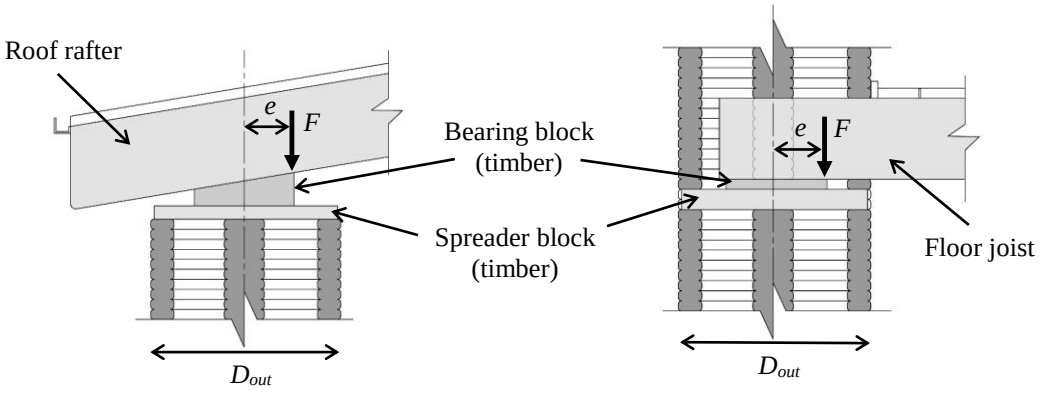

(a) Wall-to-roof connection (section view). *(b) Wall-to-floor connection (section view).*

Figure 11: Potential connection details and definition of eccentricities (e) of the applied load (F).

Additionally, for sake of conservatism the self-weight of the wall is assumed to act at an eccentricity of $0.05\ D_{out}$ to allow for any incidental geometric imperfection of the wall. The internal bending moment was calculated as the sum of each applied load P^* (i.e. P^*_{roof}, P^*_{floor}, P^*_{wall}) and its respective eccentricity, which dividing by the total compressive force N^*_c [from Eq. (6)] produces the net eccentricity:

$$e_{\text{net}} = \frac{\sum P_i^* e_i}{N_c^*} \tag{5}$$

The net eccentricity was used as the input value of e in Eq (3).

4.1.6 Optimisation of wall cross section geometry

The geometry of the 3D-printed sections in Figure 7 can be defined by two variables: the nominal wall depth (d) and average shell thickness (t). To characterise the most efficient section to fulfil a loadbearing function, an optimisation process was undertaken that minimises the material volume while ensuring that the load capacity remains sufficient to accommodate the

applied design load. As a metric of the structural adequacy, the limit-state design formula [Eq (1)] can be rearranged and expressed as the capacity utilisation (u), i.e. the ratio of the design load to the design capacity:

$$u = \frac{N_c^*(t,d)}{\phi N_c(t,d)} \tag{5}$$

where both the capacity and design load are functions of the optimisation variables d and t.

As a proxy for the material volume, we can adopt the area per unit length of the wall ($\bar{A}$), since the two are directly proportional. Therefore, the optimisation process to determine the optimal t and d can be expressed as:

Minimise $\bar{A}$, by varying t and d, subject to the constraints:

a. $u \leq 1$ (to ensure structural adequacy),
b. $t > 0, d > 0$ (positive values only),
c. $d \geq t$ (in valid sections the shell thickness must not exceed the effective depth).

To cater for varying architectural requirements on the building geometry, this optimisation was performed at different combinations of the wall height (H_w), tributary width (L_{trib}), and number of storeys (n_s). Constant inputs and their values are summarised in Table 4.

The optimisation problem was solved using two different methods in order to provide a means of cross-verifying the results and to examine alternate approaches to the representation of results. The first approach used a continuous optimiser in MATLAB, in which t and d can adopt any values along a continuous domain. The second approach used the evolutionary optimiser Galapagos in the Rhino-Grasshopper package [47] (Figure 12). The continuous-optimisation algorithm in MATLAB is the computationally faster of the two approaches; yet, implementing the optimisation in Grasshopper provides certain advantages, such as:

1) Direct link to the 3DP system (i.e. 3D printers and robotic arms), providing the ability to interface the design software with the printing tools.

2) Inclusive control over the design-to-fabrication framework, incorporating design of the geometry and other performance objectives such as thermal, lighting and environmental impacts.

3) The ability to provide visual representation of the modelling results in real time, including the building geometry and its aesthetics (Figure 13).

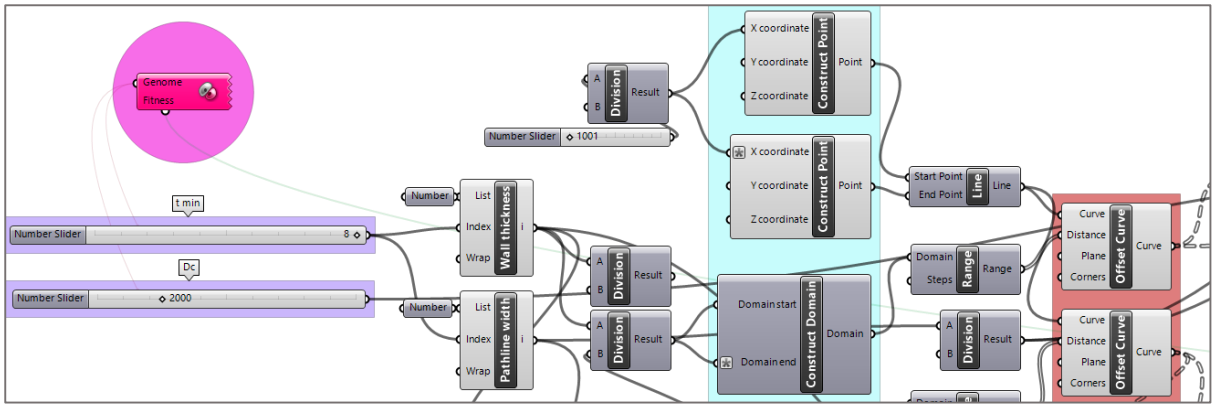

Figure 12: Part of the Grasshopper defintion for the optimisation of the wall models.

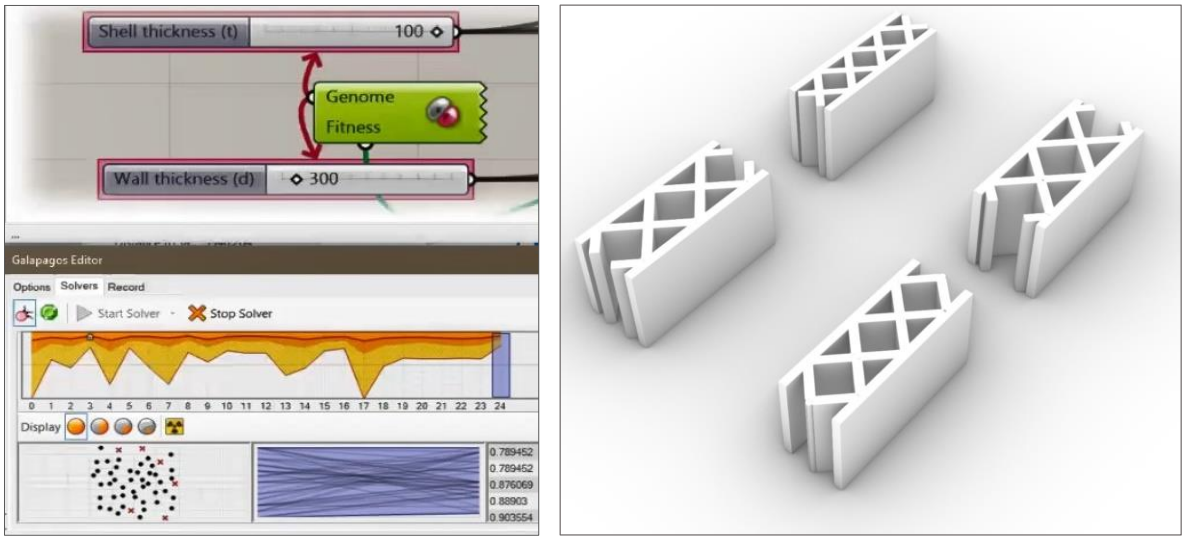

Figure 13: Visual representation of the optimisation process of Galapagos (left) and a sample of the visual generation of results for wall type C in Grasshopper (right).

4.2 Results and discussion

4.2.1 Single-scenario analysis

The typical relationship between structural adequacy versus the wall section geometry is illustrated in Figure 14, which plots contour lines of constant utilisation (u) as a function of shell thickness (t) and nominal wall depth (d). The graph corresponds to a single scenario where H_w = 2.5 m, L_{trib} = 3.5 m, and n_s = 2; however, the general trends are representative regardless of the selected values of these inputs. The thick black contour line corresponding to u=1 represents sections whose capacity exactly matches the design load. Thus, the grey-shaded area above u=1 encompasses sections that are structurally adequate. The red dashed line delineates the zones where the section is compact (governed by the material crushing) as opposed to slender (governed by local buckling), as per Eq (2). The black dashed lines bound the range of t values that correspond to available nozzle sizes in the 3DP system used in the present experimental study.

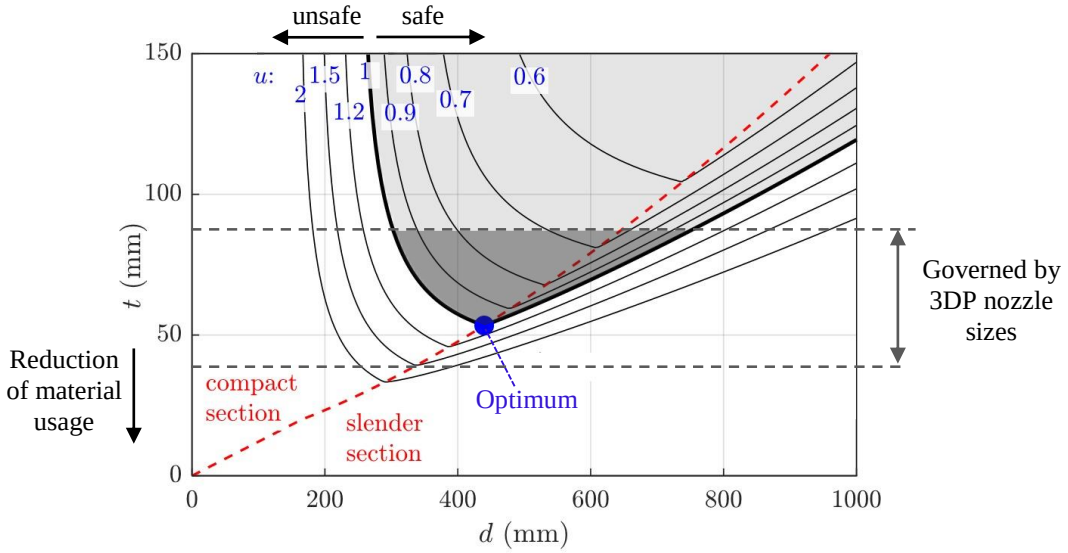

Figure 14: Typical utilisation-contour plot for varied shell thickness (t) and nominal wall depth (d). Shaded grey area indicates the zone where the wall's capacity is adequate for the design load. The dashed red line delineates compact sections (material stress failure) from slender sections (local-buckling failure). In this example: H_w = 2.5m, L_{trib} = 3.5m, n_s = 2.

For any of the printed patterns (A, B, C) the area-per-unit-length is approximately proportional to shell thickness (i.e. $t \propto \bar{A}$), thus allowing the shell thickness to be used as a proxy for material consumption. Therefore, in the graphical representation in Figure 14, the optimal section occurs at the trough of the u=1 contour line where t is minimised. Notably, the u contours follow different trajectories in the compact- and slender-section zones, and the optimal solution always occurs at the boundary that delineates them. In the compact-section zone, there is a roughly inverse relationship between t and d; this is because a section with a reduced depth requires a thicker shell to maintain the necessary section area and moment of inertia. In the slender-section zone the capacity is governed by local buckling of the shell, and hence increasing the section depth requires an increase to the shell thickness to maintain a constant capacity. The existence of an optimal section also demonstrates that hollow 3DP sections offer improved material efficiency compared to equivalent solid sections. These observations also highlight that in the practical range of interest, the design capacity of the wall is governed both by the material's compressive strength and elastic modulus, underscoring the importance of both these properties.

4.2.2 Design charts based on experimentally quantified material properties

The loadbearing capability of 3DP cob walls is examined in Figure 15 and Figure 16 by presenting model design charts for varied tributary width and wall height respectively. The figures plot the smallest required shell thickness (t) and accompanying wall thickness (d) of the optimised wall section that minimises material consumption. The constant inputs used to generate these figures are summarised in Table 4 and include the material properties established in Section 3. Figure 15 maintains a constant wall height of 3.0 m while varying the tributary width up to a maximum of 6 m. Conversely, Figure 16 maintains a constant tributary width at

4.0 m while varying the wall height between 2.5 to 3.5 m. These ranges of dimensions were selected to reflect the practical bounds of interest in a typical residential building. Each figure considers separately the alternate printed patterns (A, B, C) in either a 1- or 2-storey building. The relative efficiency of the alternate sections is presented in Figure 17 and Figure 18 by plotting the section area per unit length (a proxy for the material consumption).

Overall, the plots demonstrate that, on the assumption of the mechanical properties matching those established in the accompanying tests, loadbearing structural function in typical residential construction can be accomplished using wall section sizes that are reasonable and within the capability of the 3D printer system. The indicative range of shell thickness and wall thickness is summarised in Table 5. It is seen that in a single-storey house the section size can be kept small (t = 25–40 mm, d = 250–400 mm) relative to a 2-storey house (t = 35–120 mm, d = 320–800 mm).

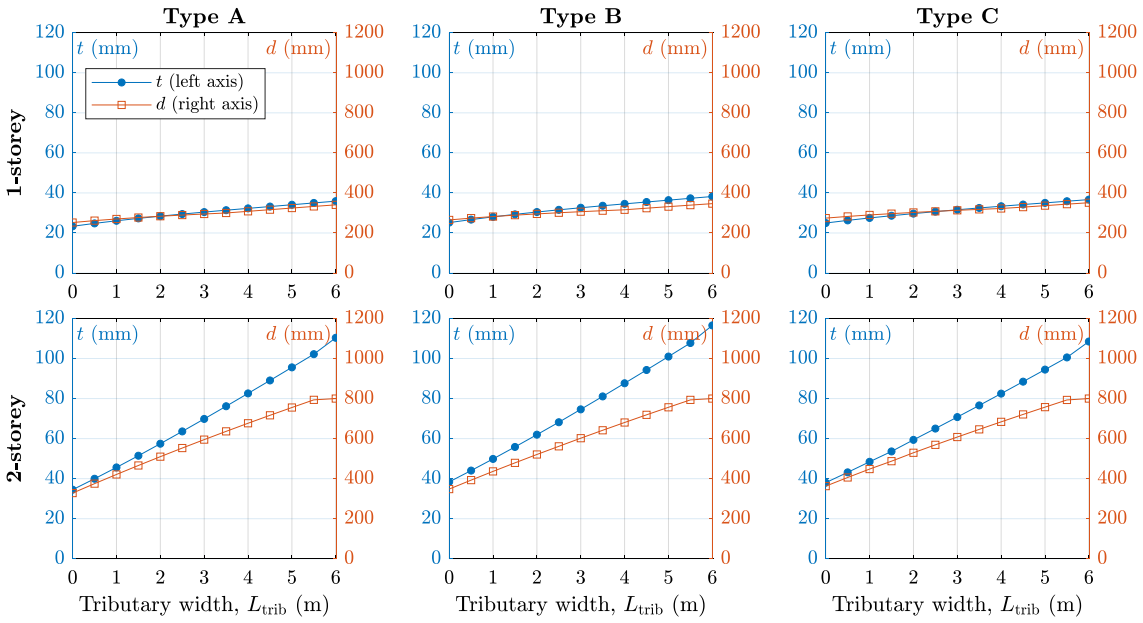

Figure 15: Dimensions t and d of optimised sections for varied tributary width (constant wall height of 3 m). All inputs including material properties are as per Table 4. Considers section types A, B, C, and either a 1- or 2-storey building. Each plot shows t on the left y-axis and d on the right y-axis.

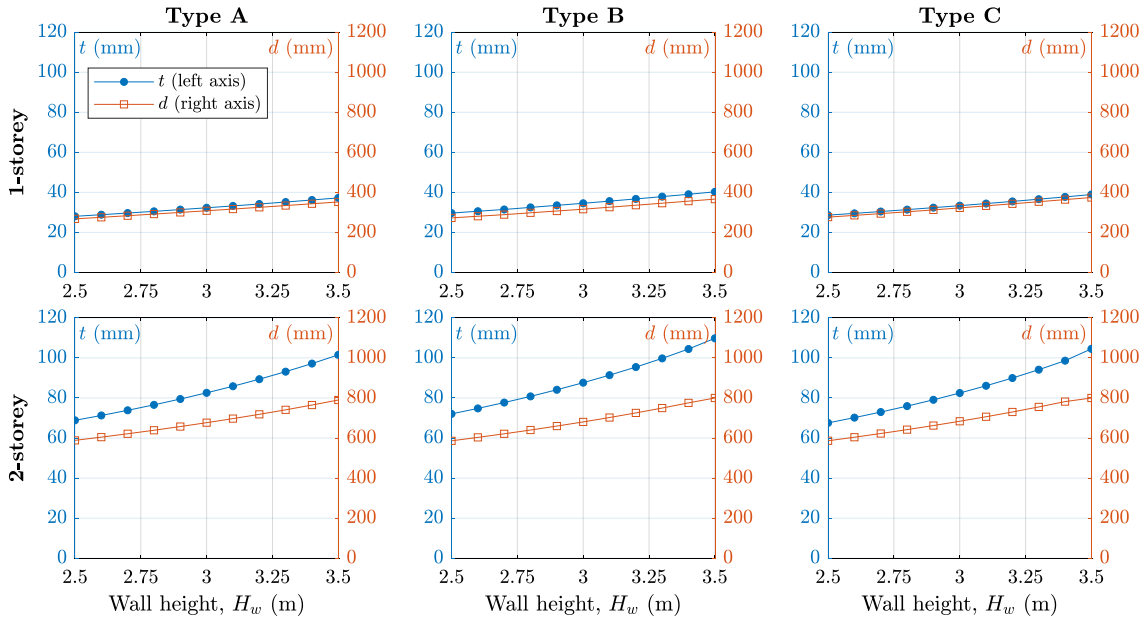

Figure 16: Dimensions t and d of optimised sections for varied wall height (constant tributary width of 4 m). All inputs including material properties are as per Table 4. Considers section types A, B, C, and either a 1- or 2-storey building. Each plot shows t on the left y-axis and d on the right y-axis.

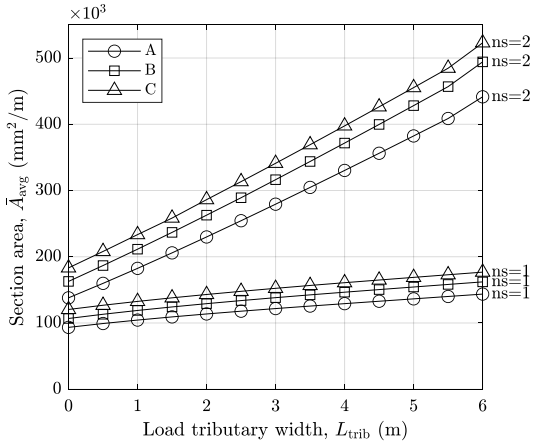

Figure 17: Section area per unit length for the optimised sections in Figure 15.

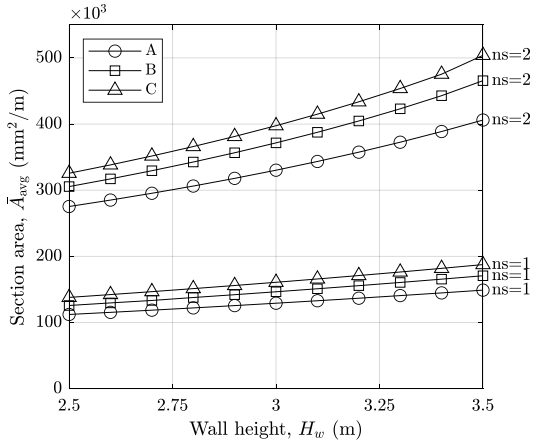

Figure 18: Section area per unit length for the optimised sections in Figure 16.

Table 5: The range of the section-defining parameters *t* and *d* corresponding to the design charts in Figure 15 and Figure 16.

	1 storey		2 stories	
	Min (mm)	Max (mm)	Min (mm)	Max (mm)
Shell thickness (*t*)	25	40	35	115
Wall thickness (*d*)	250	400	320	800

Note that in scenarios where a small section geometry may be permitted by structural considerations alone, the actual section could in practicality be dictated by other factors such as architectural requirements, aesthetics, thermal performance, standardisation of the construction process, and the capability of the 3D-printing system. For instance, a previous study by Gomaa et al. [21] found that 3D printing of large-scale cob walls requires a nozzle size of at least 40 mm, which can be used to generate an 'average' shell thickness (t) between 50–80 mm. Smaller nozzle diameters can slow down the printing process and also cause clogging of the extrusion system. On the other hand, using larger nozzles leads to reduced control over material consumption and accuracy.

The plots in Figure 17 and Figure 18 indicate that based solely on their structural performance, of the three section types, A is the most efficient, followed by B and then C. However, on any project it may also be necessary to consider other factors that may be impacted by the type of wall section. For example, from an architectural perspective, the notion of efficiency also includes considerations such as the design function, thermal performance, and environmental impacts. For instance, the thermal performance efficiency of 3DP cob was explored thoroughly in a recent study by Gomaa et al. [22], which demonstrated that the voids present in 3DP wall patterns dramatically improve thermal efficiency compared to solid cob walls. This means that the relative thermal performance of the alternate wall sections A, B or C may not necessarily match their relative structural performance. Hence, it is recommended that selecting the wall section type should be undertaken using a holistic approach that considers their structural, thermal, and environmental efficiency.

4.2.3 Parametric study into the influence of the material properties

As demonstrated by the review of experimental studies (Table 1), the mechanical properties of cob can exhibit drastic variation depending on the mix composition. To account for the limited number of material tests in the current study, a parametric study was undertaken to examine the sensitivity of the feasibility study findings on the quality of the material. To this end, the mean compressive strength (f_{cm}) and elastic modulus (E) were varied so as to cover a realistic range of the respective properties as identified through the review of past testing (Table 1).

Three scenarios were considered (Note: Symbol '*' refers to the value being representative of the accompanying tests in Section 3):

1. Varied f_{cm} = 0.6/0.9*/1.35 MPa, at constant E = 23* MPa,
2. Varied E = 20*/40/80 MPa, at constant f_{cm} = 0.87* MPa,
3. E and f_{cm} both varied in equal proportion: [f_{cm}, E] = [0.4,20*], [0.8*,40], and [1.6,80] MPa.

The purpose of the first two scenarios was to gain insight into the parametric influence of the respective properties by varying them in isolation, while the third was meant to represent variation of the overall quality of the material by changing both properties simultaneously.

The study considers wall pattern type C and varies the tributary width while keeping H_w = 3 m. Aside from f_c and E, the remaining inputs listed in Table 4 remain unchanged. The results are presented in Figures 19–24 respectively.

- Scenario 1

The first scenario (Figures 19 and 20) looks at variation of compressive strength between 0.6/0.9/1.35 MPa while maintaining E as per the current tests (23 MPa). Note that the intermediate strength level (0.9 MPa) is similar to the result of the current tests. It is observed that in the 1-storey case, the required cross section is relatively insensitive over the three levels of strength. In the 2-storey case however, the reduced strength (0.6 MPa) requires a cross section that becomes excessively large for any tributary width exceeding 1m, thus making the walls effectively incapable of performing a loadbearing function. Conversely, the improved strength (1.35 MPa) allows for a smaller section to be used, saving up to 30% in material volume.

- Scenario 2

The second scenario (Figures 21 and 22) looks at variation of the elastic modulus at levels of 20/40/80 MPa while maintaining f_{cm} as per the current tests (0.87 MPa). The lowest E value (i.e. 20 MPa) is comparable to the material of the current tests. For both the 1- and 2-storey cases, a higher elastic modulus leads to a reduction in the necessary cross section size. The improvement in increasing E from 20 to 80 MPa results in a material saving between 10–50%. It is also interesting to note that a higher elastic modulus results in an optimal cross section that has an increased wall thickness (d) while having a lower shell thickness (t); this can be explained by improved resistance to local buckling.

- Scenario 3

The last scenario (Figures 23 and 24) examines the effect of proportionally increasing both f_{cm} and E, which can be considered analogous to an overall variation in the quality of the material, i.e. low (0.4/40MPa), intermediate (0.8/40MPa) and high (1.6/80MPa) quality. The graphs indicate a strong dependence between the loadbearing capacity (i.e. required section size) and the input material properties in both the 1- and 2-storey cases. While not being directly comparable to the previous two scenarios because of different input values, a general comparison indicates that the most efficient improvement in overall loadbearing performance is achieved by simultaneously enhancing both f_{cm} and E, rather than by increasing either of these properties alone.

Overall, the sensitivity study indicates that the feasibility of cob walls to act as loadbearing is conditional on a minimum required level of material performance. The 3DP cob tested in this study meets this threshold, but it is evident that a reduced compressive strength (< 0.75 MPa) may not be sufficient for loadbearing walls in a 2-storey house. On the other hand, even weak cob (≈ 0.4 MPa) may still be sufficient to construct loadbearing walls in a single-storey house.

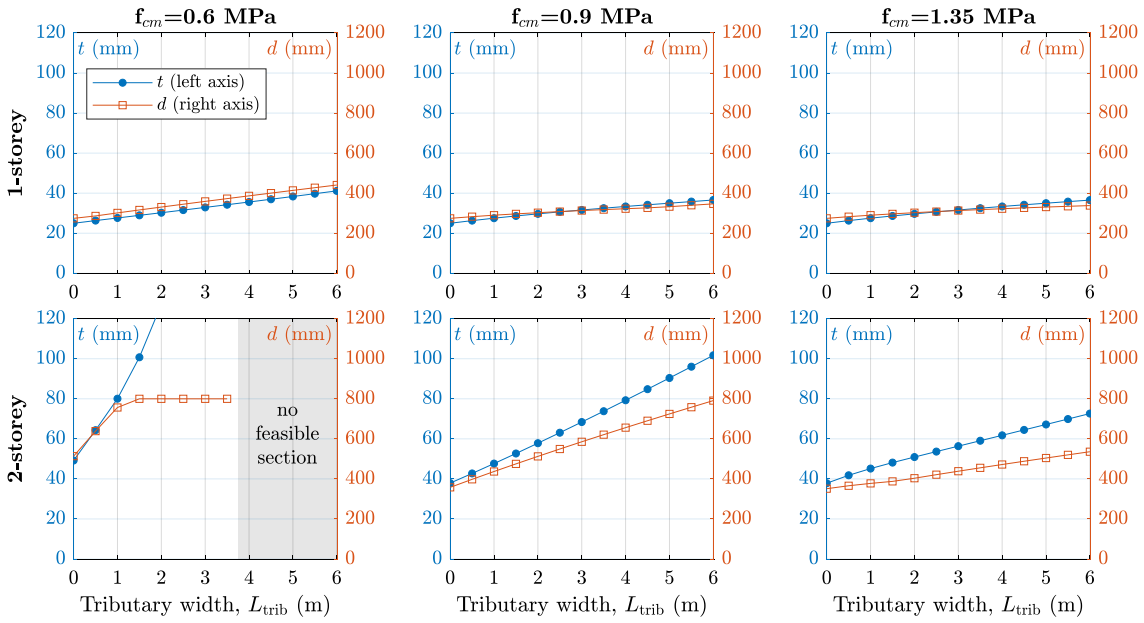

Figure 19: Dimensions t and d of optimised sections for varied compressive strength (constant E).

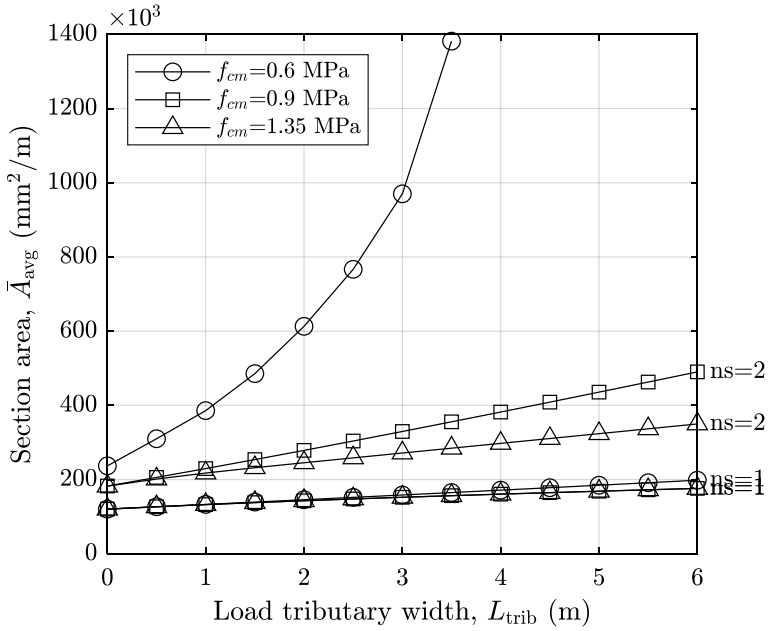

Figure 20: Material consumption of the optimised sections plotted in Figure 19.

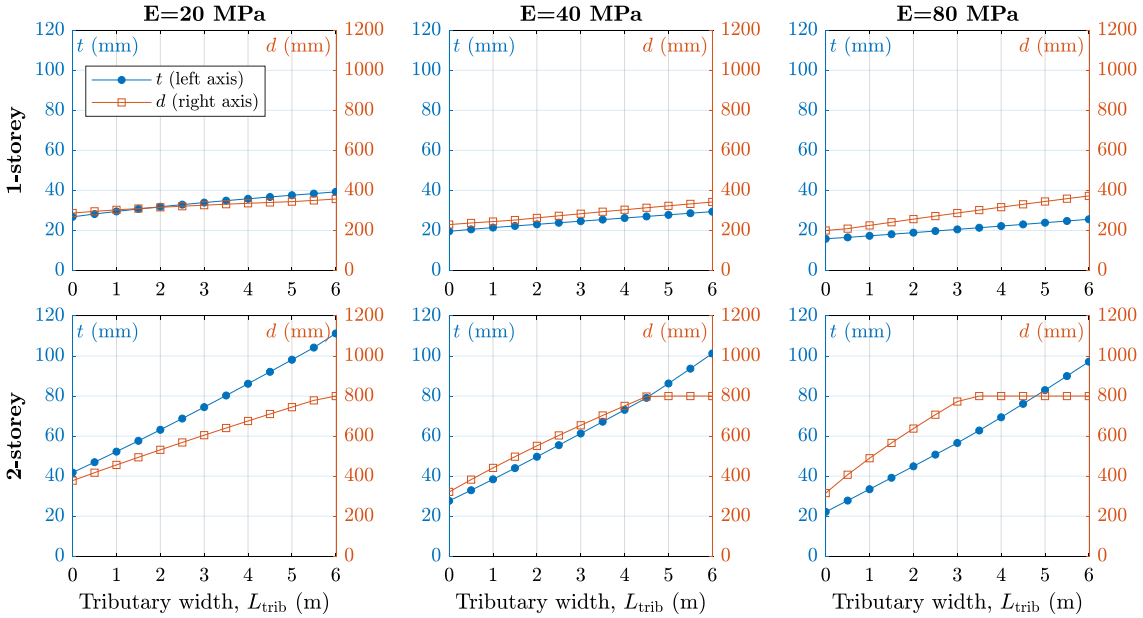

Figure 21: Dimensions t and d of optimised sections for varied elastic modulus (constant f_{cm}).

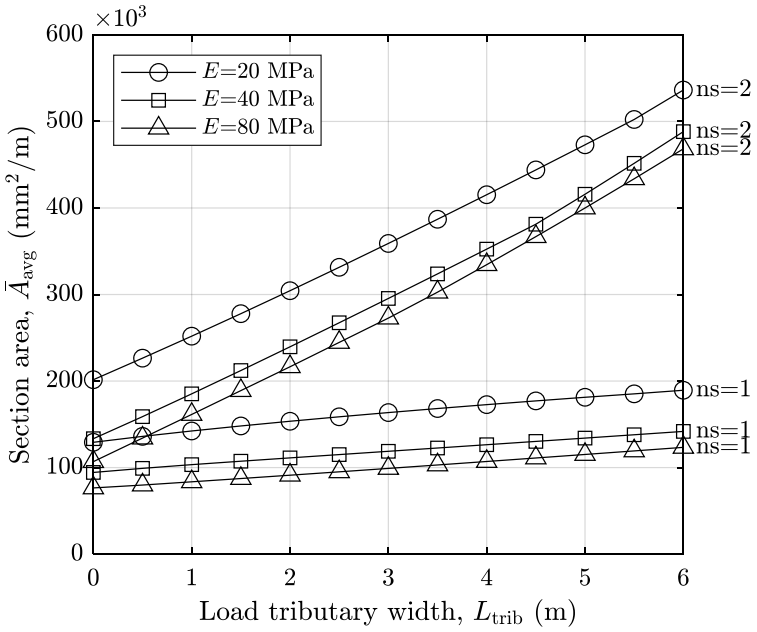

Figure 22: Material consumption of the optimised sections plotted in Figure 21.

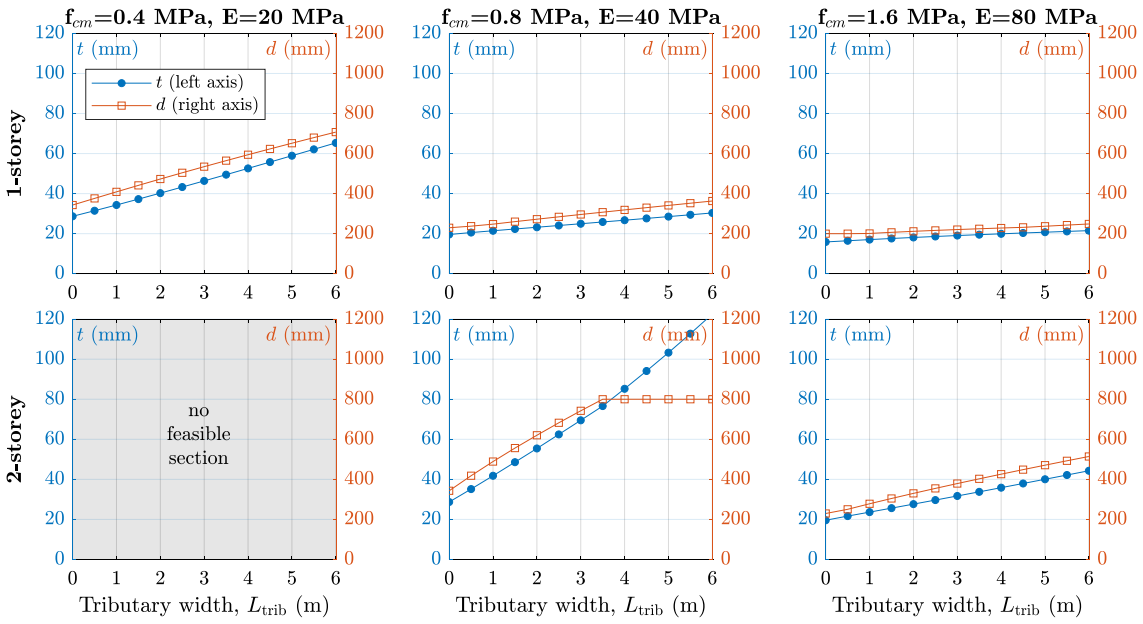

Figure 23: Dimensions t and d of optimised sections for varied f_{cm} and E, with ratio f_{cm}/E held fixed.

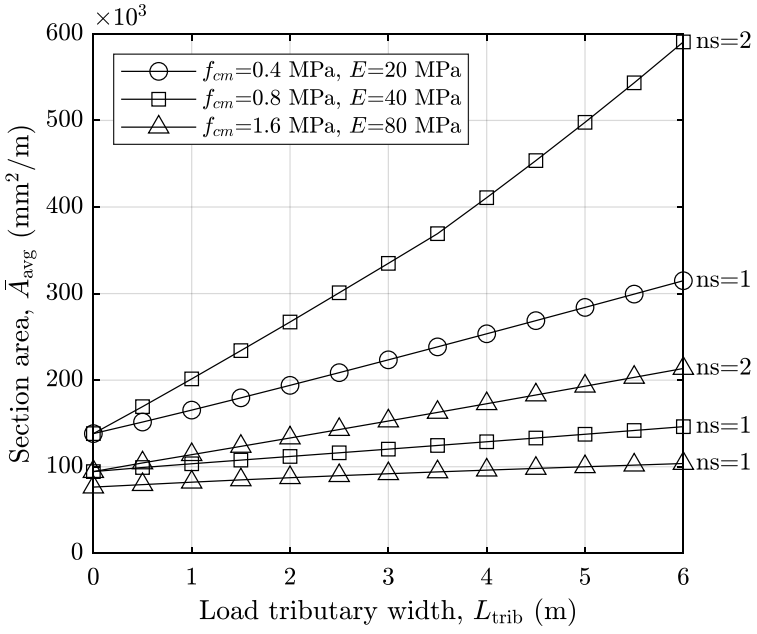

Figure 24: Material consumption of the optimised sections plotted in Figure 23.

5 Case study of a small 3DP cob house

As explained previously, the approach to leveraging the wall sizing charts (e.g. Figure 15) depends both on structural and architectural design considerations. To demonstrate the essential design process, a case study involving a small house will now be presented. The process starts with a floor plan defining the zoning and dimensions of the spaces (Figure 25). For illustrative purposes, the hypothetical house incorporates four spaces with different sizes and opening configurations, representing typical design requirements. The dimensions of the spaces range from 2m to 4 m, wall heights are set at 3m, and the number of storeys is taken as either 1 or 2. The roof (in the 1 and 2-storey cases) and the suspended floor (in the 2-storey case) are treated as one-way spanning in the directions indicated on Figure 25.

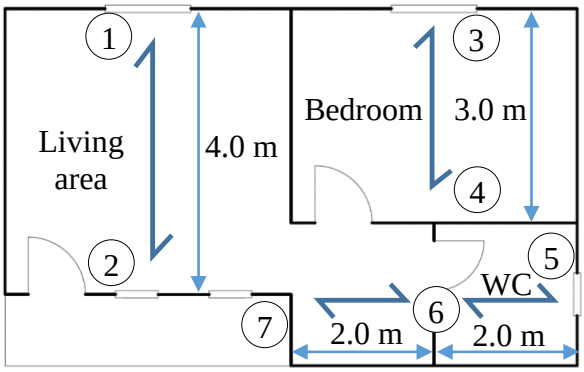

Figure 25: Basic floor plan of the idealised 3DP cob house. Half-headed arrows indicate the span direction of the suspended floor and roof. Loadbearing walls are numbered from 1 to 7.

The design parameters and final sizing of each wall are summarised in Tables 6 and 7 for the single and double storey alternatives respectively. The procedure to determine the minimum section sizes is as follows:

1. Establish which walls are loadbearing by considering the span direction of the floor/roof. In this example, walls 1–7 are loadbearing (Figure 25).
2. The ‘basic’ tributary width of each loadbearing wall is determined by considering whether the wall is internal or external and the effective span of the floor/roof being supported, using gross dimensions (refer to Figure 10).
3. If the wall has an opening, the basic tributary width is upscaled in relation to the ratio of the openings (as described in Section 4.1.4). For instance, a wall containing 50% openings (in plan view) carries an effective tributary width equal to double the basic tributary width. Note that for simplicity, the effective tributary widths in Tables 6 and 7 are rounded-up to the nearest 1m.
4. Non-loadbearing walls are analogous to having a zero effective tributary width.
5. The effective tributary width is then used to select *t* and *d* from the relevant design chart (Figure 15).

Note that the nominated section sizes in Tables 6 and 7 assume the material properties quantified in the accompanying material tests (i.e. using Figure 15). Also note that consideration is given here only to gravity loads and not to out-of-plane loads due to wind or earthquake, which are region-specific and outside the scope of the current paper.

Figure 26 illustrates the floor plan by assigning the minimum section sizes to each wall. Since the minimum required section size can be different for each wall, the designer has the choice of standardising the sizes as needed to suit the other project requirements (e.g. thermal and architectural) which may also serve to reduce the complexity of the design and improve the efficiency of the construction process.

Table 6: Design of loadbearing (1–7) and non-loadbearing (NLB) walls in the 1-storey example house.

Wall	Basic L_{trib} (m)	Opening ratio (%)	Tributary scale factor	Effective L_{trib} (m)	Corresponding t and d (mm)					
					Type A		Type B		Type C	
					t	d	t	d	t	d
1	2	25	1.5	3	30	300	35	310	35	320
2	2	50	2.0	4	**35**	**310**	**35**	**320**	**35**	**330**
3	1.5	30	1.6	3	30	300	35	310	35	320
4	1.5	15	1.3	2	30	290	35	300	35	310
5	1	5	1.1	1	**30**	**280**	**30**	**290**	**30**	**300**
6	2	30	1.6	3	30	300	35	310	35	320
7	1	40	1.8	2	30	290	35	300	35	310
NLB	0	0	n/a	0	25	320	25	350	25	380

Table 7: Design of loadbearing (1–7) and non-loadbearing (NLB) walls in the 2-storey example house.

Wall	Basic L_{trib} (m)	Opening ratio (%)	Tributary scale factor	Effective L_{trib} (m)	Corresponding t and d (mm)					
					Type A		Type B		Type C	
					t	d	t	d	t	d
1	2	25	1.5	3	70	600	75	600	70	600
2	2	50	2.0	4	**80**	**700**	**85**	**640**	**80**	**700**
3	1.5	30	1.6	3	70	600	75	600	70	600
4	1.5	15	1.3	2	60	500	60	520	60	520
5	1	5	1.1	1	**45**	**420**	**50**	**420**	**50**	**420**
6	2	30	1.6	3	70	600	75	600	70	600
7	1	40	1.8	2	60	500	60	520	60	520
NLB	0	0	n/a	0	35	350	40	370	40	390

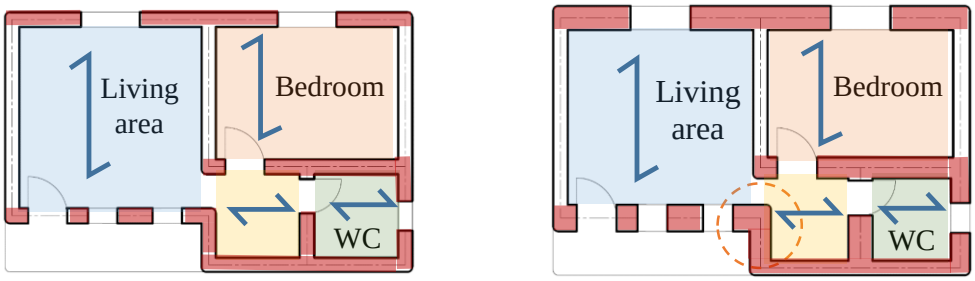

(a) Single-storey house *(b) Double-storey house*

Figure 26: Floor plan showing the minimum required wall sizes walls to scale. (Shown for pattern type A for illustrative purposes)

From Table 6 and Figure 26a, it can be seen that in the case of 1-storey house, the required sections are relatively consistent across all of the walls present (in terms of *t* and *d*), regardless of the chosen pattern (A, B, C). For example, if we consider pattern A, the required *t* varies between 30–35 mm, and *d* between 280–310 mm. The consistency in wall sizes in the case of a 1-storey building results from the required cross section being relatively insensitive to the tributary width, as reflected by Figure 15. For construction simplicity, the designer may therefore choose to standardise the wall sizes by assigning the largest required section to every wall.

In contrast to the 1-storey house, in the case of the 2-storey house the required section sizes (Table 7) vary substantially between the walls present (e.g. for type A: t = 45–80 mm, d = 420–700 mm). The resulting floor plan (Figure 26b) visually illustrates the difference in the wall thickness demands, especially between loadbearing and non-loadbearing walls. Therefore, in the case of the 2-storey building, the designer may opt for a suitable compromise between standardising the wall section sizes and economical material usage, for instance by adopting two or three different sizes across the building. Large wall thickness can also negatively impact the architectural functionality of the spaces, where, as highlighted in this example by the dotted circle in Figure 26b, the aisle linking the living area with the bedroom becomes severely narrowed due to the large thickness of the walls on both sides. Such considerations may require an iterative re-adjustment of the floor plan until both the structural and architectural requirements are satisfied.

An alternate way that the designer can balance the structural and architectural requirements in relation to wall section sizes is by dictating the gravity load path by controlling: 1) the span directivity of the floor/roof system being carried by the walls, 2) which cob walls act as loadbearing, and 3) which internal walls can be formed using lightweight partitions. To demonstrate this, Figure 27 illustrates three alternatives that maintain the same space layout as the original arrangement (Figure 25) but are reconfigured by altering the floor (or roof) spans and by implementing internal partitions to affect which walls are loadbearing.

Arrangement (a) is similar to the original configuration but rotates the floor span in south-east zone, thus allowing cob wall no. 6 (see Figure 25) to be replaced by a lightweight partition and also to reduce the size of wall no. 7. By removing some of the internal cob walls, configuration (a) arguably reduces the overall 3DP construction complexity compared to the original layout.

It does however increase the load demand on internal wall no. 4, therefore enlarging its section, and potentially hindering the functionality of the smaller rooms (i.e. toilets and lobby).

The presence of the internal cob wall (no. 4) in the original arrangement and configuration (a) also limits the freedom for future architectural changes to the internal space layout. Configurations (b) and (c) address this by replacing the internal walls in the east side of the house with lightweight partitions, thus improving the versatility for future layout alternations, but at the cost of requiring larger external walls because of a longer floor span in the east half out the house [compared to (a)].

Comparing configurations (b) and (c), a possible downside of (b) is that the central wall requires a large section since it acts as an internal loadbearing wall. By altering the direction of the floor span in the east half of the house, configuration (c) approximately halves the load on the central wall, but it does so at the cost of making the north and south outer walls loadbearing. Overall this would act to make the required wall sizes in option (c) more uniform across the house than in option (b), thus making (c) the potentially preferable option from a constructability point-of-view.

Overall, this example demonstrates that the process of selecting of the structural configuration is and exercise that involves compromise between a number of factors, including

- the dimensions and functionality of the spaces and location of openings,
- constructability and economical use of material,
- allowance for future alterations to the internal layout, and
- other factors not considered here, such as thermal insulation performance.

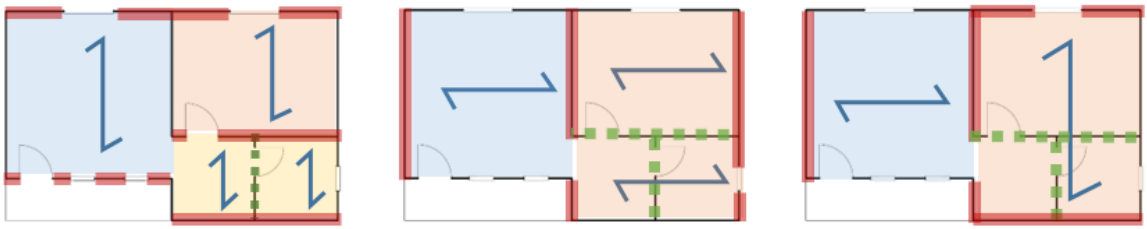

(a) *(b)* *(c)*

Figure 27. Examples of alternative arrangements of the floor/roof span directivity in the example small 3DP cob house. The loadbearing walls in each instance are highlighted in red. The lightweight partitions are highlighted in green dotted lines.

6 Conclusion

The increased uptake of 3DP technologies in construction, accompanied by a movement toward environmentally efficient materials has led to leveraging earthen materials in a contemporary 3DP process. 3DP cob has been a subject of investigation for several years now; however, while those investigations have focused mostly on the architectural aspects and environmental performance, investigation into the material's feasibility to be used for load-carrying building elements has not yet been undertaken sufficiently.

This study has conducted a comprehensive feasibility investigation into the structural capacity of 3DP cob walls under gravity loads. This was accomplished by first quantifying the basic mechanical properties of 3DP cob using a standardised compression test. The tests demonstrated that 3DP cob appears to exhibit similar mechanical performance to conventional cob in terms of compressive strength and elastic modulus. The expected load-carrying capacity of 3DP walls was then predicted using established structural mechanics concepts and limit-state design principles. These predictions demonstrate that 3DP cob walls are expected to have sufficient capacity to act as loadbearing in residential buildings up to two storeys.

The feasibility study also demonstrated the following:

- Due to the favourable geometric properties of printable hollow sections, 3DP cob walls can perform a loadbearing function with more efficient material usage compared to traditional (non-3DP) solid cob walls.
- The model design approach demonstrated in this paper provides a means for integrating the structural design process of 3DP cob into the design-to-construction framework. The generated design guidelines can be directly implemented to a Rhino-Grasshopper definition that enables visual modelling and direct interfacing with the 3D-printing system.
- The range of wall section sizes (as informed by the analysis) required for loadbearing functionality in buildings up to 2-storeys can be efficiently fabricated using available 3DP technologies and extrusion systems.

The findings of this study complete a broader feasibility investigation of 3DP cob for modern construction which combines structural performance with three other aspects: 1) constructability and fabrication process, 2) thermal performance, and 3) life cycle assessment. The results lead to the conclusion that 3DP cob construction emerges as a strong competitor to conventional and 3DP concrete construction. 3DP cob can substitute concrete-based construction in small to medium size low-rise residential projects, especially as it provides higher environmental efficiency and rationalised energy use. It can also provide novel design opportunities in addition to higher precision compared to manually constructed cob, especially for producing complex geometries. Moreover, 3DP cob construction can provide quick sheltering solutions with low cost and efficient use of local materials in expeditionary and hostile environments.

It is however important to highlight that while the current study provides promising and necessary first insight into the structural feasibility of 3DP cob walls, the findings are based on structural analysis with input from small-scale material tests. Therefore, proof-of-concept structural testing on full printed wall sections is envisaged as a crucial next step of this research.

Furthermore, while the outcomes of this study are positive overall, the accompanying sensitivity study undertaken demonstrates that the quality of the material in terms of its mechanical properties (compression strength and elastic modulus) is highly influential on the resulting loadbearing capability of the walls. Therefore, further research into the development of 3DP-suitable cob mixtures with a focus on ensuring consistently high-quality mechanical performance could yield significant additional benefit to this form of construction. Accompanying focus into other material performance aspects, in particular shrinkage and creep, is also required.

Acknowledgements

We would like to acknowledge Dr Alejandro Veliz Reyes for his valuable collaboration and support (University of Plymouth). We also extend our gratitude to Aikaterini Chatzivasileiadi and Anas Lila (Cardiff University) for their invaluable help.

Funding Resources

This work was supported financially by the Engineering and Physical Sciences Research Council (EPSRC) and The University of Nottingham under the Network Plus: Industrial Systems in the Digital Age, Grant number: EP/P001246/1. This work is also partially supported by the University of Adelaide through the Research Abroad Scholarship scheme.

References

[1] P. Feng, X. Meng, J.-F. Chen, and L. Ye, "Mechanical properties of structures 3D printed with cementitious powders," *Constr. Build. Mater.*, vol. 93, pp. 486–497, 2015, doi: 10.1016/j.conbuildmat.2015.05.132.

[2] A. Kazemian, X. Yuan, E. Cochran, and B. Khoshnevis, "Cementitious materials for construction-scale 3D printing: Laboratory testing of fresh printing mixture," *Constr. Build. Mater.*, vol. 145, pp. 639–647, 2017, doi: 10.1016/j.conbuildmat.2017.04.015.

[3] B. Zareiyan and B. Khoshnevis, "Interlayer adhesion and strength of structures in Contour Crafting - Effects of aggregate size, extrusion rate, and layer thickness," *Autom. Constr.*, vol. 81, pp. 112–121, 2017, doi: 10.1016/j.autcon.2017.06.013.

[4] B. Khoshnevis, "Automated construction by contour crafting — related robotics and information technologies," vol. 13, pp. 5–19, 2004, doi: 10.1016/j.autcon.2003.08.012.

[5] T. T. Le, S. A. Austin, S. Lim, R. A. Buswell, A. G. F. Gibb, and T. Thorpe, "Mix design and fresh properties for high-performance printing concrete," *Mater. Struct. Constr.*, vol. 45, pp. 1221–1232, 2012, doi: 10.1617/s11527-012-9828-z.

[6] A. Perrot, D. Rangeard, and A. Pierre, "Structural built-up of cement-based materials used for 3D- printing extrusion techniques," *Mater. Struct.*, vol. 49, pp. 1213–1220, 2016, doi: 10.1617/s11527-015-0571-0.

[7] L. Wang, H. Jiang, Z. Li, and G. Ma, "Mechanical behaviors of 3D printed lightweight concrete structure with hollow section," *Arch. Civ. Mech. Eng.*, vol. 20, pp. 1–17, Mar. 2020, doi: 10.1007/s43452-020-00017-1.

[8] H. Alhumayani, M. Gomaa, V. Soebarto, and W. Jabi, "Environmental Assessment of large-Scale 3D Printing in Construction: A Comparative Study between Cob and Concrete," *J. Clean. Prod.*, vol. 270, pp. 122463, Jun. 2020, doi: 10.1016/j.jclepro.2020.122463.

[9] CyBe, "3D Studio 2030 — CyBe Construction," 2019. https://cybe.eu/case/3d-studio-2030/ (accessed Nov. 20, 2019).

[10] C. Shrubsole *et al.*, "Bridging the gap: The need for a systems thinking approach in understanding and addressing energy and environmental performance in buildings," *Indoor Built Environ.*, vol. 28, pp. 100–117, 2019, doi: 10.1177/1420326X17753513.

[11] S. Ford and M. Despeisse, "Additive manufacturing and sustainability: an exploratory study of the advantages and challenges," *J. Clean. Prod.*, vol. 137, pp. 1573–1587, 2016, doi: 10.1016/j.jclepro.2016.04.150.

[12] E. Hamard, B. Cazacliu, A. Razakamanantsoa, and J. C. Morel, "Cob, a vernacular earth construction process in the context of modern sustainable building," *Build. Environ.*, vol. 106, pp. 103–119, 2016, doi: 10.1016/j.buildenv.2016.06.009.

[13] E. Quagliarini, A. Stazi, E. Pasqualini, and E. Fratalocchi, “Cob construction in Italy: Some lessons from the past,” *Sustainability*, vol. 2, pp. 3291–3308, 2010, doi: 10.3390/su2103291.
[14] T. Morton, F. Stevenson, B. Taylor, and N. C. Smith, “Low Cost Earth Brick Construction: Monitoring & Evaluation,” Fife, UK, 2005. [Online]. Available: http://www.arc-architects.com/downloads/Low-Cost-Earth-Masonry-Monitoring-Evaluation-Report-2005.pdf.
[15] L. Ben-Alon, V. Loftness, K. A. Harries, and E. Cochran Hameen, “Integrating Earthen Building Materials and Methods into Mainstream Construction Using Environmental Performance Assessment and Building Policy,” *IOP Conf. Ser. Earth Environ. Sci.*, vol. 323, pp. 012139, 2019, doi: 10.1088/1755-1315/323/1/012139.
[16] O. O. Akinkurolere, C. Jiang, A. T. Oyediran, O. I. Dele-Salawu, and A. K. Elensinnla, “Engineering properties of Cob as a building material,” *Journal of Applied Sciences*, vol. 6, pp. 1882–1885, 2006, doi: 10.3923/jas.2006.1882.1885.
[17] J. Fordice and L. Ben-Alon, “A research project dedicated to making cob legally accessible to the public,” 2017.
[18] E. Kianfar and V. Toufigh, “Reliability analysis of rammed earth structures,” *Constr. Build. Mater.*, vol. 127, pp. 884–895, 2016, doi: 10.1016/j.conbuildmat.2016.10.052.
[19] A. Veliz Reyes, W. Jabi, M. Gomaa, A. Chatzivasileiadi, L. Ahmad, and N. M. Wardhana, “Negotiated matter: a robotic exploration of craft-driven innovation,” *Archit. Sci. Rev.*, vol. 62, pp. 1–11, 2019, doi: 10.1080/00038628.2019.1651688.
[20] 3D-WASP, “3D Printers | WASP | Leading Company in the 3d printing industry,” 2020. https://www.3dwaspp.com/en/ (accessed Jan. 10, 2020).
[21] M. Gomaa, W. Jabi, A. Veliz Reyes, and V. Soebarto, “3D Printing System for Earth-based construction: Case Study of Cob Walls,” *Autom. Constr.*, vol. 124, pp. 103577, 2021, doi: https://doi.org/10.1016/j.autcon.2021.103577.
[22] M. Gomaa, J. Carfrae, S. Goodhew, W. Jabi, and A. Veliz Reyez, “Thermal performance exploration of 3D printed cob,” *Archit. Sci. Rev.*, vol. 62, pp. 1–8, Apr. 2019, doi: 10.1080/00038628.2019.1606776.
[23] A. Perrot, D. Rangeard, and E. Courteille, “3D printing of earth-based materials: Processing aspects,” *Constr. Build. Mater.*, vol. 172, pp. 670–676, 2018, doi: 10.1016/j.conbuildmat.2018.04.017.
[24] L. Keefe, *Earth building : methods and materials, repair and conservation*, 1st ed. New York: Taylor and Francis Ltd., 2005.
[25] S. S. Damluji, *The Architecture of Yemen: From Yafi to Hadramut*. London: Laurence King Publishing, 2008.
[26] Green Home Buildings, “Mixing and Applying Cob,” 2020. http://www.greenhomebuilding.com/QandA/cob/mixing.htm (accessed Jul. 03, 2020).
[27] Earth Devon, “Cob Dwellings: Compliance with The Building Regulations,” *Cob Unbaked Earth Dwellings*, vol. 2000, pp. 1–21, 2008.
[28] A. Weismann and K. Bryce, *Building with cob: a step-by-step guide*. Devon: Green Books ltd, 2006.
[29] L. Miccoli, U. Müller, and P. Fontana, “Mechanical behaviour of earthen materials: A comparison between earth block masonry, rammed earth and cob,” *Constr. Build. Mater.*, vol. 61, pp. 327–339, 2014, doi: 10.1016/j.conbuildmat.2014.03.009.
[30] D. J. Wright, “Building From The Ground Up : Understanding and Predicting The Strength of Cob , An Earthen Construction Material,” The University of Tulsa. PhD thesis, 2019.
[31] R. H. Saxton, “Performance of cob as a building material,” *Struct. Eng. London*, vol. 73, pp. 111–115, 1995.

[32] Q. M. Pullen and T. V. Scholz, “Index and engineering properties of Oregon Cob,” *J. Green Build.*, vol. 6, pp. 88–106, 2011, doi: 10.3992/jgb.6.2.88.
[33] E. Quagliarini and G. Maracchini, “Experimental and FEM Investigation of Cob Walls under Compression,” *Adv. Civ. Eng.*, vol. 2018, pp. 21–29, 2018, doi: 10.1155/2018/7027432.
[34] H. Houben and H. Guillaud, *Earth construction: a comprehensive guide*, 1st ed. London: Intermediate Technology Publications, 1994.
[35] L. Ziegert, “Konstruktion, Schäden und Sanierung, Berichte aus dem Konstruktiven Ingenieurbau,” Technical University of Berlin. PhD Thesis., 2003.
[36] K. A. Coventry, “Specification Development for the Use of Devon Cob in Earthen Construction,” University of Plymouth. PhD thesis, 2004.
[37] G. Minke, *Building with Earth: design and technology of a sustainable architecture*. Basel: Walter de Gruyter, 2012.
[38] M. Rizza and H. Bottger, *Effect of Straw Length and Quantity on Mechanical Properties of Cob*. San Francisco, 2015.
[39] G. Brunello, J. Espinoza, and A. Golitz, “Cob Property Analysis,”. Dep of Civil & Environemntal Engineering. Santa Clara University. MSc Thesis., 2018.
[40] T. Vinceslas, E. Hamard, A. Razakamanantsoa, and F. Bendahmane, “Further development of a laboratory procedure to assess the mechanical performance of cob,” *Environ. Geotech.*, vol. 7, pp. 200–207, 2018, doi: 10.1680/jenge.17.00056.
[41] A. Jiménez Rios and D. O’Dwyer, “Experimental validation for the application of the flat jack test in cob walls,” *Constr. Build. Mater.*, vol. 254, 2020, doi: 10.1016/j.conbuildmat.2020.119148.
[42] A. Fabbri, J.-C. Morel, and D. Gallipoli, “Assessing the performance of earth building materials: a review of recent developments,” *RILEM Tech. Lett.*, vol. 3, pp. 46–58, 2018, doi: 10.21809/rilemtechlett.2018.71.
[43] S. Goodhew, PP. C. Grindley, and S. D. Probeif, “Composition, Effective Thermal Conductivity And Specific Heat Of Cob Earth-walling,” *Trans. Built Environ.*, vol. 15, pp. 205–213, Jan. 1995, doi: 10.2495/STR950231.
[44] CEN, “EN 772-1. Methods of test for masonry units - Part 1: Determination of compressive strength,” 2011. [Online]. Available: https://infostore.saiglobal.com/en-us/Standards/EN-772-1-2011-A1-2015-331320_SAIG_CEN_CEN_761952/.
[45] Standards Australia, *AS 1170.1–2002 (R2016) Structural design actions Part 1 : Permanent , imposed and other actions*. Sydney, NSW: Australian / New Zealand Standard ™, 2002.
[46] Standards Australia, *Australian Standard for Masonry structures (AS 3700:2018)*. Sydney, NSW: Australian / New Zealand Standard ™, 2018.
[47] R. McNeel, “Grasshopper - in Rhino 6,” 2020. https://www.rhino3d.com/6/new/grasshopper (accessed Jul. 30, 2020).

GENERAL

We wish to again thank all of the Reviewers for their constructive feedback on how to improve the paper. We have addressed the comments from the second phase of review as follows.

Reviewer #3

1. In general, writing has been improved but further polishing is still recommended. Issues is writing were still identified regarding:
- Definite/indefinite articles,
- Usage of plurals,
- Frequent use of demonstrative pronouns and demonstrative determiners,
- Incorrect verb constructions,
- Grammatical tense (past tense often wrongly used),
- Usage of contractions is not recommended in scientific writing,
- Capitalization

We have undertaken a thorough proof-read of the paper and addressed as many of these issues as we could identify. Please refer to the marked-up paper with the changes being highlighted in red.

2. In Figure 15 and Figure 16, it is recommended to add a legend to the graphs, similar to Figure 17, denoting which series corresponds to "t" and which one corresponds to "d" (necessary for when the paper is printed in gray scale). The same recommendation applies to Figure 19, Figure 21, and Figure 23.

We have modified the figures by adding a legend as recommended by the Reviewer.

3. It is recommended to only mention future studies in the conclusion section (see Section 4.2.2).

We have identified two such instances in the main text. We deleted one, but retained the other as it is integral to the context of the discussion (on line 297), as follows:
"… thus providing impetus for future investigations into 3DP-suitable cob mix design to focus on not just the material's strength but also stiffness"

Highlights

- Basic mechanical properties of 3D-printed cob were experimentally quantified.
- Mechanical properties of 3DP cob are shown to be comparable to traditional (non-3DP) cob.
- A model technique for compression design is demonstrated using a limit-state framework.
- Loadbearing 3DP cob wall are shown to be feasible for residential construction up to 2 stories.

CRediT author statement

Mohamed Gomaa: Conceptualization, Methodology, Data curation, Formal analysis, Investigation, Resources, Software, Validation, Visualization, Writing - original draft, Writing - review & editing, Project administration, Funding acquisition

Jaroslav Vaculik: Conceptualization, Methodology, Data curation, Formal analysis, Investigation, Resources, Software, Validation, Visualization, Writing - original draft, Writing - review & editing.

Veronica Soebarto: Conceptualization, Writing - review & editing, Supervision

Michael Griffith: Methodology, Writing - review & editing, Supervision

Wassim Jabi: Resources, review & editing, funding acquisition

Feasibility of 3DP Cob Walls Under Compression Loads in Low-Rise Construction

Mohamed Gomaa[ae], Jaroslav Vaculik[b,c*], Veronica Soebarto[a], Michael Griffith[b,c], Wassim Jabi[d]

[a] School of Architecture and Built Environment, Horace Lamb Building, University of Adelaide, Adelaide SA5005, Australia.
[b] The School of Civil, Environmental and Mining Engineering, Engineering North Building, University of Adelaide, Adelaide SA5005, Australia.
[c] Bushfire and Natural Hazards Cooperative Research Centre, Melbourne, Australia
[d] The Welsh School of Architecture, Bute Building, Cardiff University, Cardiff CF10 3NB, UK.
[e] School of Engineering, B251- RMIT Bundoora East Campus, RMIT University, Melbourne VIC 3083, Australia.

*Corresponding Author
Postal address: The School of Civil, Environmental and Mining Engineering, Engineering North Building, University of Adelaide, Adelaide SA5005, Australia.
Phone: (+61 8 8313 5451)

Declaration of interests

☒ The authors declare that they have no known competing financial interests or personal relationships that could have appeared to influence the work reported in this paper.

☐The authors declare the following financial interests/personal relationships which may be considered as potential competing interests: